UNIVERSITY OF KYRENIA

GRADUATE SCHOOL OF SCIENCE

SURFACE ANALYSIS OF BIOFOULING EFFECT ON SHIP PROPELLERS IN PORT OF KYRENIA

In Partial Fulfilment of the Requirements for

The degree of Master of Science

in

Maritime Transportation Management Engineering

Volkan VARIŞLI

UNIVERSITY OF KYRENIA

GRADUATE SCHOOL OF SCIENCE

SURFACE ANALYSIS OF BIOFOULING EFFECT ON SHIP PROPELLERS IN PORT OF KYRENIA

In Partial Fulfilment of the Requirements for

The degree of Master of Science

in

Maritime Transportation Management Engineering

Volkan VARIŞLI

DECLARATION

I hereby declare that all information in this document has been obtained and presented in accordance with academic rules and ethical conduct. I also declare that, as required by these rules and conduct, I have fully cited and referenced all material and results that are not original to this work.

Volkan VARIŞLI / Kyrenia,2020

ACKNOWLEDGEMENTS

TEŞEKKÜR

To my dear wife and lovely Maya,

Kaptan Bora Ekşi anısına..

ABSTRACT

The common basis of the pioneering scientific approaches that guide the attitudes towards maritime transportation in terms of fuel consumption volume were based upon reducing hydrodynamic ship losses or reducing economic waste with high economic value, and reducing general referral losses. On the other hand, opinions on reducing high losses arising from propeller resistors are limited with the idea of recovering the efficiency of optimum propeller designs from possible biofouling with mechanical cleaning and polishing applications.

Being able to evaluate the activities such as the taxonomic classification of the propeller biofouling and the speed of spreading with gray-scale spectrum analysis method, which occurs intensely in the waiting times exceeding the average limit, is a subject that requires experimenting in a real marine environment.

The main point of this study is to evaluate the three-dimensional (3D) surface topography of biological formations in Kyrenia Commercial Port using the characteristic prop materials and to evaluate the results related to surface roughness in an accelerated, special computer environment where applicable metrological calculations. The micro-scale roughness data obtained is an expression of the result-oriented perspective, by analysing Musker's characteristics and the Rubert scale, enabling access to macro results such as increased emission values by analysing the results in the hypothesis that a real ship machine will change the instantaneous fuel consumption. For this reason, it is the aim of making the propeller more visible subject with a sample of dynamic balance disruptions originating from biofouling by compiling together with mathematical formulations of the concepts defined in the literature, in order to be the subject of discussions beyond the known ones.

Keywords: *Propeller Resistance, Biofouling, Fouling, Friction, Friction Coefficient, Fuel Economy, Emission, Reynolds, Ship Resistance, 3D Scanning, Kyrenia,*

ÖZET

Yakıt tüketim hacmi açısından deniz taşımacılığına yönelik tutumlara yön veren öncül bilimsel yaklaşımların ortak dayanağı hidrodinamik gemi kayıplarının azaltılması ya da ekonomik değeri yüksek, türlü yakıt atıklarının azaltılabilmesine, genel sevk kayıplarının azaltılması üzerine kurguludur. Diğer yandan pervane dirençlerinden doğan yüksek kayıpların azaltılması yönündeki düşüncelerse, optimum pervane tasarımlarının verimini olası biofoulingden görece ucuz, mekanik temizlik ve parlatma uygulamalarıyla geri kazanımı fikrinde ortaklaşmakla sınırlıdır.

Ortalamayı aşan bekleme sürelerinde yoğun gerçekleşen pervane biofoulinginin taxonomic sınıflandırılması ve gray-scale specturm analiz yöntemiyle yayılma hızı gibi etkinliklerini değerlendirebilmek, gerçek deniz ortamında deney yapmayı gerektiren bir konudur.

Girne Ticari Limanında, karakteristik pervane malzemeleri kullanılarak yapılan deneyde biyolojik oluşumların üç boyutlu (3D) yüzey topografyasının taranarak, metrolojik hesapların yapılabileceği, hızlandırılmış, özel bir bilgisayar ortamında yüzey pürüzlülüğüne bağlı sonuçlarını değerlendirmek bu çalışmanın temel kurgusudur. Elde edilen mikro ölçekli pürüzlülük verileri Musker's karakteristiği ve Rubert skalasıyla kıyaslanıp sonuçların gerçek bir gemi makinesinin anlık yakıt tüketimini değiştireceği yönündeki hipotezinde tahlil ederek, artmış emisyon değerleri gibi makro sonuçlara erişebilmenin olanaklı kılınması sonuç odaklı perspektifin ifadesidir. Bu nedenle araştırmanın bilinenlerin ötesinde tartışmalara konu edinilebilmesi için gemilerde direnç oluşturan, literatürde tanımlı kavramların matematiksel formülasyonlarıyla birlikte derlenerek bio-fouling kaynaklı olası dinamik balans bozuklukları gibi bir örneğe yönelik örnermeyle pervaneyi kayıp öznesi olarak görünür kılmak hedeflenmiştir.

Anahtar Kelimeler: *Pervane Direnci, Biofouling, Fouling, Sürtünme, Sürtünme Katsayısı, Yakıt Ekonomisi, Emisyon, Reynolds, Gemi Direnci, 3D Tarama, Girne*

TABLE OF CONTENTS

LIST OF FIGURES

XII

LIST OF TABLES

ABBREVIATIONS USED

A Wetted surface area, thin ship theory (m$_2$)

$A0$ Propeller disc area [π D2/4]

AD Propeller developed blade area ratio, or developed blade area (m$_2$)

AE Propeller expanded blade area ratio

AHR Average hull roughness

AP Projected bottom planing area of planing hull (m2) or projected

area of propeller blade (m$_2$)

AT Transverse frontal area of hull and superstructure above water (m$_2$)

AX Midship section area (m$_2$)

A_{VL} Longitudinal Area of the Vessel (m$_2$)

A_{VT} Transverse Area of the Vessel (m$_2$)

B Breadth of monohull or overall breadth of catamaran (m)

BAR Blade area ratio

Bpa Mean breadth over chines [= AP/LP] (m)

Bpx Maximum breadth over chines (m)

BWL Breadth on waterline (m)

c Section chord (m)

C_A Model-ship correlation allowance coefficient

C_B	Block coefficient
CD_{air}	Coefficient of air resistance [R_{air}/1/2ρa ATV2]
Cf	Local coefficient of frictional resistance
C_F	Coefficient of frictional resistance [R_F /1/2ρW SV2]
C_L	Lift coefficient
C_M	Midship coefficient [AX/(B × T)]
C_P	Prismatic coefficient [∇/(L× AX)] or pressure coefficient
C_R	Coefficient of residuary resistance [RR/1/2ρSV2]
C_S	Wetted surface coefficient [S/√∇ · L]
C_T	Coefficient of total resistance [RT/1/2ρSV2]
C_V	Coefficient of viscous resistance [RV/1/2ρSV2]
C_N	Moment Coefficient
C_x	Resistance Coefficient
C_W	Coefficient of wave resistance [RW/1/2ρSV2]
C_{WP}	Coefficient of wave pattern resistance [RWP/1/2ρSV2]
D	Propeller diameter (m)
D_{APP}	Appendage resistance (N)
D_F	Planing hull frictional resistance, parallel to keel (N)
E	Energy in wave front
$EEDI$	Energy Efficiency Index

EU	European Union
F_H	Hydrostatic pressure acting at centre of pressure of planing hull
F_P	Pressure force over wetted surface of planing hull (N)
Fr	Froude number [V/ $\sqrt{g \cdot L}$]
Frh	Depth Froude number [V/ $\sqrt{g \cdot h}$]
Fr∇	Volume Froude number [V/ $g \cdot \nabla 1/3$]
g	Acceleration due to gravity (m/s2)
G	Gap between catamaran hulls (m)
GM	Metacentric height (m)
h	Water depth (m)
H	Wave height (m)
HT	Transom immersion (m)
HFO	Heavy fuel oil
IMO	International Maritime Organization
ITTC	International Tank Towing Conference
iE	Half angle of entrance of waterline (deg.), see also 1/ 2 αE
J	Propeller advance coefficient (VA/nD)
k	Wave number
KT	Propeller thrust coefficient (T/ρn2D4)
KQ	Propeller torque coefficient Q/ρn2D5)

L	Length of ship (m)
L_{APP}	Appendage lift (N)
LBP	Length of ship between perpendiculars (m)
lc	Wetted length of chine, planing craft (m)
LCB	Longitudinal centre of buoyancy (%L forward or aft of amidships)
LCG	Longitudinal centre of gravity (%L forward or aft of amidships)
LCV	Lower calorific value of fuel
Lf	Length of ship (m)
lK	Wetted length of keel, planing craft (m)
lm	Mean wetted length, planing craft [= (lK + lc)/2]
LOA	Length of ship overall (m)
lp	Distance of centre of pressure from transom (planing craft)(m)
LP	Projected chine length of planing hull (m)
LPS	Length between pressure sources
LWL	Length on loaded waterline (m)
L/∇	1/3 Length–displacement ratio
$MARPOL$	Convention for the Prevention of Pollution from Ships
MDO	Marine Diesel Oil
MGO	Marine Gas Oil
n	Propeller rate of revolution (rps)

N	Propeller rate of revolution (rpm)
P	Propeller pitch (m) or Power (kw)
P_{ATM}	Atmospheric pressure (N/m2)
P/D	Propeller pitch ratio
P_D	Delivered power (kw)
P_E/P_{eff}	Effective power (kw)
P_L	Local pressure (N/m2)
P_S	Installed power (kW)
P_V	Vapour pressure (N/m2)
Q	Propeller torque (Nm)
R	Resistance (kN)
R_{air}	Air resistance (N)
R_{app}	Appendage resistance (N)
Re	Reynolds Number ($\rho VL/\mu$ or VL/ν)
R_F	Frictional resistance (N)
R_{Fh}	Frictional resistance of yacht hull (N)
R_{Ind}	Induced resistance of yacht (N)
rps	Revolutions per second
rpm	Revolutions per minute
R_R	Residuary resistance (N)

R_T Total hull resistance (N)

RV Viscous resistance (N)

RW Wave resistance (N)

RWP Wave pattern resistance (N)

S Wetted surface area (m2)

$SAPP$ Wetted area of appendage (m2) between catamaran demi-hull centre-lines (m)

sfc Specific fuel consumption (kg/kw.hr)

SLR Hull/Length ratio

SP Propeller/hull interaction on planing craft (N)

t Thrust deduction factor, or thickness of section (m)

T Draught (m), or propeller thrust (N), or wave period (secs)

T_{tq} Torque (N)

$TRNC$ Turkish Republic of Northern Cyprus

U Speed (m/s)

U_a Axial induced velocity (m/s)

U_r Radial induced velocity (m/s)

U_t Tangential induced velocity (m/s)

U_{aii} Axial Self-induced velocity for the i[th] component (m/s)

U_{aij} Axial velocity induced by the j[th]component on the i[th]component (m/s)

U_{tii} Tangential self-induced velocity for the i[th]component (m/s)

U_{tij}	Tangential velocity şbduced by the jthcomponent on the ithcomponent (m/s)
V	Speed (Knots or m/s)
Va	Wake speed (VS(1 − wT)) (m/s)
VA	Relative or apparent wind velocity (m/s) or Axial inflow velocity
V_{FC}	Volumetric fuel consumption/Fuel mass flow
VK	Ship speed (knots)
Lf	Speed length ratio (knots and feet)
V_R	Reference velocity (m/s)
V_p	Fuel volume
VS	Ship speed (m/s)
V_t	Tangential inflow velocity
W	Channel width (m)
wT	Wake fraction
$w_c\,(X_R)$	Circumferential mean wake fraction
w_T	Propeller effective wake fraction
w_v	Volumetric mean wake fraction
$w_x\,(X_R)$	Local wake fraction
WSA	Wetted surface area (m$_2$)
X	Longitudinal Wind Force
X_R	Non-Dimensional radius measured from the shaft axis

Y	Transverse Wind Force
Z	Number of blades of propeller
$(1+k_1)$	Form-factor, monohull
$(1+k_2)$	Tentative Form Factors

β Viscous resistance interference factor, or appendage scaling factor, or deadrise angle of planing hull (deg.) or angle of relative or apparent wind (deg.)

δ	Boundary layer thickness (m)
$\varGamma_p$	Fuel specific gravity
ε	Angle of propeller thrust line to heel (deg.)
ηD	Propulsive coefficient ($\eta 0 \eta H \eta R$)
ηO	Open water efficiency ($JKT/2\pi KQ$)
ηH	Hull efficiency $(1-t)/(1-wT)$
ηR	Relative rotative efficiency
ηT	Transmission efficiency
γ	Surface tension (N/m), or wave height decay coefficient or wave number
φ	Heel angle (deg.), or hydrodynamic pitch angle (deg.)
λ	Leeway angle (deg.)
μ	Dynamic viscosity (g/ms)
ν	Kinematic viscosity (μ/ρ) (m_2/s)
ρ	Density of water (kg/m_3)

ρa	Density of air (kg/m$_3$)
σ	Cavitation number, or source strength, or allowable stress (N/m$_2$)
τ	Wave resistance interference factor or trim angle of planing hull (deg.)
τc	Thrust/unit area, cavitation (N/m$_2$)
τR	Residuary resistance interference factor (monohull resistance)
τW	Surface or wall shear stress (N/m$_2$)
θ	Wave angle (deg.)
ζ	Wave elevation (m)
∇	Ship displacement volume (m$_3$)
Γ	Circulation
ω	Angular velocity (m/s)
λ	Lagrange multiplier

1. INTRODUCTION

The phenomenon of motion actually requires an irreversible energy consumption during movement from the stationary state to its current form and operates the reversible mechanism that slows down or tends to stop this motion with resistance factors as all of the objects.

In the earlier periods of world history, the multidimensional key points of the resistance mechanism have gained importance with the motivations to define the concepts first, then to relatively facilitate the produced work or to remove the obstacles.

However, right after the industrial revolution, consumption has started to occur much faster than the pervious demand and turned this motivation into a direct attitude towards the prevention of losses in the hands of those power and energy holders. In fact, the definition of motion scientifically includes a relativity concept has been redefined extensively in terms of being measured and prevented beyond all other conceptual definitions.

Today, even in experiments on nano-physics, the targets are not different from seeking answers to countless questions that remain unsolved in all current energy concepts. In essence, all world policies do not change and by constantly producing their own new nutrition cells, they destroy the world's seemingly infinite resources during this production by damaging them in unsustainable ways. In this sense, the question of whether resistance actually needs to be prevented is definitely the subject of another philosophical discussion.

From heat to vibration or acoustics, the basic loss issues of mechanical engineering become a complicated concept that can be defined as friction and friction losses when it comes to movement. Beyond the friction that takes place in the dry environment, there is a reversible

force is struggled in all the definitions that start or continue the movement in viscous environments.

Infact the ships that carry all the commodities of the "consuming world", where place of productional or consumptional facilities repeatedly, again thought with all her losses in a complex micro world sample.

Ships that provide movement with hydromechanical phenomena where almost any energy consumption has occurred, from hull friction resistors to wave or aerodynamic to electrical losses, and still able to serve with fossil fuels. Every ship that can fulfill the bouyancy condition is designed to be delicate but also durable so that it can survive bouyancy and its propulsion system.

In this study, overall hull efficiency will be described as conceptual only, but propeller will be explained with all details in literature to improve a multidirectional approach.

The definitions will start primarily from friction, because the resistances exposed at the point of contact with the perfectly designed viscous environment, with their losses and under major effects will be tried to be evaluated as much as on early stages. Hull resistance losses, which are frequently encountered in terms of the results it causes in the literature, are relatively less about ship propellers. In terms of strength, the propeller, which is perhaps the most durable part of the ship, can actually take control of the most robust part in a way that makes it ineffective when the micron-sized marine species that have developed a new life cycle on it started the vital growth process.

In addition to the energy losses that will arise, it can mechanically disrupt its functions and break a key ring such as ship transportation, leaving it out of efficient functionality. The biofouling process of such importance in terms of hydrodynamic movement capability for ships with large fuel expenditures and emission values, of course, may seem complicated in terms of the results of the evolutionary process of the micro-biological species of geographically

dependent and physically active components, but can be complex and enigmatic with their results.

In addition to all these, it is been aimed to make the natural bonds between the propeller, which is an inorganic substance, and the constantly renewed biological universe understandable.

In order to make this study on 15.06.2018, 5 pieces of test materials that produced from commonly used propeller alloys installed vertically and 1m.distance to each other via synthetic ropes which is electrically non-conductive to the position $35^020'35"$N-$33^019'55"$E in Port of Kyrenia, TRNC. The ropes, which will keep the parts in their position, are fixed to a buoy located to the sea surface and attached to pier on top, fixed to a eye-ring on the submerged concrete block at the bottom of the pier to keep the parts in a fixed position.

During experimental period, submerged parts daily surface control applied to the part against to risks of position changing, abnormal wave or currents caused by the vessel traffic or similar aspects that could happen. Sea-bed or any environmental natural index were not changed on installation of in the period of experiment.

Port of Kyrenia is the 2nd largest commercial port of Turkish republic of Northern Northern Cyprus (TRNC). Port of Kyrenia is a port that is capable of handling of crowded shipping traffic as technically but generally calm with routine intensity as shipping traffic because of un-named embargo. Position of the experimental installation is the berth of training and research vessels of Maritime Studies of University of Kyrenia.

Northern Cyprus is located at the climate zone called 'semi-arid' according to macro classification. Since it is located on a Mediterranean island Mediterranean climate is seen where summer is hot and dry and winter is mild and rainy. The average maximum temperature lies around 19.0°C. The warmest month of the year is July. During this month, the air

temperature lies between 37.0 ° C and 40.0 ° C during the daytime (in the shade). The coldest month of the year is usually January and daytime temperatures range from 9.0 ° C to 12.0 ° C, and the coldest nights of the year are mostly experienced during this month. In Northern Cyprus most of the rainfall occurs in October - March period where the annual precipitation is 402.8 mm (1941-1970).n The wettest month with the highest rainfall is December, and the driest months are July and August. In Northern Cyprus, which is an island country, the wind generally blows in different ways according to the topographical features of the regions. However, the dominant direction of the wind throughout Northern Cyprus is the West (W). The average annual wind speed is 2.8 m / sec. d. In Northern Cyprus where there is plenty of solar energy due to its latitude degree it is located, during the summer months it is sunny 12 hours a day. The average number of hours of sunshine per winter day is almost 5. The average daily amount of solar energy throughout the year is 417.3 cal / cm^2. The maximum amount of solar energy is 622.2 cal / cm^2 per day in July. The lowest daily amount of solar energy is 214.5 cal / cm^2 in December. The average sea temperature in TRNC is 21.3 ° C. The months when sea water is the highest temperature is in July and August. The months with the highest average sea temperature is July and August (around 27.0 - 28.0 ° C) [171].

2. LITERATURE REVIEW

2.1 Motion and Resistance

"Corpus omne perseverare in statu suo quiescendi vel movendi uniformiter in directum, nisi quatenus a viribus impressis cogitur statum illum mutare" [1].

Everybody persists in its state of being at rest or of moving uniformly straight forward, except insofar as it is compelled to change its state by force impressed [2].

This definition of Newton's first law and classical mechanics teaches a sentence describes motion exactly in Newton's second law when its concentrate on the use of quantifying devices at the far behind of a philosophical approach where stayed much more far beyond the quantum mechanics. Newton's second law calls "If a force generates a motion, a double force will generate double the motion, a triple force triple the motion, whether that force is impressed altogether and at once, or gradually and successively. The motion (being always directed the same way with the generating force), where the body moved before, is added to or subtracted from the former motion, according to they directly conspire with or directly contrary to each other; or obliquely joined, when they are oblique, to produce a new motion compounded from the determination of both" [3].

Since Archimedes, all the forces based on all impacts over a buoyant substance could have been declared according to Newton's second law. " Ships generally move with a mean forward velocity and their oscillatory motions in waves are superposed upon a steady flow field" [4]. It's always much easy to describe "breaking horsepower concept" while describing resistance as the opposite vectorial resultant of total forces or stated obstacles which are effective for an object that at the starting of a motion or an acceleration in linear space or the

ocean, in the marine engineering lectures to define engine power output transferred through a propulsor.

Pitching, rolling, heaving, surging, yawing and swaying or a combination of those dynamic reflections are called possible movements of a ship. William Froude realized that the ship resistance problem had to be broken into two separate and about manners residuary. Resistance relates to wave-making resistance and the frictional resistance were the basic definitions in his frictional drag test models processed in a viscous environment in 1873. All his experiments have been started with a series of a plate towed in bath bowl. According to Froude's definitions of frictional resistance, such an effect could be higher for high-speed crafts and it might reach approximately half of the total resistance moreover, it could be the highest resistive effect for slower ship designs.

In William Froude experiment, with 3980 mt. / M/S Merkara, surface friction between 5 to 8 Knots was 92% of ship's entire resistance effective on the mathematical model. At the same time, the smallest skin area brought the smallest resistance [5]. The following experiments pointed him back to basic frictional resistance experiments, done about pipes, ventures and elbowed objects to define eddy-making resistance. But in all pilot exercises had been eliminated from water friction calculations up to the ship's model test case II and case IV. Case II was about a plane moving edgeways through frictional fluid and Case IV about a submerged body moving through a frictional fluid. Surface friction has been taken into consideration more accurately. The tail-end of the vessel has been correlated in the factor of pressure, the intent of forwarding pressure and the eddy-making brake effect as physically. Other than the liquid mass flow conceptual impacts, liquid formal relative equilibrium was a spot effect on the plane surface particulars as hydrodynamically. This concept, in fluid mechanics, has based on D'lambert's [9] Paradox discussions after fifty years later. According to D'Alambert's post-subject was about border layers of a liquid unit. When the border layers

on the bodies are observed with more advanced systems, it is found here that the non-condensation is very effective due to the border conditions. Even if the boundary layer was thin, the drag forces could be very large because the forces were applied to the surface. It is also strong here that the flow for the long bodies separates the flow and creates very low-pressure areas in the back region, such as rotations, the turbulence which might be precisely modelable effects. This modeled approach has been a source for G.G. Stokes [10] to work beyond the workings of fluid dynamics to produce basic formulas that will direct the ship engineer to associate body and water resistance.

The calculations for defining and calculating the friction originating from total flow resistance have been transformed into equations with the support of C.L.Navier [11] and used to calculate the water friction and allow the formulation of equations that can be used for all fluids beyond conceptual. But for dynamic objects, it is still used correctly and the application was made by Reynold [12] and has become the coefficients of Reynolds, which is called Reyolds number, for ship's hull formations additionally.

"Any roughness of the surface will increase the frictional resistance appreciably over that of a smooth surface, and with subsequent corrosion and fouling still greater increases will occur. Not only does the nature of the surface affect the drag, but the wake and propulsive performance are also changed." [8].

Nowadays, drag resistance deductions on a vessel hull surface are a major subject for the researchers to improve hull performance. There are several experiments are in use to perform analysis of outer hull welding edges. "Contribution of welding seams to ship skin friction could very well be less significant than those of FCCs when the welding seam height is below 5 mm, a representative value for full-scale welding seam height" [7].

2.2 Roughness and Friction

Definition of the outer surface with surrounding the boundary surface in the solid-state of material as the surface without considering the detailed explanations of material science. However, this definition may cause an incomplete approach, which necessitates neglecting the factors that constitute the surface phase and the factors that degrade the surface phase. Therefore, a more sophisticated approach to defining surface engineering from applied sciences applies and approximates the definitions as follows: Solids are composed of bulk material covered by a surface. The surface which bounds the bulk material is called the surface phase. It acts as an interface to the surrounding environment. The bulk material in a solid is called the bulk phase. This interaction can degrade the surface phase over time. "Environmental degradation" of the surface phase over time can be caused by wear, corrosion, fatigue, and creep [13].

A Surface that forms the ideal theoretical form that has the ideal outer surface under the microscopic vectorial plane may have breaks distorts, distorts creatures to bring even the smallest vector direction difference may be called roughness. Smooth surface identification can be appllicable when the deviation from the surface theoretical form is undetermined or unrecognizable at the unit surface based on the total sampling length or area metrology. But on the other hand, if the total surface area shows large differences, break-outs in the direction of the vector, the surface called rough.

In etymology dictionaries, like an Ancient Greek and Ancient Rome term of topology has been used in different bigger scaled land metrology. "The first areal surface texture measuring instruments were made available around 1987. Instrument manufacturers such as Zygo, Wyko and others started to provide parameters calculated in a group of datas" [14]. Topographic applications have been used for military mapping and geological survey facilities mostly in the 19'th century. But in the 20'th century, it becomes more generic even in the

micro-surface analysis such as neurology in medical terms. Since the 1940's together with the improvement of automotive sector achievements, it became an obligation to improve a global system to define the International Roughness Index (IRI). Since the supports World's Bank supports in the 1970s, researches has become more popular and in the early 1980s, the highway engineering community-identified road roughness as the primary indicator of the utility of a highway network to road users. However, existing methods used to characterize roughness were not reproducible by different agencies using different measuring equipment and methods [15].

The surface finish may be measured in two ways: contact and non-contact methods. Contact methods involve dragging a measurement stylus across the surface; these instruments are called profilometers. Non-contact methods include interferometry, digital holography, confocal microscopy, focus variation, structured light, electrical capacitance, electron microscopy, and photogrammetry. Technical friction concept is one of the mesauremental subject in the field of science. It may be useful to strengthen the concept design of tribologic expressions by constructing this definition of friction in the field of applied sciences. Creation of a lubricating oil or development of the frictionless environment is the subject of tribology. Tribology covers topics and applications related to the movement of surfaces in interaction with interdisciplinary science and technology. Tribology includes physics, chemistry, solid mechanics, heat transfer, material science, lubrication science, reliability and performance science [16].

"One often thinks that Tribology, which concerns lubrication, friction, and wears, is born with the industrial development of the 19th and 20th centuries. None of that. From time beginning human beings have looked for reducing friction and avoiding wear. From antiquity (more than 2000 years before Jesus Christ) bitumen was used for diminishing the friction of the pottery wheel pivot, Egyptian "bas-reliefs" before Jesus Christ shows the use of lubricant

for facilitating the displacement of heavy loads. Meantime, generally there is an ignorance that Romans had invented the thrust ball bearing. Much closerly, Leonard de Vinci, well known for his painting and sculpture, was also a remarkable mathematician, whose works on friction, machines, and mechanisms were used more than two centuries after his death" [17].

Since there is a need for energy for the movement of objects, it is desirable for many engineering applications to have no friction forces, but to be minimal. Because there is a slight roughness among the objects made of all materials. An example is a piston moving in the cylinder block, the fluid flowing in the channel and the air movement of the bullet core. In some cases, it is attempted to utilize frictional forces such as brakes, clutch discs, belt pulley mechanisms, and cams. On the other hand, both the movement and stability of the car depending on its frictional forces. It is also possible for a person to walk and to stop utilizing friction forces. From this point of view, it is necessary to maximize and minimize these forces. Friction losses occur as heat energy between objects sliding on each other. The wear of friction objects is another indication of lost energy.

Tribology theories were based on relations and laws of Robert Hook's rolling friction in 1680 and shortly thereafter the definition of the viscosity Isaac Newton sourced from the friction of the fluids in the viscous environment. On the other hand, Guillaume Amontons approached Leonardo Da Vinci's friction laws in 1699 and a hundred years later, Charles Augustin Colomb proved these laws certainly. But it should not miss out on the coefficient of friction was analytically defined by Leonard Euler in 1750. In 1825, George Rennie began to define lubricant abilities by calculating friction coefficients for different materials by performing friction and wear measurements in the tribology field. Viscosity definitions of Claused Loui Navier allowed foundations of the hydrodynamic theory of George Gabriel Stokes and Navier in the fundamental theme of this study, directly. While Osborne Reynolds

was working on the hydrodynamic pressure equations, the friction approach of mechanical engineering was acquired a new theoretical aspect [18].

Friction is a force acting opposite to the direction of relative motion. Friction rises on the interface between bodies, but may also develop within the body. Examples of the latter include air and hydrodynamic friction, where the friction rises between the fluid layers. Friction is not a fundamental force, but rather a manifestation of electromagnetic and gravity forces. The friction that occurs up to the threshold of motion is called 'static,' and the friction that occurs after motion starts is called 'kinetic' friction. The magnitude of the static friction force is variable, and at any stage, the body equals the horizontal force applied at that moment.

The sources of tribology talk about static friction and kinetic friction as well as rolling friction. For example, at the moment when a car wheel 'slippery' turns, the lowest point of the tire is in contact with a spot on the ground. The contact of those points with the very short drapery; entire friction force between the wheel and the ground is concentrated on these two points while being tilted backward at the same speed when viewed from the center of the wheel, it is motionless when viewed from the ground. Since the points are not in motion concerning each other, this is a static frictional force and if the force threshold value has not been reached, then the magnitude can not be calculated from normal forces and the dynamic equations of the system must be written and solved. But the important thing is that; since the dots are not moving against each other, there were no any work was against this frictional force. Therefore, theoretically, during this 'rolling over', there should be no loss of energy due to friction. However, tires that are not ideal materials due to their elasticity are deformed as long as they are rolled, and they are also subject to plastic shape changes in part. The energy absorbed by this inelastic component of the shape change is irreversible and is converted into heat. On the other hand, there are some frictional losses in the wheel axis due to the friction of the metal to

11

the metal. As a result; a third for the account of these losses; friction coefficient of rolling without slip is defined.

If the coefficient of friction or the frictional force from the square is too small, it can be assumed that the objects are smooth by simplification. The irregularities of the recesses and protrusions show that the actual contact surfaces of the objects are much less. In other words, the frictional force is independent of the contact area. The friction force generated between the objects that are forced to move relative to each other is parallel to the contact surfaces and the direction of motion is opposite to the direction of the action. If there is no effect on the formation of the relative motion, the friction force can not be mentioned.

2.3 Ship's Motional Energy and Losses

Shipping is the world's largest logistic method which is known and accepted that more than 90 percent of global trade is carried by sea, nowadays. Throughout the last century, the shipping industry has seen a general trend of increases in total trade volume. Increasing industrialization and the liberalization of national economies have fuelled free-trade and growing demand for consumer products. Advances in technology have also made shipping an increasingly efficient and a swift method of transportation. Because of its importance "Ships are expected to meet their design speeds and the propulsion units can only deliver the ship speed element provided all other related factors are also in place. Such elements growth, corrosion or damage to the hull will clearly affect overall performance" [19].

In shipping literature, most of the sources about the development of propellers indicate that, inventor Joseph Ressel in 1826 was the first to use propeller for ship propulsion since Archimedes's Screw and Leonardo Da Vinci's drawings of the helicopters. The boat propeller had multiple blades made out of bronze that were fastened around a conical base and was installed on a small boat that was manually driven. Moreover, in 1839, the first steam-powered

propeller system has been designed and installed to vessel "SS Archimedes" by developed accidentally by Francis Pettit Smith. In 1845, early in the history of steam navigation, the effectiveness of the screw propeller was established when the steam sloop Rattler, equipped with such a propeller, towed the steam sloop. Alecto, equipped with paddle wheels, stern first at a speed of nearly three knots in a tug-of-war staged by the British Admiralty [20].

Propulsion represents the main source of energy consumption, as it accounts for 68% of the annual ship energy demand. This also translates into the main engines consuming the largest share of the overall energy input of the system (87,9 %). Hence, efforts directed towards the reduction of propulsive power are highly justified for the ship under study [21].

Studies point that main propulsive energy production remains 16-20 percent defined loss of energy for a marine Merchant vessel. The main propulsion engine power output is about 90 percent of total power production on board according to the Sankey diagram on Figure 2.3.1 left and the difference of used energy potential is getting lost according to Grassman Diagram on Figure 2.3.2. Combined efficient description of the details is the available data included in Table 2.3.1. On the other hand,it is widely visible to see energy losses categorized according to selected vessels as an example below and the following table 2.3.2

Table 2.3.1: Summary of Input and Output Exergy Flow [21]

Summary of Input Exergy Flows.			
Input flow	Flow type	$\dot{B}\left[\dfrac{TJ}{year}\right]$	$\dot{B}\left[\%_{in,tot}\right]$
Fuel to MEs	Chemical	199.6	87.9
Fuel to AEs	Chemical	18.1	8.0
Fuel to Boilers	Chemical	9.3	4.1

B : Produced/available energy to be used

Summary of Output Exergy Flows.			
Output flow	Flow type	$\dot{B}\left[\dfrac{TJ}{year}\right]$	$\dot{B}\left[\%_{in,tot}\right]$
Propulsion	Work	67.6	69.0
Tank cleaning	Heat	0.9	0.9
Fuel heating	Heat	0.7	0.7
Hotel facilities	Heat	0.9	0.9
Nitrogen compressors	Electricity	2.1	2.1
Cargo pumps	Electricity	0.8	0.8
HVAC	Electricity	1.8	1.8
Engine room	Electricity	1.5	1.5
Boiler auxiliaries	Electricity	2.7	2.8
Miscellaneous	Electricity	2.6	2.7
Exhaust gas (ME)	Waste heat	13.8	14.1
Exhaust gas (AE)	Waste heat	1.9	1.9
Exhaust gas (AB)	Waste heat	0.2	0.2
Radiated heat (ME)	Waste heat	0.0	0.0
Sea water cooling	Waste heat	0.1	0.1
Shaft losses	Waste heat	0.2	0.2
SG losses	Waste heat	0.2	0.2

Table 2.3.2: Distribution of energy losses (%) in selected case ships. [22]

	Tanker/bulk		Container		General cargo		RoPax	
Speed (knots)	15.6	10.9	21.2	15.5	13.4	9.5	20.1	14.7
Bunker	100	100	100	100	100	100	100	100
Engine								
Exhaust	25.5	28.4	25.0	28.0	25.5	28.4	25.5	28.4
Shaft	49.3	45.4	50.5	46.5	49.3	45.4	49.3	45.4
Heat	25.2	26.2	24.5	25.5	25.2	26.2	25.2	26.2
Propulsion								
Propeller loss	16.3	14.3	15.6	13.0	19.7	15.3	15.5	14.4
Propulsion power	32.1	30.2	33.7	32.4	28.1	28.8	32.6	29.9
Transmission loss	1.0	0.9	1.3	1.2	1.5	1.4	1.2	1.1
Propeller								
Axial loss	6.3	5.3	4.8	3.5	8.8	5.6	4.8	4.3
Rotational loss	3.9	3.4	5.3	3.9	6.0	4.5	5.0	4.7
Frictional loss	6.0	5.7	5.5	5.6	4.9	5.2	5.7	5.4
Hull								
Wave generation	6.4	4.1	8.6	3.9	12.8	5.9	5.3	3.9
Air resistance	0.6	0.6	1.0	1.1	0.7	1.0	1.0	0.9
Hull friction	16.2	16.6	13.9	15.6	8.3	12.0	15.9	14.7
Residual resistance	2.7	1.9	1.8	1.4	2.8	3.2	2.2	1.4
Weather and waves	6.2	6.9	8.4	10.3	3.5	6.7	8.3	9.1

Identification of the energy requirements on ship specific approach consumptionel equipment factor is the another method based on power generation. In this preface, M.Yoshimura [22] categorization does not contain energy distributional datas on his approach in the table 2.3.2. Regarding to cargo equipment on quantity, tankers have widely higher number of the equipment in the shipping transportation. There two different look out and approaches on this manner to optimize energy critization.
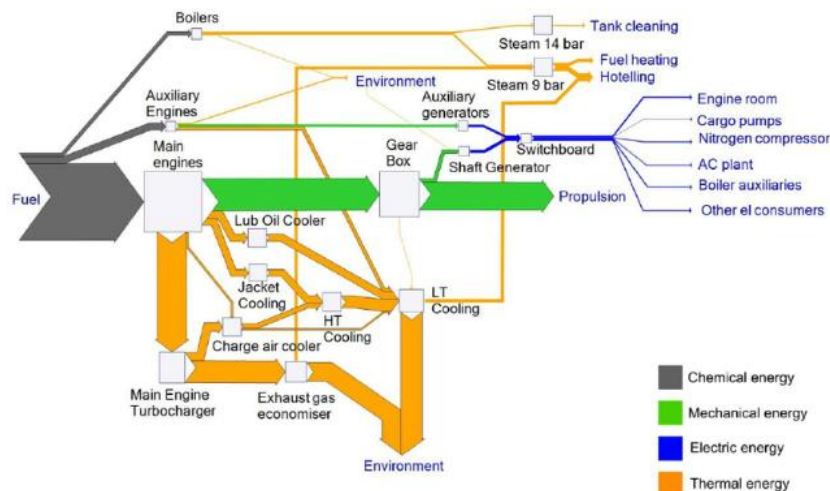
Figure 2.3.1: Sankey diagrahm of ship energy systems [21]
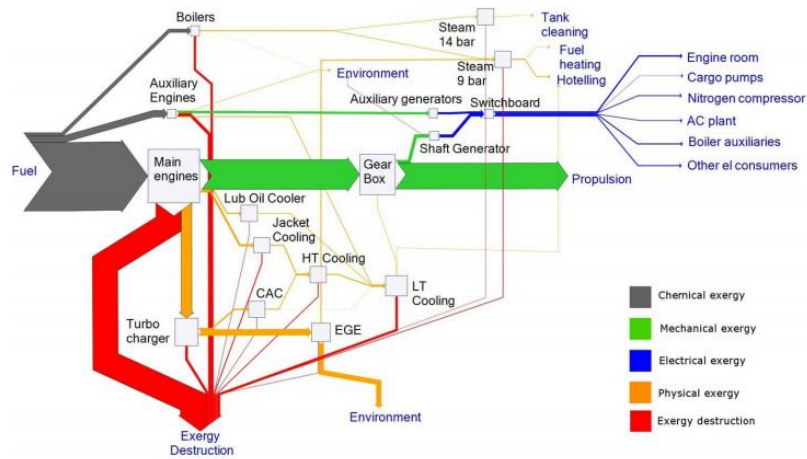
Figure 2.3.2: Grassman diagrahm of ship energy systems [21]

In these days, for a modern ship design efficiency, optimization criteria must include a multifunctional literal concepts: Squat limits, air-draft limits and wind resistance of superstructures, bow shape and block coefficient factors, aft-ship design, rudder blade design, draft and frictional effect, hull area, and water resistance, sea chest's effect, stability factors, cargo and load factors with allowable free board limits, constructional application failures, hull cleaning and pollutant factors, cavitation loss, propeller resistance, vibrational loss, shaft and propulsion system loss and several other variable oceanographic and meteorological substances. "For a successful manufacturing in a long run, a broad range of factors must be taken into account when products are designed and developed. Product manufacturing today requires skillful decision-making in scenarios that are more complex and demanding than ever before, and the use of optimized system technologies has become essential" [22].

There are different types of ships that are navigating in the world's trading fleet with different losses in connection with variables in the origin of use and operational possibilities, such as ship form, cruising speed. Fuel consumption and the environmental impacts which they produce also vary according to that significant. For example; in a comparison of tankers

15

and container vessels, the frictional losses from propellers are only about 7%, in a voyage with a similar speed with having equal propeller powers but hull-body friction varies by 15% between each other. However, when the same container ship starts sailing about one and a half times faster, body friction is reduced to 11% and propeller friction is reduced to only 2%. A similar example correlations is widely visible according to the case-study vessels of IMO, energy efficiency evaluation work groups by worldwide scientists and experts.

For a marine merchant vessel, there are different significant losses based upon a dynamic total in relation with the bunker consumption which is the most effective variable also in relation with Energy Efficiency Design Index (EEDI) may be described below simply:

* Heat loss, which exists always a derivative on mechanical and internal/external combustible machinery,

* Exhaust loss, where not in post-usage of internal combustion engines, transmission loss where used a shaft, gearbox, shaft bearings and stern-tubes with other related transfer mechanisms,

* Frictional loss, of ship's hull underwater, flying deck in the air and propellers,

* Rotational Loss, such as propeller cavitation, slip reductions, etc.

* Axial Loss, which is the relative interruption of waterline axis of the ship in sailing route in thrust segment

* Weather and waves

* Residual resistance such as biofouling and chemical fouling

* Hull resistance which is related with the motional performance of the ship's hull in a viscous environment

* Air resistance, which is the resistance effect of the superstructure and all other deck components above the waterline

* Wave generation that is self-produced waves of the ship's hull while in motion in a viscous environment

The potential for improvement in an area is related to the losses in the various areas. For instance, hull friction is an important area for tankers and bulk ships. Generally, propeller losses decrease at reduced speed while the proportion of frictional resistance increases relative to other losses. Thus Operating speed and operational direction may induct with an influence which areas constitute the larger loss areas. Naturally, the available space on deck and in machinery compartments, as well as weight/stability margins, may restrict the possibilities for installing additional equipment. Therefore, the possibility to use various techniques, the potential for improvement and the associated cost-effectiveness are very variable between ships and ship types [23].
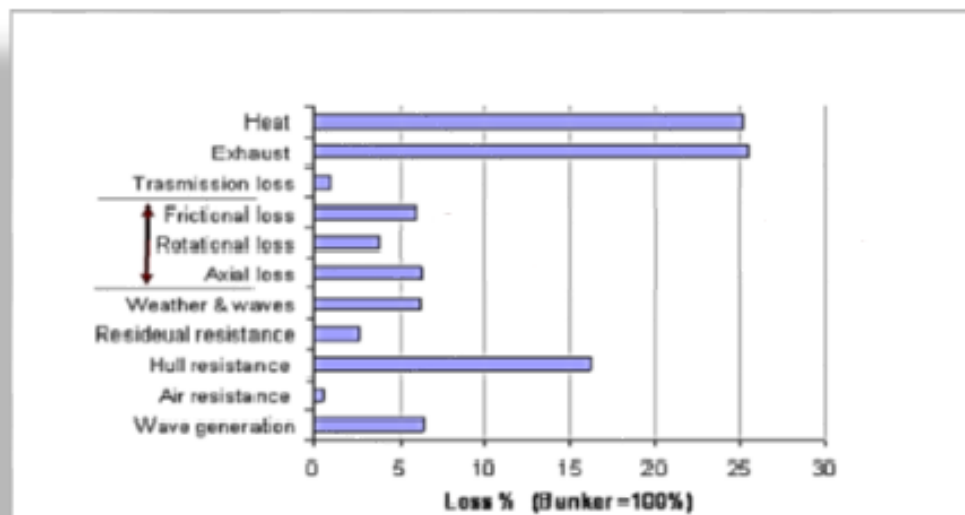
Figure 2.3.3: Fuel Consumption Loss- propulsive energy loss relation / Ref. [23]

Hull fouling will increase the frictional losses and reduce the speed that is attained at a given power. Propeller fouling will reduce the efficiency of the propeller. Engine fouling, wear and non-optimized balancing and adjustment will contribute to reduction of shaft power

and higher heat losses. Options to improve the ship principally aim to reduce these losses, while the aim of maintenance actions is to prevent these losses from increasing [23].
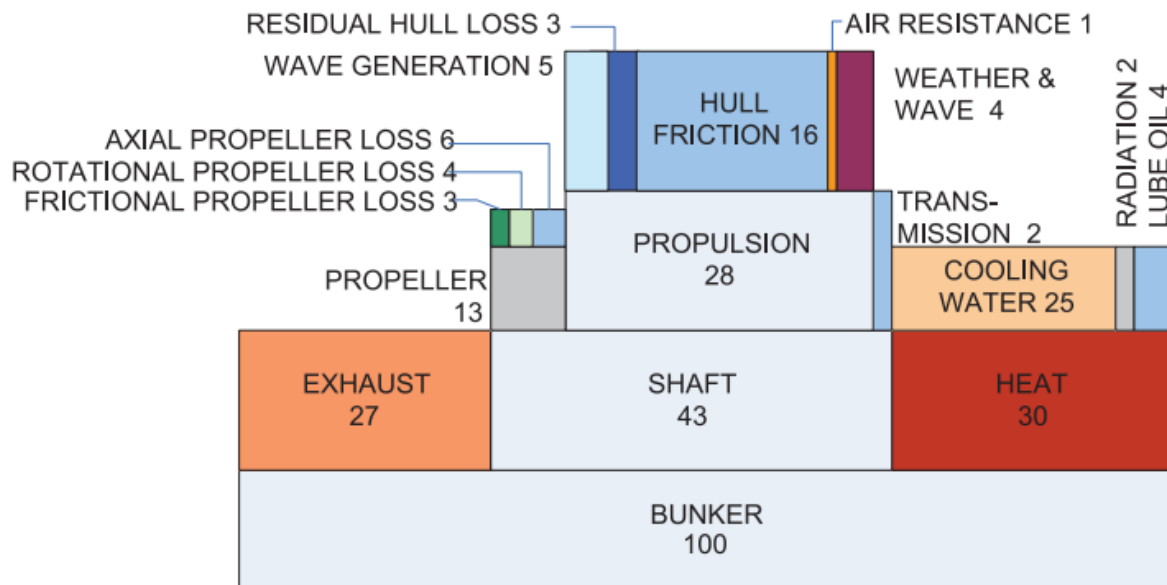
Figure 2.3.4 : Use of Propulsion energy on board a small cargo ship (ahead under, 6 Beaufort) / Ref. [23]

2.4 Ship Resistance

There are different approaches in the calculation of ship resistance in modern and traditional naval architectural literature. Classfication of these methods to 4 (four) common strategic styles since the invention of ships, such methods start based on standard hydrodynamic formulations and improved through the computerized estimations. On of the basic method, traditional and standard series formulations comprises strategies that are based on tests conducted by different researchers. It is more of a hypothetical approach than common sense, based on charts and perceptions by outstanding researchers within the field of naval architecture. On the other hand, direct model tests as a method, based on towing tank tests that are continuously developed and re-circulated by the conferences or special applications based on a specific design for the ship owners or shipbuilders. Moreover, the regression method of

ship resistance prediction based on statistical analysis has been a subject of some interest for several years. Beyond all these methods, modern computing facilitation that is based on computational fluid dynamics to multifunctional equations is one of the most critical solutions in ship resistance theory.

The issue of ship resistance, which has been dealt with many times in the literature with different methods, is being reconsidered again and again as a problem of economic crises that can change the perspectives of the world many times in a short period with elementary approaches to reduce energy losses wand necessitates more detailed evaluations. Without a doubt, propeller skin performance, as well as ship's hull performance, becomes a critical criterion stands in front. In addition to the economic penalty due to surface roughness, fouling results in detrimental results on the propulsive performance of the ship [6]. Based on the combination of these different methods that may assess all the resistance components of the efficiency of an entire ship, this study includes the factors that directly affect the propeller regime and its results, and other resistance factors will be only be included with their functional descriptions.

2.5 Ship Resistance's Definitions and Comprehensive Factors

Ship resistance is an analytic combinations of factores described in the following section. These factors will be used to explain general definitions of these concepts. In this study propeller roughness is the main variable. Its definitions will be explained with more details in further other sections.

2.5.1 Hull Resistance

As an outcome of traditional and standard series formulations and regression methods, the basic concepts developed by Reynolds and Froude have been used by researchers and naval architects to develop today's methods for calculating the power required to move a ship. On the other hand, as an observation of direct model tests method with computational fluid dynamics model, formulation of the recommended method by the International Towing Tank Conference to calculate the resistance of a full-scale ship is the ITTC Performance Prediction Method (ITTC 1978, ITTC 2011a)

$$C_{TS} = (1 + k)C_F + C_R + \Delta C_F + C_{AA} + C_A \qquad (1)$$

Before reflecting details of this common equation details, in regards of core variable hull Frictional coefficient "C_F" was used that more than hundred years, on wet surface friction, has been discussed and W. Froude's formulation was realized that "Hull Friction" varied with the wet surface and the square of speed (SV²) and mildly affected by length of the ship's hull called L_{OA}.

$$R = fSV^{1.825} \qquad (2)$$

where;

R : Resistance in kgs.

S : Surface in m²,

L : Length in m

V : Speed in knots as a simple formulation.

But on the other hand, according to the viscous/fluid mechanics theory, the viscosity may also be accepted as the resistance to flow or to shear within the fluids. So that frictional resistance can also be mentioned that a ratio of viscosity (ν) to surface length and speed. Core theory has been based on flow theory inside the laminar flow inside the pipes and founder of

the core formulation was done by Osborne Reynolds who conducted tests of liquids flowing through pipes of various diameters and lengths, at varying velocities and discovered that for each specific value of viscosity, $v \div (L \times V)$, the dynamic conditions were applicable and comparable. It's more essential to consider that reciprocal flow value that is known L V/v (layered length has velocity and viscosity comparison ratio) was assigned as "Reynolds Number" (Re) is listed in the special charts for more recent calculations of friction that is ratio of the inertial force to its viscous resistance and without any dimensions. Main formulation for frictional resistance is as similar though; namely, $R = C_f \times S \times V^2$ with a new coefficient of friction (C_f) now varying with the Reynolds Number, according to charts by various researchers. The graph most commonly accepted and followed today by research facilities worldwide is one by Schoenherr. The Resistance figures given by the much earlier Froude formula are still quite acceptable for smaller boats.

On the other hand, the size of the resistant body is also affected by identified another resistance model called wave-making resistance and confirms differences of the model/tank tests and real hull resistance differences. It's a thin boundary layer of viscous environment that is pulled along by the surface and the thickness of this layer increases as one moves aft. Within this layer, the water particles shear on one another so that the layer closest to the hull is 'pulled along' with hull speed, while the outside layer of this boundary does not move at all relative to the water adjacent to and outside of it.

On return our modern main equation explanatory basis of [27], the frictional resistance coefficient "C_F" of the ship is calculated using the ITTC 1957 model-ship correlation line:

$$C_F = \frac{0.075}{(\log_{10} R_{EL} - 2)^2} \tag{3}$$

This formulation was used for a period that basis on Hughes (1954) equation in the previous period:

$$C_F = \frac{0.067}{(\log_{10} R_n - 2)^2} \qquad (4)$$

The residual resistance coefficient "C_R" and the form factor $(1+k_1)$ can be determined using model tests defined by the ITTC standard procedure.

$$C_R = C_{TM} - (1+k_1)C_{FM} \qquad (5)$$

The air resistance coefficient of a full-scale ship "C_{AA}" is a function of the transverse projected area of the ship above the waterline "A_{VS}", wetted surface area "S" and the air resistance coefficient determined through wind tunnel tests "C_{DA}". The air resistance coefficient is determined through wind tunnel tests as a function of relative wind direction or taken as 0.8 as a default value (ITTC 2011a)

$$C_{AA} = C_{DA}\frac{r_A A_{VS}}{r_S S} \qquad (6)$$

The correlation allowance, "C_A", is used to account for all sources of discrepancy between the model and full-scale results. The ITTC (1990) recommended that the effect of coating roughness be separated from the correlation allowance with the modified equation for C_A:

$$C_A = (5,68 - 0,6\ Re_L)*10^{-3} \qquad (7)$$

Before writing $\mathit{\Delta}C_F$ variable where frictional resistance due to hull roughness and reaching an overall equation, it's essential to define other conceptual explanatory of the components as resistance factorials one by one.

2.5.2 Frictional Resistance

Concept can be explained as the resistance component obtained by adding to the direction of ship movement the tangential forces (shear stresses) formed on the wet surface of the ship due to the viscosity of water. The reason for friction resistance is viscosity and surface roughness. The frictional resistance can be calculated by

$$R_F = C_F \left(\frac{1}{2}\rho V^2\right) S \tag{8}$$

But Froude (1886) calculated the friction resistance with the following formula;

$$R_F = fSV^n \tag{9}$$

This is the equation where expressed at the beginning of this section as the W. Froude's (1886) equation which is recognized with extension in details:

$$R_F = \frac{\gamma \lambda_t}{1000} SV^{1.825} \tag{10}$$

Where "λ_t" in this formula;

$$\lambda_t = \left(0.1392 + \frac{0.258}{2.68+L}\right)[1 + 0.0043(15 - t)] \tag{11}$$

2.5.3 Pressure Resistance

The fore and aft components of the pressure force "*P*"acting on each element of the hull surface can be summed over the hull to produce a total pressure resistance. The frictional drag arises purely because of the viscosity, but the pressure drag is due in part to viscous effects and hull wave-making. An alternative physical breakdown of resistance considers energy dissipation. [28] With other wording pressure resistance is the part of the resistance with the integration of the normal stresses over the surface of a body in the direction of a certain movement.

According to the aforementioned disclosure, the pressure resistance is the resistance component obtained by the addition of normal stresses to the ship's movement direction on the wet surface of the vessel or in other words, pressure resistance is the component of the forces in the direction of the ship's movement that affect vertically to the surface of the ship.

2.5.4 Viscous Pressure Resistance(R_{vp}) and Viscous Resistance(R_v)

Due to the viscosity, friction occurs between the surface of the ship and the fluid and the boundary layer is formed and the pressure distributions around the ship change, creating a resistance component called viscous pressure resistance. A pressure increase occurs from the stem to the stern of the ship. With other wording, viscous pressure resistance is the force associated with the loss of energy in the formation of the vortex moving in the downstream direction. Viscous pressure resistance consists of the component of normal stresses caused by viscosity and turbulence in the direction of ship movement. This resistance cannot be measured directly, except for objects in water (equal to the pressure resistance). According to Hughes (1954), the viscous pressure resistance is calculated by multiplying the calculated friction resistance by a constant coefficient "*k*". This *k* value, which depends entirely on the ship form,

is called the *form factor*. It is assumed that the **k form factor** does not change according to the speed or scale of the ship. As a formulation for Hughes Method;

$$R_V = R_F + R_{VP} = (1 + k)R_F \text{ or } C_V = C_F + C_{VP} = (1 + k)C_F \tag{12}$$

or

$$1 + k = \frac{R_V}{R_F} = \frac{C_V}{C_F} \tag{13}$$

where $(1 + k)$ is a constant value for a given vessel form.

The form factor k, which indicates the friction resistance ratio of the viscous pressure resistance of the vessel, can be found in many ways. In some methods of finding total ship resistance, the k form factor is used. (ex. Hughes Method (1954)) Below are two more commonly used methods to find the form factor.

By using the form factor "k" using empirical formulas, If the ITTC 1957 formula is used to calculate the friction resistance coefficient of the ship and model, the following formula may be used to calculate :

$$k_{ITTC} = \frac{32.8C_B^2}{(L/B)^2(B/T)} - 0.03 \tag{14}$$

By using the most appropriate empirical formulas which are given for the " k " form factor, approximately one k form factor can be obtained by low Froude numbers in model tests. The waves and wave-making resistance of the ship moving at low Froude numbers are negligible. In such a case, the resistance of the vessel caused by the water is equal to the viscosity resistance caused by the viscosity. So the total resistance of the ship is equal to the viscosity resistance. This is the same for the model and its test. Once the friction resistance coefficient of the model is obtained, the "k"form factor can be found.

$$C_{Vm} = C_{Fm} + C_{VPm} = (1 + k)C_{Fm} \qquad (15)$$

$$k = \frac{C_{Vm}}{C_{Fm}} - 1 \qquad (16)$$

The "k"value found for the model is the same for the full-scale vessel and

$$k_s = k_m = k \qquad (17)$$

Viscous losses in a model will result in a change in momentum flow between the transverse planes in front and behind the vessel. This is called viscous resistance. It is referred to as wake resistance in some literature. Viscose resistance is a resistance component associated with the energy consumed due to its viscosity effect. The viscous resistance depends on the underwater geometry of the ship, the roughness, and the area of the ship's wet surface. As expressed in finding k form factor with the help of model tests in low Froude numbers, the waves and wave-making resistance of the ship moving at low Froude numbers are negligible. In such a case, the resistance of the vessel caused by the water is equal to the viscosity resistance caused by the viscosity. So the total resistance of the ship is equal to the viscosity resistance. $R_{Tm} = R_{Vm}$. There are many methods for finding viscous resistance like the determination of viscous resistance with the form factor formula $C_V = (1 + k)C_F$ proposed by Hughes while plotting the graph of $\frac{C_T}{C_F}$ the ratio of against to $\frac{F_n^4}{C_F}$ numbers as suggested by Raymon J. Prohaska (1987). However, the general formulas are as follows:

$$R_V = R_F + R_{VP} \qquad (18)$$

or

$$R_V = R_T - R_W \qquad (19)$$

2.5.5 Total Wave Resistance

Most of the researches has been devoted to the theoretical methods of calculating wave resistance. The methods can be divided into two groups:

Method A: The flow around the hull is determined and hence the normal pressure distribution. Then the fore- and aft components of these pressures over the hull surface are integrated.

Method B: The wave pattern generated by the ship a great distance astern is calculated. The wave resistance is then determined from the flow of energy necessary to maintain the wave system.

Method A was developed by Michell [29]. The object of Michell's work by using his own words "to give a general solution of the problem of the waves produced by a ship of given form moving with uniform velocity in an inviscid liquid and to determine the consequent wave-resistance to the motion of the ship. The only assumption made to the form of the ship is that the inclination of the tangent plane at any point of its surface to the vertical median plane is small.'' In his paper, Michell gives the wave resistance in the form of an integral that is called Michell's integral nowadays [29]. Michell's integral has been used many times to calculate the wave resistance. But it must be pointed out that these theoretical methods are based on the thin ship theory of wave resistance. The methods can, therefore, be unacceptable from a practical point of view and, in many cases, they yield estimates wrong by as much as 100% The improving of method A as well as method B has elucidated many wave-resistance problems.

The wave pattern analyses have led to the discovery of the additional drag component associated with wave-breaking and to a better understanding of the effect of the bulbous bow of full large ships at low Froude numbers. For such ships, the bulbous bow is effective in reducing the magnitude of the bow wave and thereby avoiding wave-breaking. In high-speed vessels, a bulbous bow promotes beneficial interference between waves generated at different points along the length of the hull. Thus the bulb reduces the wave resistance, and this reduction

can often be predicted by the use of one of the theoretical methods. It is very difficult to establish a theoretical method that can include nonlinear effects and effects of viscosity in the calculation of the wave resistance [30] .

$$D\overline{R_{AW}} = 2\int_0^\infty \frac{R_{AW}(w_e)}{x_0^2} SV(w_e)dw_e \qquad (20)$$

Where, $SV(w_e)$ is wave spectrum and x_a, significant wave height and w_e frequency.

2.5.6 Wave Making Resistance and Wave Pattern Resistance

Wave making resistance is the resistance component associated with the energy consumed by the generation of gravity waves, that is, surface waves. This component can be divided into two parts. The first wave pattern resistance is "**R_wP**" and the other is a wave breaking resistance "**R_wB**". *Wave pattern resistance* is the component of resistance derived from measurements of wave amplitudes that move away from the ship or model, assuming that the velocity field on the free water surface and therefore the momentum of the fluid can be associated with the wave-forms obtained by linear theory. The resistance thus obtained does not include wave breaking resistance. Wave breaking resistance is the resistance that occurs while the waves generated by the ship, especially bow waves, are broken. In general, the wave resistance means that the wave breaking resistance is neglected and only the wave-making resistance is considered. Wave makine resistance is related with the underwater surface of the vessel and vessel speed in all approaches. Froude number of the subject concept is:

$$F_R = \frac{V}{\sqrt{gL}} \qquad (21)$$

Concept is also related with the speed/lenght ratio of the vessel.

$$\frac{V}{\sqrt{L}} \qquad (22)$$

It is notable that where this ratio equals to "1" $F_R = 0,3$

2.5.7 Eddy-Making Resistance

Identifiable structures in a turbulent flow, particularly those that spin is called eddies. [31] An 'eddy' eludes precise definition, but it is conceived to be a turbulent motion, localized within a region of size l, that is at least moderately coherent over this region. The region occupied by a large eddy can also contain smaller eddies[32]. In the open water motion condition of a buoyant body with a certain speed, moves through the water, the frontal structure alters the flow around the vessel thereby reducing turbulence and the eddy effect. With the same effect, in a dynamic movement of the vessel, stem pressure reaches a maximum value and it reacts on a motion from the bow to the stern, up to a point where there is flow separation. That is the place where the flow separation and eddies emerge. Turbulent eddies are comparatively larger than the eddies formed elsewhere near the ship due to the hull motion. Hence, these eddies possess greater turbulent kinetic energy, the source being the kinetic energy of the ship itself. This causes a resistance to the hull dynamic motion in the water and called eddy making resistance.

Following flow separations on the ship streamlined surface will be generated and subject eddy making resistance will decrease the shipping speed. Eddy making resistance has another cost function to increase its effect with larger hull beams on larger bodies which increases both friction effectiveness and form resistance. Another consideration is the ship's streamlined body in a viscous environment. As long as there is any undulation on it, eddies by flow separation will be produced triggering the eddy-making resistance and finally slowing down the ship.

Depth of the water is an increasing factor for a limited eddy making resistance. Hydrodynamic motion eddies whirl around the ship and absorb its emotional potential energy. Design coefficients of the hull may another effective variable and weak models increase more

eddies. Thus, it becomes a definition that a smoother flow around the vessel will decrease eddy making capability.

While experimental studies of wave–structure interaction are usually timeconsuming and expensive, the large-eddy simulation (LES) is believed to be a useful tool for the early-stage design of water-surface vehicles [33].

On the other hand, the ship's propeller design results from the basis of a maximized pressure on propeller airfoil tip and decreases from noose to tail center of the propeller hub. Such effect acts with a vapor effect when it is compared with seawater pressure that may evaporate and may be formed in bubbles. This cavitation bubble being surrounded by high pressurized fluid flow implodes violently and forming a dent on the ship propeller. As the main pressure separation lead with flow separation and caused a resistance that distorts the ships propeller.
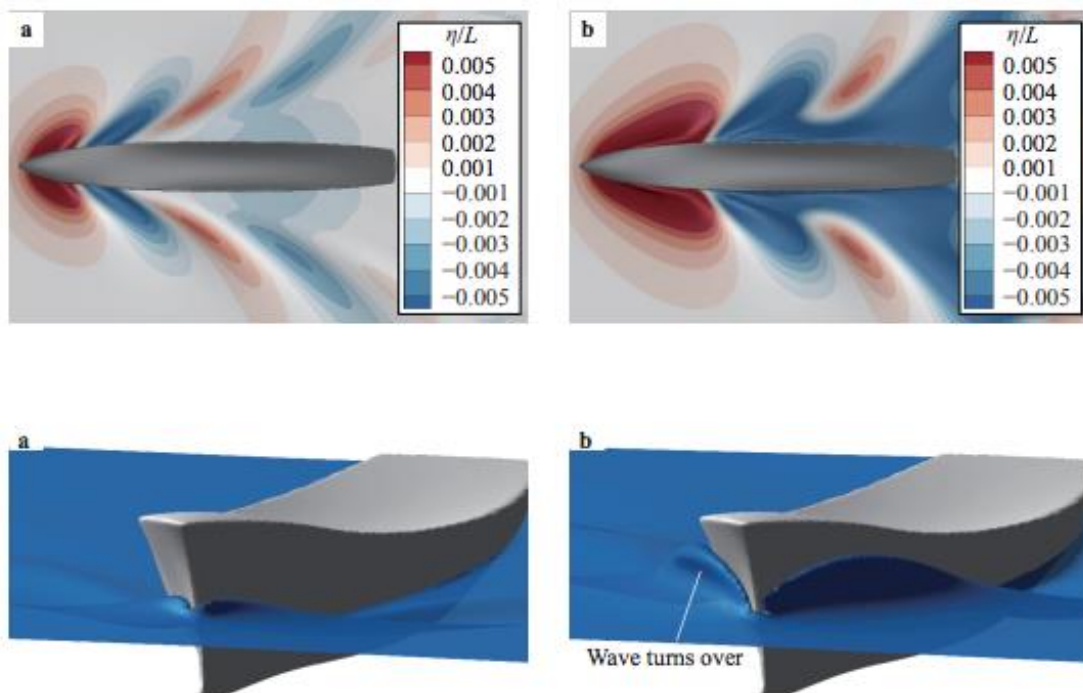
Figure 2.5.7.1: An Eddy-Making Resistance Experiment a) Bow wave at a *Fr* : 0,28 and b) *Fr* :0,67 cases [34]

2.5.8 Appendage Resistance

The appendage resistance concept points a determination out a harmonized result which is normally kept with general assumptions in terms of the results of theoretical and experimental studies about the resistance of ships. This context leads to the expression of most of the important other aspects of a design structure and constructional differences which does not in count only with limited perception. Needless to say, the inclusion of appendages will alter the resistance of the ship. The wet surface area of the appendages causes an increase in the total frictional drag. If the appendages have abrupt curvatures, the flow may separate and cause separation drag. Also, as the appendage modifies the flow around the hull it may affect propulsion performance [35] .

Resistance elementary examples: Rudders, skeg or thrusters as maneuvering aids of a ship, fins, and stabilizers as motion inhibitors, propeller boss and stern-tube seals with propeller shaft as propulsion aids, structural elements such as boss brackets, hydrofoil struts, navigational and operational aids such as sonar and speed log domes as similar as healing and draft sensors, bulbous bow, stern flaps, and propeller ducts as energy-saving components may be expressed. They are the effective derivatives of this concept to be evaluated in dynamic buoyant motion.

It is important to make adequate corrections for appendage effects on HSMV model test results. Two methods are commonly used to account for appendage effects:

(i) Testing the bare hull and then separately accounting for the lift and drag of individual components using analytical methods

(ii) Testing the hull with and without appendages and expanding the values based on the local Reynolds number of each component.

Testing both with and without appendages has the advantage of providing more information for expanding the test data using different methods. Trim moments caused by

appendage forces not correctly represented in the experiment should be accounted for using equivalent shifts in the center of gravity location and displacement. If these corrections are made after the tests are completed, the results can be obtained by interpolating between results from tests with a different center of gravity locations [36] .

Criteria of the Appendage resistance is based on naked hull resistance and assumption are taken into consideration for basic design models as the vessel's speed and hull waterline length ratio.

Table 2.5.8.1: Basic design assumptions fort he naked hull resistance speed/length ratio [37]

Ship type	Speed/length ratio		
	0.70	1.0	1.6
Large fast quadruple-screw ships	10-16%	10-16%	
Small fast twin-screw ships	20-30%	17-15%	10-15%
Small medium V twin-screw ships	12-30%	10-23%	
Large medium V twin-screw ships	8-14%	8-14%	
All single-screw ships	2-5%	2-5%	

The Appendage resistance [38] :

$$R_{APP} = \frac{1}{2} r V_s^2 C_F (1 + k_2)_{equiv} \mathring{a} S_{APP} + R_{BT}$$

(23)

Where ; k_2 Tentative Form factor with appendage component

Table 2.5.8.2: ($1+k_2$) Tentative Form Factors of. [39]

Appendage Type	($1 + k_2$)
Rudder behind skeg	1.5–2.0
Rudder behind stern	1.3–1.5
Twin-screw balanced rudders	2.8
Shaft brackets	3.0
Skeg	1.5–2.0
Strut bossings	3.0
Hull bossings	2.0
Shafts	2.0–4.0
Stabilizer fins	2.8
Dome	2.7
Bilge keels	1.4

2.5.9 Spray Resistance

Vessel speed and length ratio is another objective that's agreed on resistance comprehensive factor, reached during most of the studies as common. Based on calm water resistance considerations, the appropriate selection of a particular type of hull form is mainly dependent upon its operational speed/length ratio (**SLR**). As you all know, this is defined as the speed in knots " V_s " divided by the square root of the load waterline length (LWL) into meters or feet. Thus,

$$SLR = V_s/LWL^{1/2} \tag{24}$$

The following paragraphs present a very brief description of the hydrodynamic phenomenon associated with increasing SLR and how they influence the geometric configuration of the hull form. Because of the hull generated waves and negative pressures on

convex surfaces a self- generated wave system represents an irrecoverable expenditure of propulsive energy that is a consequence of the "wave-making" resistance of the hull. On the other hand, one other major hydrodynamic phenomenon associated with high speed itself is the generation of negative pressures along convex surfaces of the hull i.e. convex longitudinal buttock lines or convex curvatures in the transverse plane—particularly in the bilge area. The influence of this effect on hull form selection is also discussed subsequently. The ship is climbing up the back of its bow wave. At these speeds, the flow along the convex geometry of the hull bottom develops large suction pressures that further increase the squat and trim of the vessel.

If, $2,0 < SLR < 3,0$: The hull rises to essentially its original static draft and the trim angle decreases with increasing speed. The round bilges develop a spray formation that rises rapidly with increasing speed. This spray climbs up on the sides of the hull and can reach the deck level at SLR approaching 3,0. For further increases in speed, the trim is further reduced, the spray is intensified and the total wet area becomes significantly larger than the static wet area. For $SLR > 3$, the resistance of the hull usually increases very rapidly. In this condition, spray resistance will be a more critical and effective and resistance component related to the energy consumed to form the spray, especially in high-speed ships [40]. That's the very rare subject in literature because of the trading vessel's special shooting subject and hull geometric sub-functions relation which is determined in other aspects mostly.

2.5.10 Steering Resistance

The steering gear is no longer expressed as a maneuvering facility of a buoyant in a viscous environment, but also a very important factor for new ship energy optimization programs. "Attention is drawn to the possible inability of the equipment accurately to maintain set headings when at slow speeds and/or in heavy seas. The performance of heading control

systems is dependent upon correct control settings suited to the prevailing conditions of the ship's speed, displacement and, particularly, the sea state. Use of the heading control system must be restricted to conditions within the designed parameters." This wording is directly from SOLAS [41]. On the design stage, moreover in the operational stages, the main maneuvering system of a vessel will change most of the vector design aspects of a hull performance related to propulsive efficiency. Efficiency improvement of all the systems on board ships is an important research field worldwide in order to reduce polluting emissions.

The concept of 'green ship' concerns various aspects such as propulsion, on board generation, loads, and drives. Most of the research is devoted to enhancing the propeller efficiency, which is generally 50%-70% [42].

In the past, common using criteria of commercial ship autopilot designs aimed a minimized rudder activity for specified heading deviation, But much present opinion demands that a minimum of propulsion losses caused by steering control be adopted as a criterion for autopilot efficiency in the open seas areas free of navigation hazards. In this regards, it is important to distinguish between total added resistance or propulsion losses of a ship sailing on a "straight" course and those losses attributable to or caused by the steering gear [43].

2.5.11 Shallow Water Effect

The general character of experimental results dealing with the effect of shallow water on ship resistance may be stated briefly as follows: At low velocity the resistance in shallow water is greater than in deep water, the speed at which the excess is first appreciable varying with the type of vessel. As the speed increases, the excess resistance increases up to a maximum at a certain critical velocity, and then diminishes. With still further increase of speed, the resistance in shallow water ultimately becomes, and remains, less than that in deep water at the

same speed. The maximum effect is the more pronounced the shallower the water. [44] The prediction of an inland ship hydrodynamic resistance in shallow water conditions is important for the estimation of the on board power design requirements. Shallow water can affect viscous and wave resistance, sinkage and trim, propulsive efficiency, and far-field wave systems [45]. This impact may be the basis of major economic assessments and solution proposals for ships operating on coastal voyages or for vessels sailing near by the shore. The inland ship's dimensions have to comply with the existing waterway infrastructure, reduced length, breadth and draught, according to the locks and bridges capabilities [46].

It has been confirmed by recent mathematical investigations by [47] that the wall effect on wave-making resistance mathematically treated for a depth-breadth ratio of such restricted watercourses as are generally experienced, like very shallow experimental tanks, canals, etc, does not enlarge the range of speed to a very great extent, and that the resistance increasing rate in the rising part is very small. While when the sectional area ratio has a considerable value and so the restricted water-effect is evident, the range of critical speed is wide enough to cover approximately the rising part in the pure shallow-water effect, and within the range of critical speed it is clearly observed by experiments that a notable change in the conditions of water around the ship consequent on the creation of back water renders the wave-making phenomena in the pure sense of the words very obscure. And in this case it may be inferred that the so-called residuary resistance is for the most part occupied not so much by wave-making resistance, as by resistance due to back water, and others. Now, as will be touched further on, the quantity of such special resistances cannot be calculated on pure theory, but are each of a nature to include a coefficient to be experimentally determined [48].

2.5.12 Air Resistance

Air resistance of the ships is the resistance in the atmosphere where called dry boundary resistance of the hull-body or with other wording, wind resistance of the hull and its parts over the water surface with its deck houses, superstructure and all other components above the water level. This resistance depends on the speed of the ship, the total area and the aerodynamic shape of the structures. It also depends on the speed, relative direction, and intensity of the accumulated wind.

Some typical values of air resistance for different ship types, as a percentage of calm water hull resistance, are given in Table 2.5.12.1.

Table 2.5.12.1: Hull types examples in the aerofloating resistance [24]

Type	L_{BP} (m)	C_B	D_W(tonnes)	Service speed(knot)	Service power(kW)	F_r	Air Drag (%)
Tanker	330	0.84	250,000	15	24,000	0.136	2.0
Tanker	174	0.80	41,000	14.5	7,300	0.181	3.0
Bulk Carrier	290	0.83	170,000	15	15,800	0.145	2.5
Bulk Carrier	180	0.80	45,000	14	7,200	0.171	3.0
Container	334	0.64	100,000 10,000 TEU	26	62,000	0.234	4.5
Container	232	0.65	37,000 3,500 TEU	23.5	29,000	0.253	4.0
Catamaran Ferry	80	0.47	650 pass 150 cars	36	23,500	0.661	4.0
Passenger Ship	256	0.66	2,000 pass GRT90,000	22	32,000	0.222	6.0

The wind, which affects the parts of the ship above the water, causes a increasing or deduction on the ship speed and hull may heel to the sides and the ship to deviate from its route

37

even and after following a route with steering facilities to keep the course. Moreover, the ship's heel and rudder effect, the resistance of the ship changes, with other words, "Induced resistance occurs"[25]. The impact of the wind force on the upper parts of the ship is divided into longitudinal forces, lateral forces and yaw moment. These components are calculated:

$$C_X = \frac{X}{\frac{1}{2}\rho_A V_R^2 A_{VT}} \tag{25}$$

$$C_Y = \frac{Y}{\frac{1}{2}\rho_A V_R^2 A_{VT}} \tag{26}$$

$$C_N = \frac{N}{\frac{1}{2}\rho_A V_R^2 A_{VL} L_{OA}} \tag{27}$$

Where;

C_X : Resistance Coefficient

ρ_A : Density of Air

X : Longitudinal Wind Force

Y : Transverse Wind Force

C_Y : Side-force Coefficient

N : Wind-Spinning Moment

C_N : Moment Coefficient

L_{OA} : Length Overall

A_{VT} : Transverse Area of the Vessel

A_{VL} : Longitudinal Area of the Vessel

V_R : Relative Wind Speed [26]

2.6 Roughness Resistance and Incremental Resistance Coefficient (C_A)

The relationship between the geometry of a surface and its hydrodynamic friction is unknown. The main difficulty in this respect is a rough surface cannot be described solely by a single parameter such as the average roughness height. [49] While the inclusion of a Reynolds number dependence allows for calculations, the roughness parameter was still only based on a simple measure of the roughness height and did not take into account other roughness texture characteristics. [50] As a part of the overall resistance of a vessel, hull roughness is one of the parts as a critical and large effective constituent, propellers surface roughness is the another dominant. For the full scale of a ship, the total resistance coefficient is composed of

$$C_T = C_F + C_R + C_A \tag{28}$$

Correlation allowance C_A is an empirical addition, derived from analysis of the correlation between extrapolated power predictions and trial measurements according to the ITTC-78 extrapolation method that is count surface and paint roughness, corrosion and fouling. [51] Here below implemented other formulation for the *CA* that's is expressed in 1974 by [52]

$$C_A * 10^3 = 105(k_s/L_{pp})^{1/3} - 0.64 \tag{29}$$

Townsin's Proposal in 1984, has been used with the formulation below [50]:

$$\mathrm{D}C_F = \left[0,044(AHR/\ L)^{-1/3} - 10R_e^{1/3} \right] + 0,000125 \tag{30}$$

where; average hull roughness (*AHR*) can be considered to be equal to k_s [53].

The roughness of the ship surfaces can be classified into three regimes: Micro roughness regime spans surface wavelengths of the order of several microns to a few millimeters. The macro roughness regime extends from the millimeter scale to the centimeter scale. Structural roughness has a wavelength range that extends from centimeter scales to higher values [54].

Three flow regimes exist for turbulent flow over rough surfaces, (hydraulically smooth, transitionally rough and fully rough flows) primarily depending on the size of the roughness elements relative to the viscous sub-layer. For k-type roughness, the equivalent sand grain roughness Reynolds number $k^+=U\tau\,k/v$ can be used as an indicator of the rough wall turbulence regime as follows: hydraulically smooth wall for $0<k^+\leq5$, transitionally rough regime for $5<k^+<70$ and completely rough regime for $k^+\geq70$ [6].

2.7. Residual Resistance Coefficient of Fouling and Biofouling

Apart from the wet surface area and speed the major factor in determining the frictional roughness is the roughness of the hull. For slow ships the frictional resistance is the major part of the total and it is important to keep the hull as smooth as possible [55]. The formulas for computing CF, where influence of roughness of a plate on C_F, are applied to the flat plates with smooth surface. The rough surface (of a ship) will result in the increase of C_F. Roughness (on the surface of a hull) may be classified into 3 types.

1. Structural roughness: Caused by welded joints, waviness of shell plating on the hull based on Schoenherr's (1932) formula which was examined and compared with Rotta's (1950) formulations.

2. Corrosion

3. Fouling/Biofouling: Inorganic environmental contamination and organic subsistence of marine environment such as seaweeds, shells and barnacles.
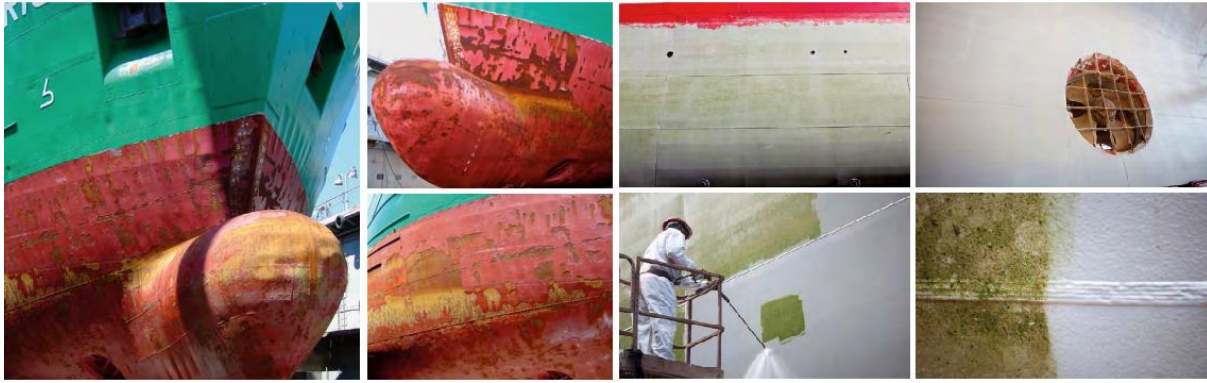
Figure 2.7.1 : (Left Side) A Hull 6 years after launch, using conventional antifouling coating which had been repaired in drydock 2 – 3 before. (Right side) Two years after application of glassflake vinylester resin STC and routine in-water cleaning, showing almost no damage to the coating and no coating deterioration years but having biofouling [56]

In this study, structural resistance factors caused by hull form and hydrodynamic relatives explained with their numeric components in various relations. Corrosion and fouling/biofouling subjects are the core factors that may be thoriated only and after in a ship in operation.

The marine environment (the seawater and atmosphere) is the most aggressive natural environment, the concentration of which — mainly of sodium chloride ions in water — gives an electrochemical nature to the influence of corrosion on the surface of the material of an offshore structures (vessels, ports, shipyard infrastructure, drilling platforms, and wind farms). The development of material engineering resulted in the creation of technical groups of alloys (which are relatively cheap, but which have electronegative potential concerning the reference electrode), which apart from good mechanical values also show good resistance to general corrosion thanks to the spontaneous creation of a thin protective passive layer on their surfaces [57].

The results revealed that this corrosion environment is characterized by repetition of dryness and wetness. The conditions for laboratory corrosion tests were determined based on the results of these measurements [58].

41

When a developed steel was used on a marine merchant vessel, deterioration behavior of the coating after use for approximately 5 years, together with the results of an evaluation of the corrosion behavior of the steel [59]. This determination is far most true for the environment only re-fill/discharge criteria for a ballast tank. Moreover, hull dynamic surface will have additional di-electric combinations in their motional activity.

Nowadays, waste generation of World's population have a catastrophic effectiveness on both in the oceans and very intensively in ship's port of calls. A progressive evaluation of the anorganic fouling materials, their ability to adhere to surfaces may only be defined with relative approaches but effectively in experimental studies. But, biofouling, which is a biological phenomenon can occur at anywhere in world seas and cause detrimental effects on ships performance. These kinds of organisms tend to attach to the underwater surface of a ship that can critically change the surface characteristics of ship hull. Although today many anti-fouling products exists, biofouling has not an exact solution since its quiet complicated, interdisciplinary as covering issues which are related to biology, chemistry and ship engineering, also it's an unstable problem depending on sea water properties [60]. There are experimental approaches to biofilm and biorganic foulers investigated in past twenty years that energy discussion was extensively and dramatically increased. In fact, the spectrum of mechanism of fouling of surfaces range from purely probabilistic,what is in the water column attaches or settles, to succession,requiring a series of molecules and then organisms attach before the next more complex level of fouling can occur [61].

Barnacle type	Dimensions (diameter and height)
Big	10 mm and 5 mm
Medium	5 mm and 2.5mm
Small	2.5 mm and 1.25mm
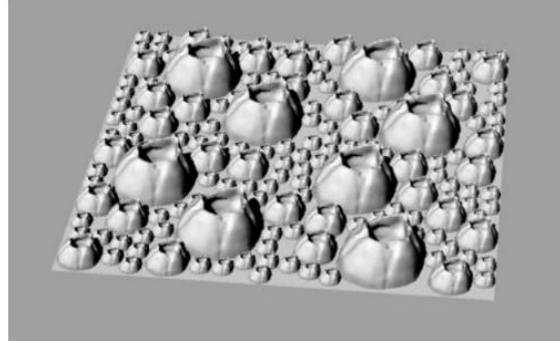
Figure 2.7.2 : An experimental barnacle figures used on towing test bath [60]

In this study, it's been taken a model of a common reference texture by Demirel's (2015) [62] determination based on Schultz [63] experimental approach. At this point of view,

$$\frac{0,242}{\sqrt{C_F}} = \log_{10}(R_e C_F)$$

(31)

Where;

m = 0 Acception and A = 0,242 based on Schultz [63] experimental result.

According to ITTC Recommended Procedures of Fresh water and Sea water properties, report code 7.5-02-01-03 [64] it is clear to understand frictional coefficient and propulsive efficiency % changings without test misalignments factor.

$$C_{RS} = C_{TS} - C_{FS}$$

(32)

$$C_{RS} = C_{Rr}$$

(33)

$$C_{Fr} = C_{Tr} - C_{Rr}$$

(34)

$$\frac{(C_{Fr} - C_{Fs})}{C_{Fs}} x100 = \%DC_F$$

$$\frac{(C_{Tr} - C_{Ts})}{C_{Ts}} x100 = \%DP_E$$

(35)

43

2.8 Fouling and Effects on Underwater Structures

In the construction of ship hulls, there are several different composite materials such as steel, aluminum, polymer reinforced glass are the fatal choices of the builders. On the other hand, ships follow very different routes and can remain in the light layer for a long time in places with high yields. There are various coatings are used to protect the body as well as protection for de-ionization applications such as anodes which are made from zinc, aluminum and copper alloys. However, these coatings are insufficient to protect the body from calcium carbonate residues, extra-cellular secretions and inorganic salts produced by fouling organisms.

Fouling event is observed in various aquatic environments. Underwater structures at sea are of various categories, but 24% of them are ship hulls [65]. The densities could also be different at the locations wherever many various species settle within the hulls, and numerous results may have an effect on manoeuvrability from propulsor to rudder or dynamic the sound signature of the ship could also be modified which can reflect echoes to effect active and passive navigational instrument systems.

High friction resistance due to roughness results in a reduction in speed and maneuverability. Even a small amount of bio-film can have an effect on the friction resistance of ships (up to 80% for a film of 1 mm thickness) Marine biofouling begins to accumulate on the submerged portion of an oceangoing vessel within minutes of making contact with the water. Over time, this accumulation increases the drag of the vessel, causing the physical resistance of the vessel to increase. As a result of fouling drag on the vessel, higher fuel consumption to maintain a given speed or lower speeds at a maintained power will occur [66].

To compensate for this, excessive fuel consumption is required, leading to an increase in the release of harmful compounds. 40% increase in fuel consumption increases travel costs by up to 77% [67].

Corrosion deterioration due to corrosion facilitates change in electrical conductivity of material and color fading. But on the other hand, it causes the emergence and proliferation of unnatural, invasive, invasive or non-native species. Polluted waters may be harmful either directly through toxic effects, or indirectly e.g. through depletion of oxygen or reduction of the solar radiation available for photosynthesis. Silt and other suspended matter may asphyxiate sessile organisms or produce substrates unsuited for the attachment of many forms and may also interfere with the food assimilation of animals that use water filtering. On the contrary, some contaminants may enrich the nutrient supply and thus enhance the fouling. It is also widely known that the problem of fouling is not as pressing in deep waters as in coastal areas. Marine bacteria and marine organisms, in general, are much less plentiful in oceanic waters compared to coastal waters. Depth is another parameter affecting the intensity of fouling, but it does not influence in the case of ships as they are always in contact with superficial waters [68].

2.9 Biofouling and Population Growth in Viscous Environment

One engineering challenge solved in nature, but plaguing a variety of industries, is biological fouling, commonly referred to as biofouling. This is the accumulation of unwanted biological matter on surfaces, with bio-films created by micro-organisms and macro scale biofouling (simply called macro-fouling) created by micro-organisms. In addition to biofouling, inorganic fouling is composed of deposits from corrosion, crystallization, suspended particles, oil, and ice. The term fouling describes both biofouling and inorganic fouling. The type and extent of fouling depend on the local environment, inorganic deposits and organisms; this varies significantly between medical, marine and industrial applications. In general, medical biofouling includes only the bio-film, whereas marine and industrial

45

biofouling generally include a combination of bio-film, macro-fouling and inorganic fouling [69], [70].

A bio-film 1mm thick can increase the ship's hull friction by 80 percent, which translates into a 15 percent loss in speed. [71] Furthermore, a 5 percent increase in biofouling increases ship fuel consumption by 17 percent, with a 14 percent increase in greenhouse gases CO_2, NO_x and SO_2 emissions [72].
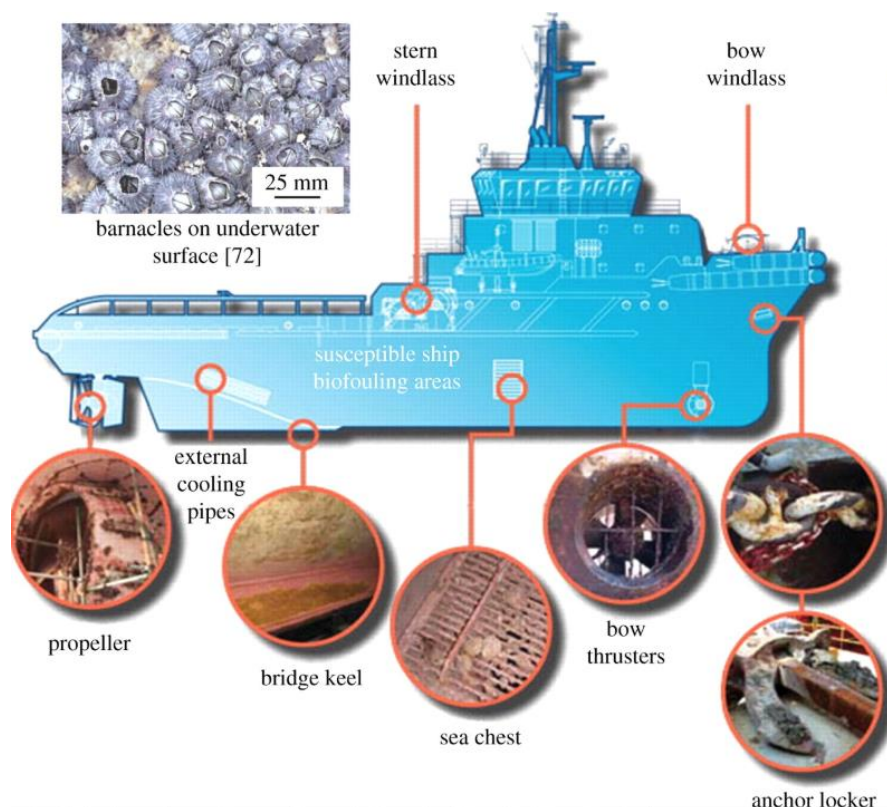
Figure 2.9.1 : Marine biofouling examples. Areas are susceptible to biofouling on a typical ship (middle) and the common hard-shelled barnacle (Tetraclitella purpurescens) (top left). Adapted from Mermaid Marine Australia, Ltd; photographs courtesy of Ashley Coutts, Cawthron Institute, John Polglaze, URS Australia and Helix ESG. (Online version in color.)

In aquatic environments, colonization (spreading), fouling and biofouling can be used in similar meanings. In the marine environment, any solid exposed undefended surface will become fouled. Similarly, fouling may effect numerous species that are able to tolerate a certain degree of epibiosis. In contrast, many others actively maintain their body surface clean of

epibionts with a known wording: antifouling [73]. Biofouling refers to the process of biological fouling and differs from other forms of fouling, such as corrosion, crystallization, chemical reactions, which vary on surfaces in terms of origin and deposition of different deposits. As a result, biological fouling; This is a special case involving the coating of surfaces by living organisms in aquatic environments [74].

A pile of microorganisms that are secreted by holding onto various surfaces and formed in the extracellular polymeric slurry matrix is called biofilm [75]. In particular, it has been reported that biofilm bacteria formed on wet surfaces are phenotypically different from their planktonic states. Based on this difference, these "living layers" have been deemed appropriate for sloppy communities called biofilms. Various surfaces are important settlements for microorganisms since surfaces accumulate by retaining nutrients.

Bacterial adhesion is influenced by many factors such as the electrical charge of the surface, its physical and chemical behaviors against/in water and surface topography. The properties of the surface alone can lead to changes in the formation of the biofilm. In seawater; negatively and positively charged ions, proteins, as well as humic acids, sugars, and fats are important. Further, the cell surface properties may have more effective by long-chain polymers, cell extensions, surface-active agents, and similar factors that give rise to or support key conditions with playing a role in the strength of attachment. Studies have shown that more than 4000 species cause fouling. However, the species identified constitute a very small amount of the species that are not known. Traditionally, fouling takes place in 4 steps:

In the first step, polysaccharides, proteins and proteoglycans, and inorganic compounds are deposited on the surface and occur in the first minutes. This process consists of Brownian motion, electrostatic relations, van der Waals forces. For the second stage, the surface is required to remain submerged for about 24 hours, so that bacteria and unicellular algae can adhere to the surface [76].

In literature, there are several determination for the initial stage of the biofouling process is similar to that of most organic processes, whereby the amount of carbon that can be absorbed promotes microbiological growth. Accumulation of organic substances on the surface causes the formation of the bio-film matrix with the adherence function of bacteria on these surfaces. The next process is the spreading of micro and macro-fouling organisms to the surface.
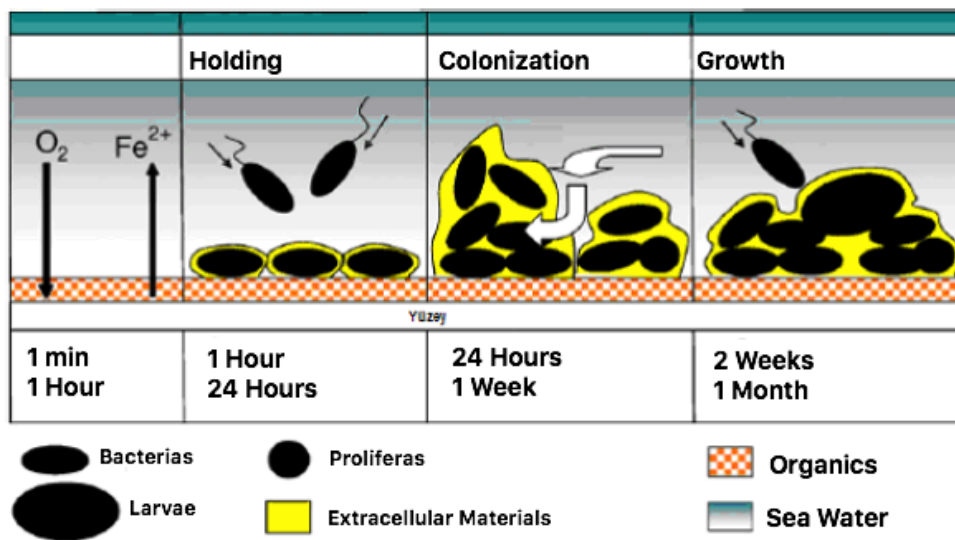
Figure 2.9.2 : Development stages of biofouling [77]

The regionally diverse biofouling event is closely related to many environmental variables. Geographical region, water conditions (salinity, temperature, pH, dissolved nutrients and oxygen concentration) and the course of the ship are the most important environmental variables. As a result, these variables cannot be altered to control the growth of fouling organisms. Of course, the temperature is one of the most important variables. The commonly known view is that fouling is more intense in areas where the water temperature is relatively high. Rather, it is associated with the proliferation and growth of marine animals. In regions with seasonal changes, especially during low temperatures, the growth of many species is suppressed, and in the warm period reproduction starts again. On the other hand, tropical climates with small temperature variations are both richer in species and the fouling continues uninterrupted throughout the year. Besides, some species can easily adapt to changing

environmental conditions and can be found in many parts of the planet [78].

Table: 2.9.1: Adhesion stages of organisms attached to surfaces in sea water [79]

Processes	Organisms in hold	Condition of Biofilm	Approximate start time period
1.Step: Electrostatic	**Adhesion:** Proteins, polysaccharides,	Regulator	Early minutes
Interactions Brownian	glycoproteins and other		
movements and Van der	organic molecules,		
Waalls forces required	cling to surfaces		
physical forces	starts		
2nd. Step: Recyclable	**Bacterias:** Pseudomonas	Microbic Biofilm	1-24 Hours
adhesion, physical forces	putrefaciens, Vibrio		
and between species	alginofyticos, **diatoms**;		
interactions	Achnantes brevipes,		
	Amphora coffeaeformis,		
	Nifzschia pusilla		
3 rd. Step: Compacting	**Spores of Microalgea**	Biofilm	1 Week
microorganisms	Ulothrix zonata		

	Enteromorpha intestinalis		
predators, toxic			
substances and environmental	and **protozoa**;		
protected from changes and	Vaginicola sp.,		
new microorganisms	Zoolhamnium sp.,		
Enough food is provided	Vorticella sp.		
4.th Step: Particle and macrorganism increase in larvae and irreversible film formation and irregular microbial colonies roughness formation	**Larvaes of Macro-foulers** Balanus amphitrite (Crustacea), Laomedia flexuosa (Coelenterata), Electra crustulenta (Bryozoa), Spirorbis borealis (Polychaeta), Mytilus edulis (Mollusca) and Styela coriacea (Tunicata)	Sea invertebrates and macroalgae adherence and development	2-3 Weeks

2.10.1 Geometric Scales of Biofouling on Surfaces

Marine organisms can cling to surfaces or each other with an effective defense mechanism to maintain their populations on nature, to complete their evolutionary processes, and to apply the life forms required by their mutuality or commensal activities. The topographic deformation process of this mechanism can often be in different forms that can be explained by adaptation to physical processes.
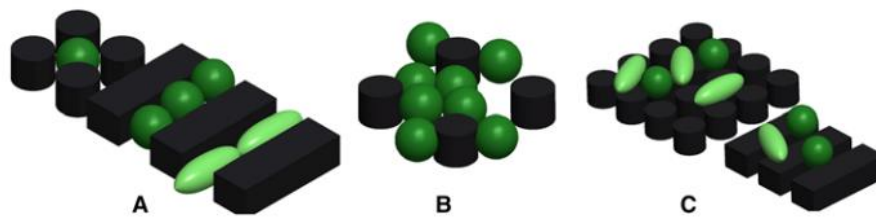
Figure 2.10.1.1 : Settlement of organisms on topographically varied structures. (A) Organisms (green and light green) fitting well between adequately spaced topographical features. (B) Organisms leaning on each other and on topographies that are spaced too far apart. (C) 'Bridging' of organisms on multiple topography features [80]

Biofouling and inorganic fouling depend on surface factors such as wettability, microtexture, color and contours [81]. For instance, bryozoan and mussel larvae prefer hydrophobic surfaces [71] hydroids, bryozoans, and ascidians prefer microtextured surfaces; larvae, sponges, barnacles, ascidians and mollusks prefer light-colored surfaces; barnacles prefer convex contours; and calcareous sponges prefer concave contours [65]. Surface wettability influences fouler colonization, which ranges from water-fearing superhydrophobic to water-loving superhydrophilic surfaces [81].

A hydrophobic surface exhibits low wettability and low surface energy, whereas a hydrophilic surface exhibits high wettability and high surface energy. Water droplets on a hydrophobic surface will 'bead up', while droplets on a hydrophilic surface will spread out evenly. The preface 'super' indicates higher tendencies in either direction, such as superhydrophobic and superhydrophilic. The degree of wettability is determined by contact

angle measurements, where contact angles less than 10° are superhydrophilic and over 150°

are superhydrophobic.
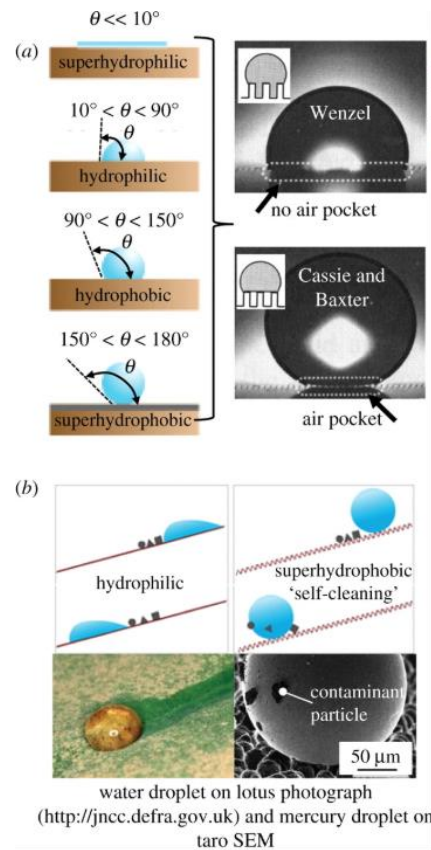
Figure 2.10.1.2. Various parameters describing wettability and self-cleaning. (a) Schematic shows droplet contact angles (left) and photographs of droplet regimes (right). Adapted from Nosonovsky, Bhushan (2008) [82] (b) Schematic shows the self-cleaning effect (top) and superhydrophobic examples (bottom). Adapted from Barthlott, Neinhuis [83]

Close examination of the liquid-solid–air interface reveals that the Wenzel regime

(1936) does not contain an air pocket, unlike the Cassie–Baxter regime. This difference, owing

to surface roughness, influences the surface wettability as the air pocket affords a larger contact

angle θ, which relates to wettability [82] Nosonovsky -Bhushan Equations (36). Description

of the Wenzel equation (37) (no air pockets), where θ is the contact angle, θ_f the contact angle

of the droplet on the solid surface, R_f the roughness factor, A_f the flat solid-liquid contact area

and A_{SL} the projection of the solid-liquid area. Equation (38) describes the Cassie–Baxter

equation (with air pockets), where fSL is the fractional solid-liquid contact area [84]. Furthermore, the contact angle hysteresis (CAH) is the difference between the advancing (downhill side) and receding (uphill side) contact angles, which is low for Cassie–Baxter and high for Wenzel regimes. As the CAH increases, so does the adhesion strength, which explains the deformed shape of a water droplet adhered to a vertical window [82].

Wenzel regime:

$$cos\theta = Rfcos\theta f \tag{36}$$

where

$$Rf = \frac{A_{SL}}{Af} \tag{37}$$

Cassie–Baxter (1944) regime:

$$cos\theta = Rf \int SLcos\theta f - 1 + \int SL \tag{38}$$

Micro-organisms prefer to settle in areas slightly larger than themselves for maximum protection and surface area contact with the substrate. Fewer attachment points between the micro-organism and substrate translate into lower bioadhesive strength [85].
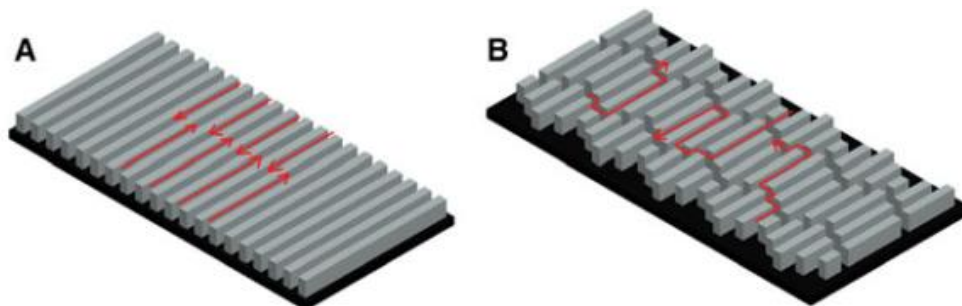
Figure 2.10.1.3 : Tortuosity of topography with different complexity. Grooves in (A) are less 'tortuous' because organisms perceive the option to move only along one axis (indicated by red arrows); while riblets in (B) have higher 'tortuosity' because organisms are allowed the option to explore the surface along with several directions. [80]

The topographies studied were designed at a feature spacing of 2 μm and all significantly reduced spore settlement compared to a smooth surface. An indirect correlation between spore settlement and a newly described engineered roughness index (ERI) was identified. ERI is a dimensionless ratio based on Wenzel's roughness factor, depressed surface fraction, and degree of freedom of spore movement. Uniform surfaces of either 2 μm diameter circular pillars (ERI = 5,0) or 2 μm wide ridges (ERI = 6,1) reduced settlement by 36% and 31%, respectively. A novel multi-feature topography consisting of 2 μm diameter circular pillars and 10 μm equilateral triangles (ERI = 8,7) reduced spore settlement by 58%. The largest reduction in spore settlement, 77%, was obtained with the Sharklet AF™ topography (ERI = 9,5) [86] .
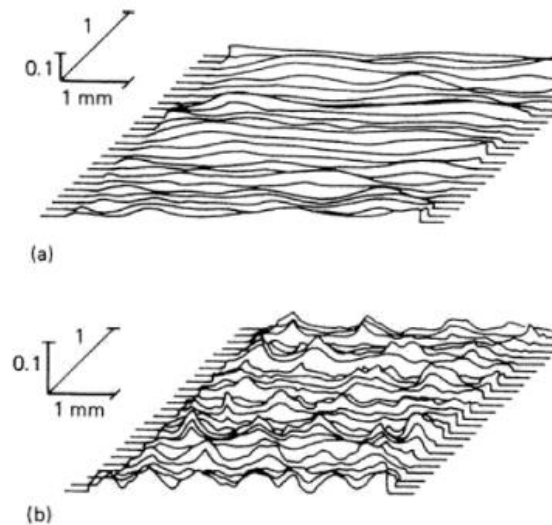
Figure 2.10.1.4 : Example of two different textures having approximately the same roughness amplitude [92]

Surface micro-structures may affect the boundary-layer flow and the hydrodynamic drag (skin friction) of the surface. The skin friction was empirically measured in a flow channel using a sub-set of the tested micro-textures. The measurements of skin friction showed that the orientation of the micro-structures is important, with minimum friction when the grooves are

parallel to the flow. For one of the micro-textures, the skin friction was ca 10% lower compared to a hydraulically smooth surface. It is concluded that, depending on the flow speed, micro-textures will not significantly increase skin friction when arranged parallel to the flow, even at moderate protrusion through the viscous sub-layer [99].
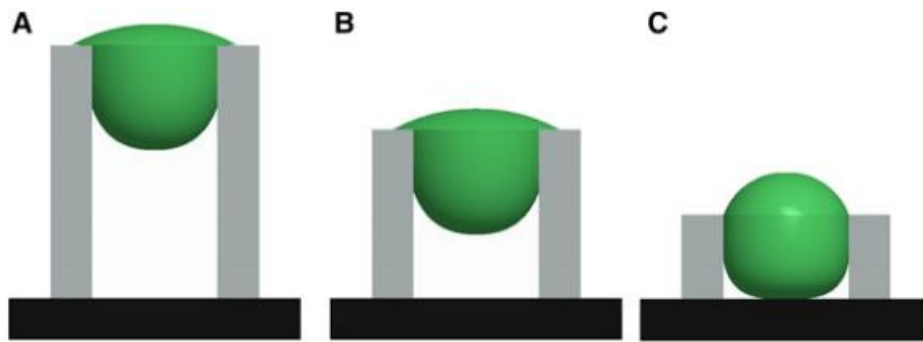
Figure 2.10.1.5 : Effect of topography feature height towards effective spore attachment. Spore adhesion is the most effective in (C) because there is significant contact between spore and surrounding areas of the topography feature (i.e. walls, floor). Spore settlement in (A) and (B) is less effective since topography feature height is too high to allow spores more contact with its surroundings, especially the floor of the substrate [87]

A micro-spore reproduction may be taken as an example of maintaining the vital form and reproductive efficiency. Ulva spores are quadriflagellated, pyriform microorganisms that are motile and selective about surfaces that are suitable for settlement. Upon initial contact with the surface, a spore gauges potential for settlement by spinning in place while being anchored presumably by a temporary adhesive to the same spot. The spinning motion allows the spore to test its adhesion strength to the surface which depends on factors such as the surface's chemical properties. The longer the spinning duration, the more likely the spore will permanently attach to the surface [80].

There are forms in which the reproductive mechanism involves a hierarchy if vital colonization increases to larger scales. For example, Hierarchical structures of micro peaks on irregular micro-cells reduced Chlorella (9-10 μm) and Nannochloropsis Maritima (1-2 μm) settlements [88]. The micro peaks were 0,3 μm wide with an average height of 2 μm and were

densely packed on cells that had an average width of 30 μm. This topography exhibited antifouling properties because gaps between peaks were too small (2-3 μm) to accommodate high settlement densities of both types of spores. 'Bridging' of spores between peaks also indicated that this topography was high in tortuosity which made it difficult for spores to establish contact with the substrate to adhere effectively [80].

Most of the studies commonly express formations with a size of 1-5 mm. visible dimensions are called macro topographic colonies and algeas are the well-known group of the characters. Diatoms exhibit passive settlement onto a substrate and subsequent motility only when physical contact is made with the substrate to select preferred attachment sites. Therefore, diatoms could have settled passively onto random areas on the substrate and migrated to elevated areas of bumps which would be the most strategic position for diatoms to reach sunlight and other nutrient supplies [89].

The "rugophilic"; behavior (e.g. the preference for settling in concavities) of barnacles is well documented. In contrast, little is known about the settlement preferences of other species with regard to surface microtopography. In a randomized block design, five different rugosities (smooth, 0,1 mm, 0,5 mm, 1 mm, 5 mm) were exposed to natural fouling in the Baltic Sea. In four experiments, test panels were colonized by Mytilus edulis, Polydora dliata, Balanus improvisus, diatoms, hydrozoa, bryozoa, and several ciliates. Settlement densities and microtopographical preferences for pits or elevations as a function of grain size were evaluated. Rugosities influenced settlement densities and the microtopographical preferences of almost all investigated species. Settlement densities were generally lowest on smooth panels, with most species showing distinct preferences for different rugosities. While a preference for pits was frequent, in some species the proportion of individuals settling on elevations significantly increased with roughness. These datas on microtopographical preferences of different species

give new insights into interactions between settlement behavior, surface roughness, boundary layer hydrodynamics and community structure [90].

Many studies have tested the effects of micro topographies on the settlement behavior of barnacle cyprids and these studies consolidate the importance of topography scale in relation to the size of the cyprids. The larvae, which are the first periods of these macro structures, are mentioned in the micro topography, except for the macro topographic structures that fall outside the content of the time limits.
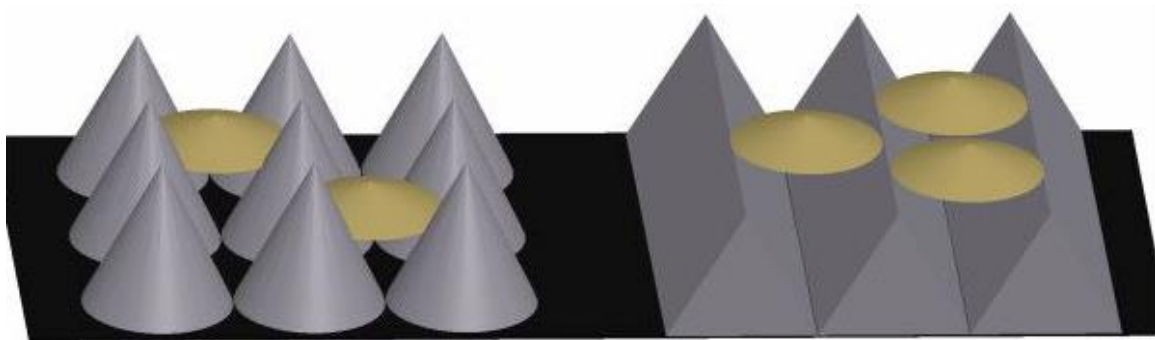
Figure 2.10.1.6 : Influence of isotropy on similarly scaled but geometrically different topography. The illustration shows that peaks are better than the more isotropically inclined V-shaped grooves of approximate size at providing secure settlement points for the attachment of cyprid base plates (beige). [80]

Micro topographies that ranged from 8-64 μm and 500-1000 μm enhanced cyprid settlements. Sine wave grooves that were 16 μm in wavelength were very supportive of B. amphitrite attachment which suggests that this size could be a critical dimension for this particular cyprid species. However, it is difficult to ascertain the reasons for this finding and further studies are warranted to determine this. Similar grooves which were 32-64 μm probably provided strong anchor points for attachment because cyprid antennular discs (30 μm) were compatible in size to these grooves. Topographies that were 500-1000 μm were expected to encourage cyprids to settle because cyprids were close in size and would be able to attach easily onto topographies of this range [91].

57

2.10.2 Biofouling and Roughness Relation

The turbulent movement of ship propellers in a viscous environment can only be expressed in comparison to the basic hydraulic principles in cellular areas where there is a steady flow. However, any effect that disrupts the flow order will inevitably disrupt the turbulence order and change the efficiency of the work performed. In other words, turbulent flow in each cellular area in which the surface form is degraded is much further away than can be expressed by laminar flow principles.

Just as if the cavitational possibilities began to occur in the viscous environment after the first round of turbulence of the propeller, the continuation of the same turbulence would change as soon as the surface phenomena were included in the activity. The fouling or biofouling effect may significantly also affect propeller performance as soon as the homogeneous surface activity resistance is broken.
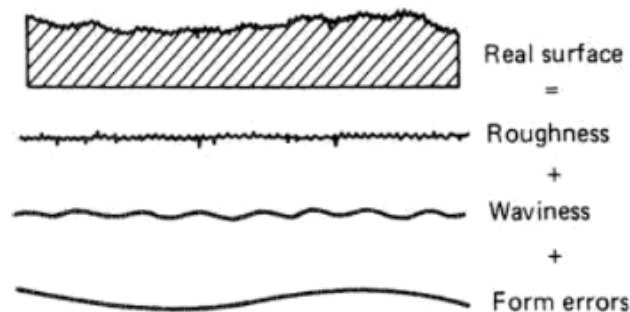
Figure 2.10.2.1: Reduction of the Surface Profile in to Components [92]

Surface Roughness has the effect of increasing the activity of turbulent eddies in the vicinity of the wall and therefore the transfer of momentum in the boundary layer, manifesting itself by an increase in the Reynolds stresses. The viscosity of the fluid will annihilate the effect of roughness and therefore the flow will not be different from the flow on a smooth surface. This regime of flow is termed as a "hydraulically smooth" regime. The values of roughness can make the assumption that the effect of roughness can be expressed as a decrease in the ability of the wall to "damp" the turbulent eddies in viscous and buffer sub-layers. This is

equivalent to saying that the viscosity will only partially annihilate the production of turbulence by roughness elements [6].
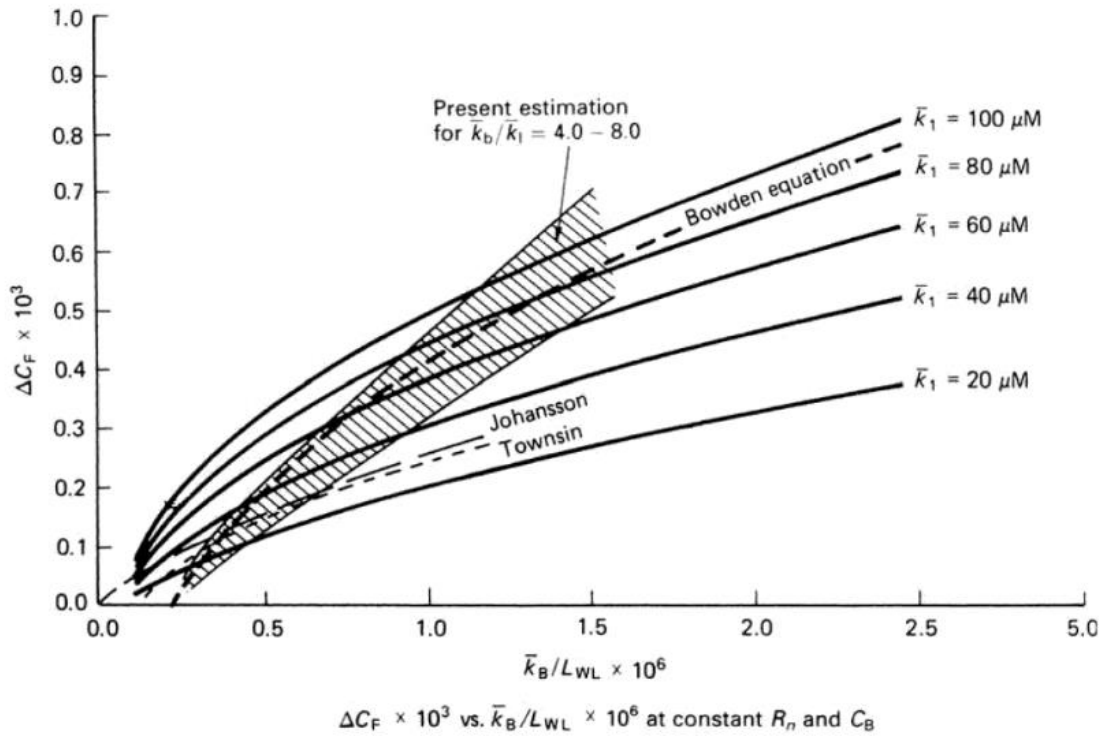
Figure 2.10.2.2 : Comparison of roughness ΔC_F values [92]

Many studies determined that uniform arrays of single-layered, micro-topographies are effective at deterring the initial settlement of fouling organisms. In contrast, most studies that tested uniform arrays of single-layered, macro-topographies concluded that these topographies are not suitable for anti-fouling applications. Both single-layered, micro-topographies and single-layered, macro-topographies were determined to have limitations at mitigating biofouling. This resulted in the interest to develop hierarchical topographies. Hierarchical topographies are surfaces that consist of features that are varied in size and shape. It was suggested that the diverse nature of hierarchical topographies might be able to deter biofouling from a wider array of organisms [93].

In this study ship's overall resistance and propeller, resistance will be categorized in different sections. Because most of the researches were generated on the ship's hull performance with tank towing tests in full scales in laboratory conditions but propellers are mostly difficult to scale in the laboratory environment as they computed. Because hydrodynamic estimations on surfaces with critical heterogeneity in harshness and fouling may serve to assist illustrate this. The estimates are based on results from laboratory-scale drag measurements and boundary layer similarity law analysis. In the present work, predictions are made for a mid-sized naval surface combatant at cruising speed and near maximum speed. The results indicate that slime films can lead to significant increases in resistance and power, and heavy calcareous fouling results in powering penalties up to 86% at cruising speed [94].

Marine biofouling roughness is generally randomly distributed in space, and also varies in shape and texture. The common practice in the hydrodynamic analysis is to ignore the details and express them simply by means of a representative length scale dimension [95]. Where taken this is as an approach towards the surface of the propeller which is much smaller than the hull, it will be possible to consider the causes of power losses beyond the expectations. In order to address more realistic roughness conditions, as typically observed on ships' hulls, 'low' and 'high' roughness densities were introduced into the same types of coating, in the second test campaign [96].

In this study, it was aimed to present an applicable procedure for surface effects for propeller turbulence that are intended to be interpretable only when datas are obtained from points close to the boundary layer of the turbulence. The development of this intellectual consensus lies in the following sentence: For shipowners and operators who may not wish to access advanced computer programs, a simplified method has been proposed to calculate the propeller roughness penalties. There is a good agreement between the two simplified and detailed propeller analysis methods [97].

2.11 Propeller Resistance Factor's Definition

2.11.1 Propeller Environment

Seawater is a complex natural environment and it is the principal environment in which marine propellers to operate. However, it is not the only environment since many ships and boats, some considerable size, are designed to operate on inland lakes and waterways. Consequently, the properties of both freshwater and sea-water of interest to the propulsion engineer [98].

There are common environmental derivatives that are effective in propellers' viscous dynamic motion as similar to all motional activities under rules of fluid mechanics. There are physical or chemical variables such as density, salinity, temperature, viscosity, vapor pressure, dissolved gases in the seawater, surface tension, weather, fouling. As a biological and biofouling is another factor that can also be influenced by all of these and can produce the results of this effect with its effectiveness and needs further evaluation.

Of course here are the symptoms included in the accounts as limited areas that are meant for a propeller manufacturer or ship designer. In most of the options, seawater density can be seen in almost all conditions as a fundamental variable in material selection. For example, seawater density can be seen as a fundamental variable in material selection and drag calculations at almost all conditions. But an important variable when in a comparison with the ship's hull and resistance conditions. On the other hand, mostly taken as 1.025 g/cm^3. When it's taken as a constant, on design manners, easily dismissed as a difference. It will not be wrong to make the same interpretation in terms of salinity. The temperature will be the variable of kinematic viscosity, which can affect density and salinity. It is not customary for a propeller designer to consider temperature alone when evaluating surface components or performance, nor will it result in a drastic change. Although vapor pressure and dissolved gases stand before us as an important calculation factor, from material selection to cavitation losses, they are

generally considered as limiting variables in terms of limit values and are sometimes capable of causing modifications even after long periods of production and assembly.

Since this situation can be evaluated from a result, it also emphasizes the commitment to the limit values at the design stage. Weather and sea conditions make it necessary to consider the hydrostatic and hydrodynamic factors that the surface stress factor and common other stresses will encounter during the transfer of energy from a design point of view. However, all of these can be expressed in coefficients in the back-ground of the design and can be solved with designs that can often fall within the security limits. Fouling and biofouling are unpredictable, and the results, including the user factor, lead to serious evaluations in the field of basic and ancillary sciences and continuous new experiments. On the other hand, Optimum propeller design is also correlated with ship hull components and resistances, therefore, manufacturers are having experimental results from the conferences such as International Towing Tank Conference (ITTC) that's been going on since 1932.

2.11.2 Propulsive Efficiency Definitions

Propulsive power has two main components that are thrust which is the thrust "T" as the reaction force of propeller according to Newton's third law and the torque, "Q" rotational force with other wording to define the moment of force according to momentum theory. On the other hand, there are power predictions mentioned as "w", " t " and "η_R" are frequently referred to as propulsion factors or propulsion coefficients.

w : *Wake Fraction Coefficient*

t : *Thrust Deduction Coefficient*

η_R : *Quasi Propulsive Coefficient*

Q_l : *Quality Index*

2.11.3 Thrust and torque

According to Foude's theory of momentum (1889) , which is more frequently interpreted after the manufacture of wind turbine blades, the impeller with thrust blades implies the reversible force generated by the actuator disc image produced during rotation. The propeller imparts a uniform acceleration to the water passing through it and the thrust generated by the propeller is uniformly distributed over the entire disc. The flow is frictionless and water quantity through the propeller is endless. In this study, water will be taken into consideration together with the frictional resistance subjects for the propellers.

$$Q = V_A(1 + a)A_0 \qquad (39)$$

Where,

Q : Flow rate of water through the propeller actuator disc

V_s : Vessel speed

V_w : Wake speed

V_A : Speed of advanced ($V_A = V_s - V_w$)

a : Axial-inflow factor 1

b : Axial-inflow factor 2 ($b = 2a$)

A_0 : Disc Area

r : Density of the water

$$T = r A_0 V_A^2 b(1 + b/2) \qquad (40)$$

63

For the prediction of the required propulsive power, the efficiency of the propeller in open water conditions has to be determined. It has appeared that the characteristics of most propellers can be approximated well by using the results of tests with systematic propeller series [100].

The power transmitted to a propeller should be defined as the force which rotates it directly, as constant as possible in the X-axis direction of a rotational optimized machine shaft and which can rotate radially in the Y-axis direction. With this definitionin a prediction of the following formula in any environment:

$$P_p = \eta_g P_e \tag{41}$$

Where,

P_e : *Propeller Effective Power*

A propeller operating in open water can be characterized by two non-dimensional parameters which are both functions of " *J* " as propeller advanced ratio according to propeller water speed " V_p " and vessel speed " V_s "

$$J = V_p / \eta_p D \tag{42}$$

For better understanding, a definetive formulation with more equations about thrust and torque coefficients:

Thrust Coefficient:
$$K_T = \frac{T_0}{r h_p^2 D^4} \tag{43}$$

Torque Coefficient:
$$K_Q = \frac{Q_{P_0}}{r h_p^2 D^5} \tag{44}$$

These exceptions are optimal for a propeller without hull and it's resistance in a viscous environment. Where required to define a thrust power independent from a shaft power, it's necessary to improve a new equation based on the open water propeller efficiency.

$$h_0 = \frac{T_0 V}{2ph_p Q_{p0}} = \frac{J(V)K_T}{2pK_Q}$$

(45)

where K_T and K_Q are linear and enreached form of the formulation for a steady condition of the vessel. Such form is also the basic formulation of the towing tests in literature.

$$Rt = \frac{1}{2}rC_r A_w U^2$$

(46)

2.11.4 Effective Propulsion Coefficients

A propeller in a viscous environment has different efficiency factors than it is installed to a dynamic designed ship's hull. Because of pressure increases at the stern, a propeller is in the boundary layer or way of the ship and water particle velocity induced by ship-generated waves will be the different dominant relatives.

As expressed before, the speed of advance of the propeller 'V_a' relative to the water in which it is working is lower than the observed speed of the vessel 'V_s'. This difference in speed is called wake. Water block velocity near the propeller is not the same as the ship velocity and this concept is mentioned as wake fraction in hydrodynamic literature.

Basically, wake fraction is the ratio of the speed difference to the observed speed and concept of wake fraction can be formulated:

$$w = \frac{(Vs - Va)}{V}$$

(47)

In Naval architecture literature wake fraction was identified by Froude and Taylor with their name's. Froude regenerated this formulation as below:

$$Va = \frac{(Vs)}{(1 + wf)}$$

(48)

65

Taylor's regeneration is a different look out according to the effective factors:

$$Va = Vs(1 - wf) \tag{49}$$

This conceptual view has enabled us to define negative and positive vessel and retention propeller speeds, situations in which vessel speed or propeller retention speeds are greater or smaller than each other. At the same time, the relative formulation is now known as the Froude and Taylor formulations.

$$Wt = \frac{(wf)}{(1+wf)} \tag{50}$$

or

$$Wf = \frac{(wt)}{(1-wt)} \tag{51}$$

The process where the propeller speed is smaller than the vessel speed is defined as a positive wake and represents the situation for most single propeller ships. However, if the propeller speed is greater than the speed of the ship, this applies only to hi-speed crafts.

In essence, the propeller will be needed for a ship already designed, the nominal wake concept has been defined and it is a wake measurement near the ship's stern without a propeller in the absence of propeller. In practice, it is necessary to using pitot tubes for such a measurement. Of course, an effective wake measured in the presence of the propeller.

The measurements show that a propeller at a rotating speed "n" behind a hull advancing at velocity, "Vs", delivers thrust "T". By comparing it to the results of the same propeller in the open-water tests, with the same revolutions "n", the propeller will develop the thrust "T" but at a different speed (usually lower), known as the effective speed of advance, "Va". The difference between Vs & Va is considered an effective wake [101].

Thrust is generated in the propeller where high propeller efficiency is obtained with a large propeller rotating at low speed. Ideally, the number of blades should be minimized, to

reduce blade area and frictional resistance. Typical design restrictions are limitations on diameter, cavitation, and loading. The size of the propeller may be limited by the design of the ship, by restrictions on draught in expected areas of operation or by engine torque [103].

Basically, in a ship, the propulsive efficiency concept contains relative rotative efficiency, open water efficiency, actual propeller efficiency which is related to hull efficiency, shaft efficiency in detail. For a more detailed examination, it is necessary to define the theoretical content behind these concepts and their relationships with each other in a propeller specific manner.

2.11.5 Relative Rotative Efficiency (η_r) :

The relative rotative efficiency is the difference in torque absorption characteristics of a propeller when operating in the mixed wake and open water flows. This concept is a ration of open water condition and propeller present condition behind the hull.

$$\eta_r = \frac{P_{Do}}{P_D} \tag{52}$$

Where,

P_{DO} : Delivered power in open water condition

P_D : Delivered power behind condition

With other wording, $\qquad \eta_r = \frac{Efficiency\ behind\ the\ hull}{Efficiency\ in\ open\ water}$

In general acceptance *"ηr"* taken in consideration and calculations in such condition according to propeller type: $0.95 \leq \eta r \leq 1.04$

In many cases the value of *"η_r"* lies close to unity and is generally within the range [102]. Such a definition should point out a reality of the vessel aft shape may bring other

variables and constraints. For this reason vessel, aft structural shapes were categorized in terms of their wake fractions.

w (wake fraction)		
$0.5C_B$-0.05	for single screw	Taylor's formulae
$0.55C_B$-0.20	for twin screw	
0.30	C_B=0.70	for moderate speed cargo ship
$0.4 \approx 0.5$	C_B=0.80 $\approx$ 0.85	for large bulk carrier
0.25	C_B=0.60 $\approx$ 0.65	for containership
$0.10 \approx 0.15$	C_B=0.50	for twin screw ferry
0.05	at cruising speed	for high speed frigate
-0.05	at full speed	
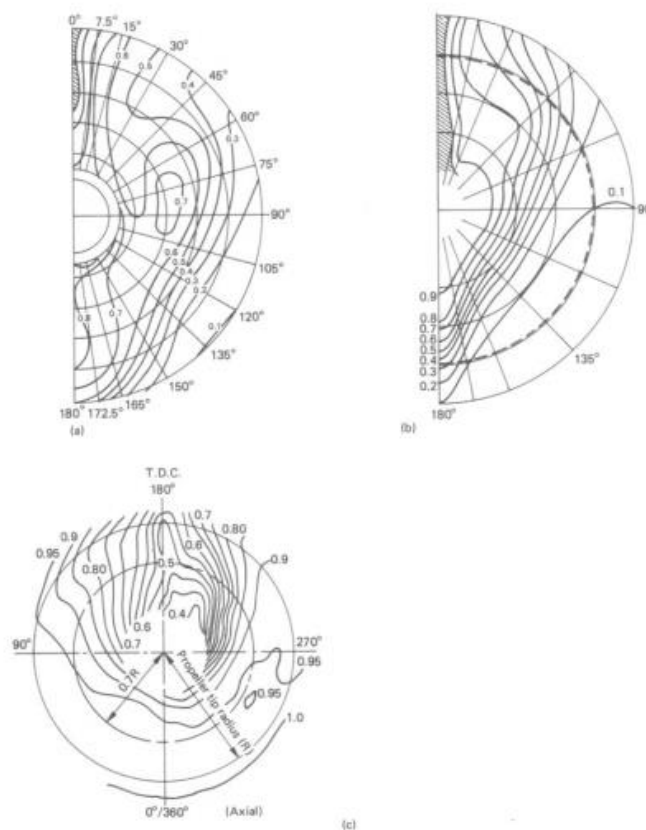
Typical wake contours: a) U form hull; b) V form hull; c) twin-screw hull

Figure 2.11.5.1: Hydrodynamic Characteristics Of Propellers [159]

In this study, a physical experiment has been applied in the condition of an open water basis. Therefore aft shape or a general effect of the hull may only be primitive effective in consideration. So that, calculations will be applied to real vessel data from an earlier experiment with applicants approach.

2.11.6 Thrust Deduction Coefficient (t)

When a hull is starting a dynamic motion, there is an area of high pressure over the stern, which has a resultant forward component to reduce the total resistance. With a self-propelled hull (in the presence of the propeller), the pressure at the stern is decreased due to the propeller action. Therefore, there is a resistance augment due to the presence of the propeller. If " T " is the trust of the propeller and " R_T " is the motional resistance of a hull at a given speed " V_s ", then so that the propeller propels the hull at this speed, " T " must be greater than " R_T " because of the resistant augment. The normalized difference between " T " and " R_T ", is called the thrust-deduction fraction, and denoted by " t ".

The application of the source and sink concept to the system ship and propeller leads to a satisfactory explanation of the various phenomena summarized under the notation "thrust deduction." The quantitative analytic evaluation of the forces involved, although in principle successful, meets still some difficulties and there are some important gaps between the results of theory and facts. Thus, there remains a wide field for systematic experimental investigations that can be planned and guided by the present theory. [104]

So that " t " will be effected from hull shape but also additional factors such as rudder blade, fins, nozzles or supportive bearings.

Where,

" R_T " is the naked hull resistance

" T " is the thrust after subtracting the resistance of the rudder and stern appendages.

$$t = \frac{T - R_T}{T} = 1 - \frac{R_T}{T}, \quad \text{thus} \quad R_T = \left(1 - t\right)T$$

(53)

2.11.7 Quasi Propulsive Coefficient (η_R)

Quasi-propulsive coefficient is defined as the ratio of the effective power to the delivery power as horse power or kw.

$$h_D = \frac{P_E}{P_D} = \frac{R_T V_s}{2\rho nQ} = \frac{TV_A}{2\rho nQ} \times \frac{R_T V_s}{TV_A} = h_B \times h_H = h_0 \times h_R \times h_H \tag{54}$$

$$P_E = R_T \times V_s \tag{55}$$

Where,

P_D : Delivered Horsepower $= 2\pi nQ$

$$h_D = h_0 \times h_R \times h_H$$

η_0 : Efficiency of a propeller in open water

η_R : Relative rotative efficiency

η_H : Hull efficiency

$$P_D = \frac{P_E}{h_H h_R h_o} = \frac{R_T V}{h_H h_R h_o} \tag{56}$$

For the design calculations equation is in use mostly:

$$P_D = \frac{(1+C)P}{h_D}, \quad h_D = h_H h_R h_o \tag{57}$$

Where X is a correlation allowance or with other wording as load factor. It depends principally hull roughness of the newly painted weather, LOA and cruising type of the vessel and it's fouling condition.

Where $\hbar_s$ is the shaft efficiency,

$$P_s = P_D / \hbar_s \tag{58}$$

as the final power requirement of a vessel.

2.11.8 Quality Index *(Q$_I$)*

Ideal efficiency comes from Actuator Disk consideration on axial energy losses ηI consideration on axial energy losses [105].

$$Q_I = \frac{\eta_o}{\eta_I} \tag{59}$$

$$\eta_I = \frac{2}{1 + \sqrt{1 + C_T}} \tag{60}$$

There are two more predictive coefficients are in terms of literature for drag and lift coefficients but mostly they are taken from the tables on calculations theory.

2.12 Propellers Roughness and Biofouling Correlation

Propeller roughness is a complementary problem to that of hull roughness and one which is no less important. As in the hull roughness case, propeller roughness arises from a variety of causes, chief of which are marine growth, impingement attack, corrosion, cavitation erosion, poor maintenance, and contact damage [106].

A smooth surface is essential to keep power requirements down on a propeller blade [107]. Attempts have been made for many years to estimate the penalty in power incurred by increased propeller roughness [108]. For example, conducted his studies into the power loss incurred by propeller roughness by increasing the drag coefficients of the propeller blade to approximate the surface roughness and demonstrated that a considerable power loss occurs

71

when a surface becomes rougher. One important geometric measure of a surface's curvature is given by the Gaussian curvature (1827) k, which describes the local shape of a surface and is obtained by taking the product of the maximum and minimum principal curvatures k_{max} and k_{min} at a point [109].

The propeller blade has two main hydrodynamic surfaces. The surface of the blade which faces aft and is referred to as the face or suction side, and the surface which faces forward which is referred to as the back or pressure side. The tip of the blade joins the leading edge of the propeller to the trailing edge where the face and back intersect, which occurs at the maximum radius from the center of the hub to which the blade is attached [110].

Propeller surface roughness can be measured in scales by Rubert propeller roughness comparator other than the modern surface topographic tools. Rupert Rougness gauge consists of six examples (A, B, C, D, E, and F) of surface finish that range from an average roughness amplitude $R_a = 0.65\mu m$ to an amplitude of $R_a = 29,9$ µm5.

Propeller roughness and it's effects should be evaluated in propeller lift surface analysis requirements with blade sectional and surface drag coefficients. blade drag is accounted for by the inputting of the appropriate blade section drag coefficients usually denoted by the term, C_D. On the hand, it must be formed based upon the calculation of the drag coefficients corresponding to various degrees of blade roughness [97].

The increase in section frictional resistance due to roughness can be represented by the expression:

$$1000DC_F = 8.1R_e^{0,093}\left[\frac{1}{3}(h^{'} / c) - 4,5R_e^{1/3}\right]$$

(61)

Where;

R_e : Blade section Reynolds' Number

c : Section chord length

h' : Roughness parameter as defined by Musker [111]

Table 2.12.1: Musker's characteristic roughness measure of Rubert gauge surfaces [111]

Rubert Surface	h' (μm)
A	1.32
B	3.4
C	14.8
D	49.2
E	160
F	252

The sum of the frictional drag and the form drag will give the increase in total drag:

$$\mathrm{D}C_D = 2(1 + t/c)\mathrm{D}C_F \tag{62}$$

where ; t is the maximum thickness of the blade section.

Whe in a correlation for an investigation, it has been assumed that the new or polished propeller has Rubert B blade surfaces, the drag of which is represented by the design C_D values. The increase in C_D caused by blade roughening means biofouled as in our study, is then given by the difference between the ΔC_D values corresponding to the Rubert surface in question and that for Rubert B. Where taken as an example of Rubert D.

$$C_{DD} = Design C_D + (\Delta C_{DD} - \Delta C_{DB}) \tag{63}$$

As an example: When the effect of the increased roughness on the drag coefficient for the section at r/R = 0.7 is:

Table 2.12.2 : Drag coefficients of Rubert surfaces (Design = Rubert B) [112]

Surface	Design	Rubert D	Rubert E	Rubert F
C_D	0.00838	0.01003	0.01138	0.01206
% Increase		19.7	35.8	43.9

Colebrook and White (1937) and their comprasion with Nikuradse (1933) its's been concluded that the transition from a smooth to a fully rough regime is better characterized by the maximum roughness height, "k_m". They modified the roughness Reynolds number to take the following form based on maximum roughness height [27].

73

For smooth boundary layers, Given x (longitudinal distance along the boundary layer), some estimate for Ue, ρ, and μ , can be used to determine y values that give 30 < y+ < 0.1δ+ (x), which are usually accepted as valid values for y+ in the log layer [170].

$$C_f = \frac{0,455}{\ln^2(0,06\,\mathrm{Re}_x)} \tag{64}$$

Improving a roughness function Reynolds number of the propeller surface and a drag coefficient should be determined in the special tables are observed in literature especially for the lower "C_f" as a non dimensional coefficient. But there are very limited low coefficient correlation examples in literature which is determined. Therefore, for a specific surface, it should be determined with a computerized system which were based on turbulent flow requirement satisfcation. Correlative solution of the equations may improve a certain performance criteria for different vessels. Roughness-performance relation formulation is also widely different from each other. It seems that the acceptable formulation should be based on a towing test or a consumptional performance evaluation as engine manufacturer's apply.
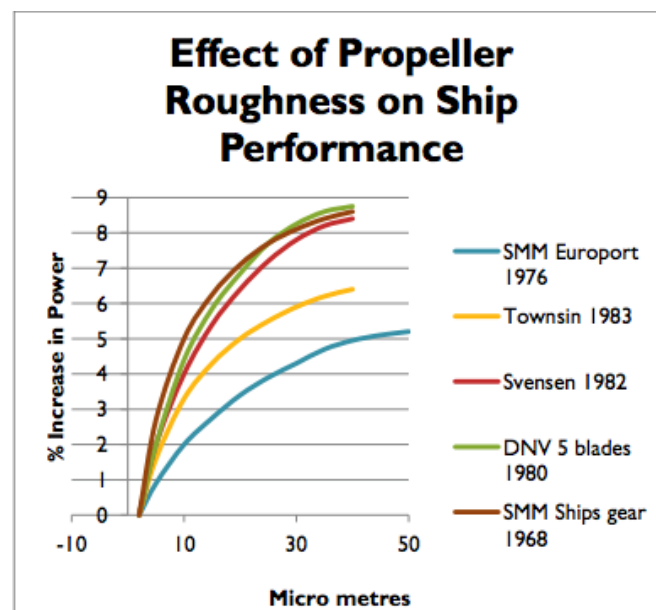
Figure 2.12.1: A Comparison Graph of Different Roughness Effectiveness Of Propellers Approaches [113]

74

2.13 Propeller Definitions and Inputs

This section completely based on [114] geometric definition reports which are simple and well-illustrated as 2D & 3D in different axes.

2.13.1 Basic Geometry of the propellers

1. *Diameter*: The diameter of the imaginary circle scribed by the blade tips as the propeller rotates.

2. *Radius*: The distance from the axis of rotation to the blade tip. The radius multiplied by two is equal to the diameter.

3. *Blade Face*: Pressure Side, Pitch Side. Aft side of the blade (surface facing the stern).

4. *Blade Back*: Suction Side. The forward side of the blade (surface facing the bow).

5. *Leading Edge*: The edge of the propeller blade adjacent to the forward end of the hub.When viewing the propeller from astern, this edge is furthest away. The leading edge leads into the flow when providing forward thrust.

6. *Trailing-Edge*: The edge of the propeller adjacent to the aft end of the hub. When viewing the propeller from astern, this edge is closest. The trailing edge retreats from the flow when providing forward thrust.

7. *Blade Number*: Equal to the number of blades on the propeller.

8. *Blade Tip*: Maximum reach of the blade from the center of the hub. Separates the leading and trailing edges.

9. *Hub*: Solid cylinder located at the center of the propeller. Bored to accommodate the engine shaft. Hub shapes include cylindrical, conical, radius, & barreled.

10. *Blade Root*: Fillet area. The region of transition from the blade surfaces and edges to the hub periphery. The area where the blade attaches to the hub.

11. *Rotation* : (Right hand is shown below) When viewed from the stern (facing forward): Right-hand propellers rotate clockwise to provide forward thrust. Left-hand propellers rotate counter-clockwise to provide forward thrust.
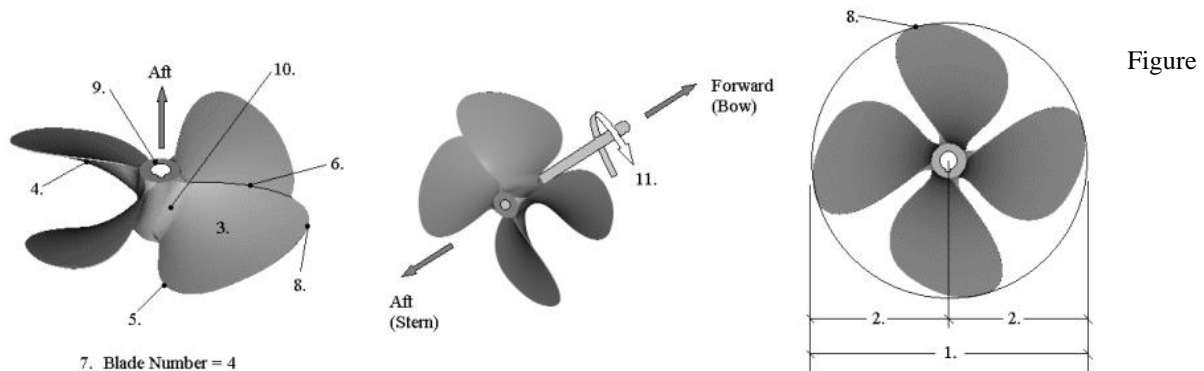
2.13.1.1: Propeller Geometric Definitives in 3 Axis [114]

2.13.2 Motional Geometric Elements of A Propeller:

1. *Pitch*: The linear distance that a propeller would move in one revolution with no slippage.

2. *Cylindrical Section*: A cross-section of a blade cut by a circular cylinder whose centerline is the propeller axis of rotation.

3. *Pitch Reference Line*: Reference line used to establish the geometric pitch angle for the section. This line may pass through the leading and trailing edges of the section and may be equivalent to the chord line.

4. *Geometric Pitch Angle, α*: The angle between the pitch reference line and a line perpendicular to the propeller

axis of rotation.

5. *Circumference*: A geometric property of a circle, defined as the linear distance equal to 2 x π x Radius. The length of the perimeter of the circle.

6. *Helical Line or Helix*: The corkscrew-shaped line traced by a fixed point on an object undergoing both rotational and linear motion.

76
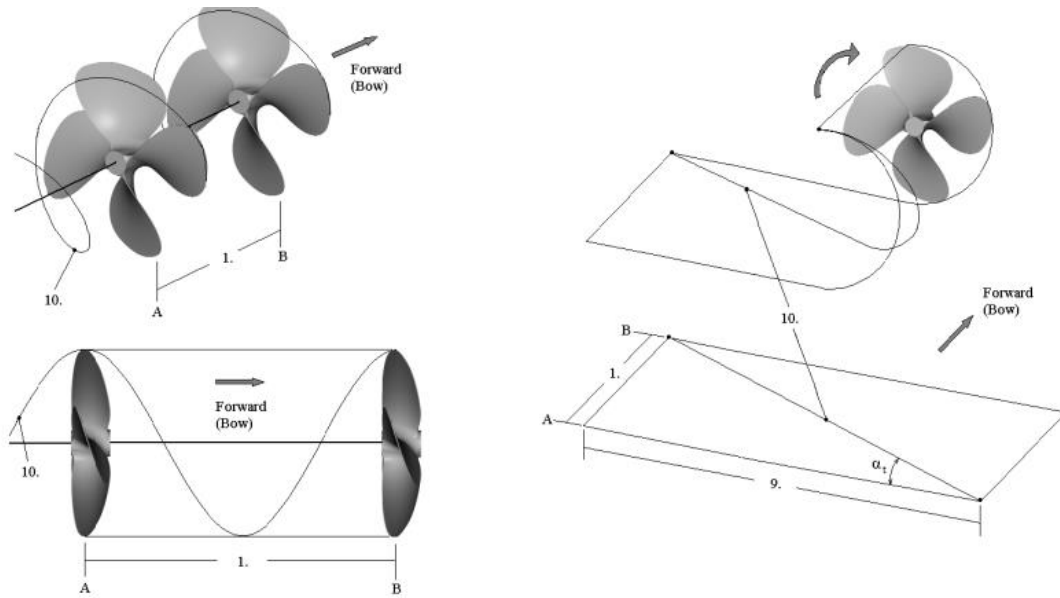
Figure 2.13.2.1: Propeller Motional Geometric Definitives in 3 Axis [114]

r_h = The radius of a cutting cylinder near the hub. The cylindrical section near the hub is located on the surface of this cylinder.

r_t = The radius of a cutting cylinder near the tip. The cylindrical section near the tip is located on the surface of this cylinder.
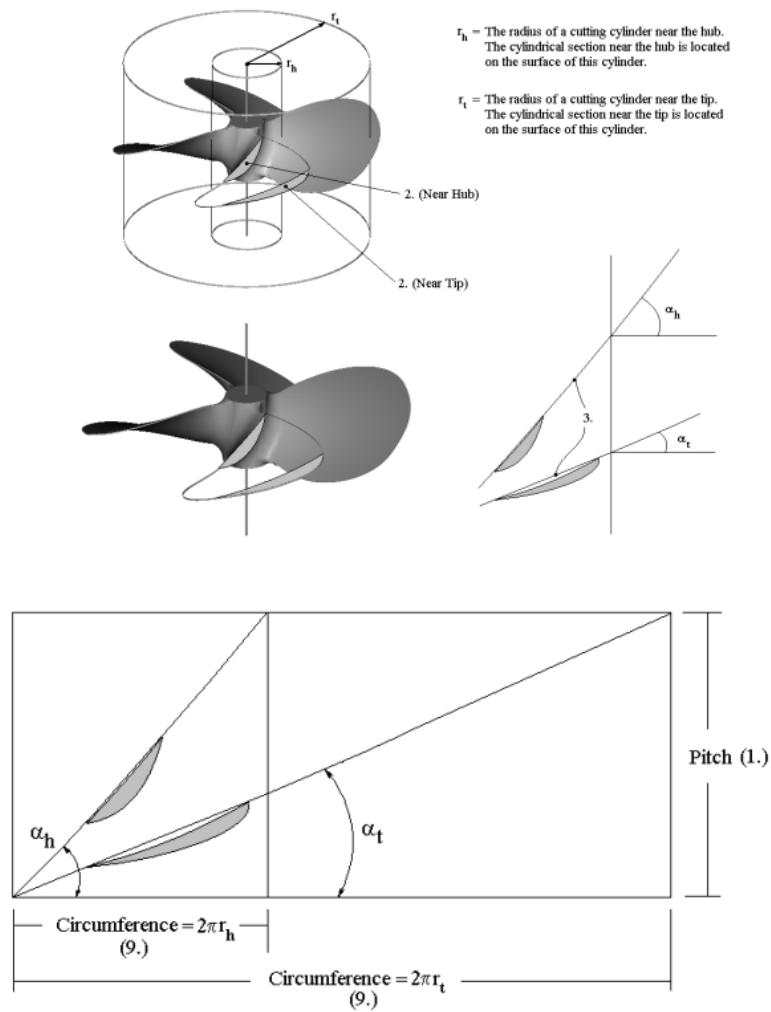
Figure 2.13.2.2: Pitch Definitive Relatives [114]

77

2.13.3 Skew, Rake and Cup Concepts of Propellers

1. Rake : The fore or aft slant of a blade with respect to a line perpendicular to the propeller axis of rotation.

1a. Aft Rake Positive Rake :Blade slant towards aft end of hub.

1b. Forward Rake Negative Rake :Blade slant towards forward end of hub.

2. Track : The absolute difference of the actual individual blade rake distributions to the other blade rake distributions. Always a positive value and represents the spread between individual blade rake distributions.

3. Skew : The transverse sweeping of a blade such that viewing the blades from fore or aft shows an asymmetrical shape.

3a. Aft Skew Positive Skew : Blade sweep in direction opposite of rotation.

3b. Forward Skew Negative Skew :Blade sweep in same direction as rotation.

4. Cup Small radius of curvature located on the trailing edge of blade.
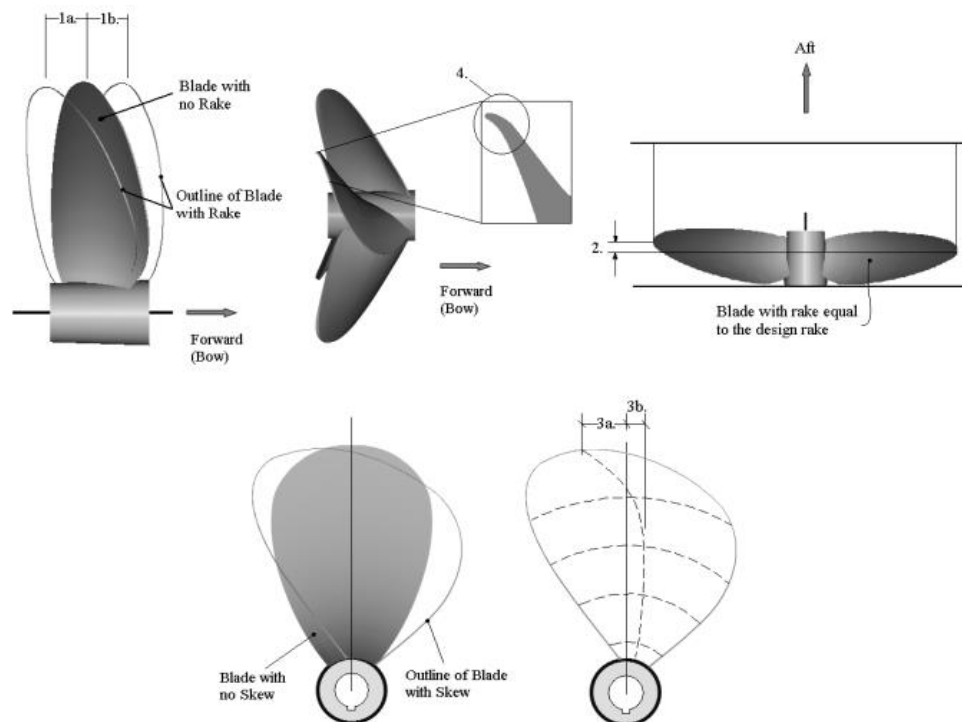
Figure 2.13.3.1: Skew, Rake and Cup Concepts [114]

78

2.13.4 Dimensional Effectives of The Propeller

1. Projected Outline The outline of the silhouette created on a screen just forward of the propeller, by a light directly behind the propeller, shining directly forward.

2. Developed Outline : An attempt to show the shape of the 2D body that would be attained by flattening a blade having zero thickness into a planar figure.

3. Expanded Outline : This is the outline created when the pitch reference lines of blade cylindrical sections are expanded (drawn as straight lines, not as a helix) and swung parallel to one another.

4. Disc Area : The area of the circle scribe by the blade tips.

5. Chord Line A helical line that connects LE to TE at a given radial location. In an expanded view, the chord line becomes a straight line and can be referred to as the nose-to-tail line.

6. Chord Length : The length of the chord line.
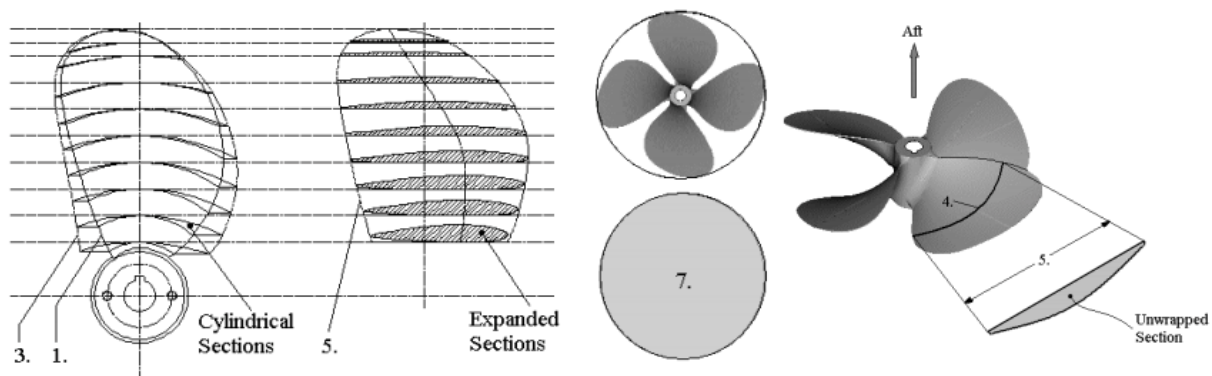
Figure 2.13.4.1: Dimensional Effective of The Propeller [114]

2.14 Optimal Propeller and Manufacturer's Finishing

The propeller placed on the stern of the ship is operating in a complex flow field. Hydrodynamic forces acting on the propeller produce fluctuating pressure on the hull surface. And hence, a designer of the marine propeller is trying to find a way to increase the efficiency without additional hydrodynamic energy loss such as cavitation [115].

An Optimized hull design represented in a parametric manner using a small number of variables, such as length, beam, and draft as well as other geometric characteristics, including the length of parallel keel and draft at the bow and stern. Constraints may be applied both to these variables and to other parameters. Results are shown for both monohulls and catamarans, in cases for which the constraints are largely inactive, for a large range of displaced volumes and forward speeds. These illustrate the hulls generated in the extreme case in which resistance is the only factor of interest [116].

Propeller design methods should satisfy vibrations with decreasing their forces and minimize pressure fluctuations caused by the hull with its pitch, wake, optimized area, and another compulsory divergence. Mainly there are three different propeller optimization approaches are used up to 2016. These methodic approaches are:

- Panel Method,

- Finite element method,

- Weak coupling of fluid-structure interaction (FSI) [117].

Panel Method, The geometry of wake surface changes linearly. The wake surface that is shed to downstream from trailing edge along the direction of the mean camber surface and its pitch are linearly changes to the average value of the geometrical pitch distribution of the propeller with respect to the rotating angle. Perturbation potential ϕ, potential-jump $\Delta\phi$ and are all assumed to be constants within each panel. Then, the integral equation can be written as liner equations:

$$
\begin{aligned}
&\sum_{j=1}^{N}(\delta_{ij} - C_{ij})\varphi j - \sum_{l=1}^{N_w}W_{il}\Delta\varphi l \\
&= -\sum_{j=1}^{N}B_{ij}(\vec{V}_0.\vec{n}_Q)
\end{aligned}
\qquad i = 1,2,....\ ,\ N \qquad (65)
$$

Where N and NW stand for the numbers of the panels on the propeller blade surface and the wake surface respectively, and δ is the Kronecker function.

B_{ij}, C_{ij}, W_{ij} are influence functions:

$$\left\{ C_{ij} = \frac{1}{2\rho} \sum_{k=1}^{z} \int \int_{S_j} \frac{\partial}{\partial n_l} \left(\frac{1}{R_{ijk}} \right) dS_j \right.$$

$$\left\{ W_{il} = \frac{1}{2\rho} \sum_{k=1}^{z} \int \int_{S_l} \frac{\partial}{\partial n_l} \left(\frac{1}{R_{ilk}} \right) dS_l \right.$$

$$\left\{ B_{ij} = \frac{-1}{2\rho} \sum_{k=1}^{z} \int \int_{S_j} \left(\frac{1}{R_{ijk}} \right) dS_j \right.$$

(66)

Where ; S_j and S_l are the surface panels on the propeller surface and the wake surface. R_{ij} and R_{il} are the distances from the boundary point on the ith panel to integration points on Sj and S_l [118].

Meanwhile, to overcome the panel method's shortcoming of not taking viscosity into account and added the viscous elements by combining the Prandtl–Schlichting law with the frictional resistance formula. The formula is

$$C_f = \frac{0,455}{(\lg R_e)^{2.58}}$$

(67)

The Reynolds number of the blade section is generally defined as

$$R_e = \frac{v_{r0} c_r}{v}$$

(68)

Determination of the Reynolds number by expression:

$$R_e = \frac{1}{v} \sum_{k=1}^{Nc} v_k l_k$$

(69)

Here to replace the conventional in the definition expression of Reynolds number. This is considered be able to include the effects of the geometry of the blade section and the non-uniform velocity.

Finite element method was a vectoral system in designed for a coordinate system basis. The blades are assumed to be made of homogeneous, isotropic and linear elastic material. [119]

Weak coupling of fluid-structure interaction (FSI) method was based on hydraulic effective force thru the blade that may deform the blade. It is a similar method to all of the possible interface coupling conditions and load transfer conditions among the structural mechanics, fluid dynamics, heat transfer, electromagnetic, and acoustics fields are discussed, and the resulted coupled equations are presented. The direct matrix assembly (DMA) method, direct interface coupling (DIC) method, multipoint constraint (MPC) equation-based, Lagrange multiplier(LM)-based, and penalty method (PM)-based strong coupling methods are proposed for different types of strongly coupled problems [120].
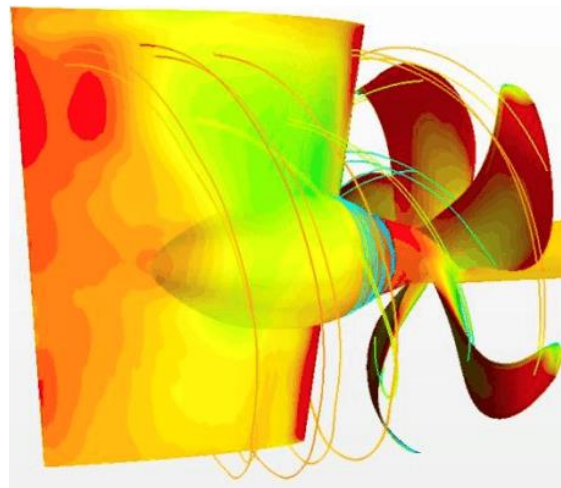
Figure 2.14.1: Effective Propeller Vortex [121]

ISO Surface finishing requirements are highlight manufacturer final limits for the surface tolerances. Classification societies observes related requirements accordingly. Propeller manufacturers tend to propose blades of great surface finish, even mirror-polished.

However achieving such surface finish increase manufacturing costs. Modern manufacturing means allow very smooth finish to be obtained while maintaining geometrical accuracy that hand-driven finishing can't assure [122].

Table 2.14.1: ISO Surface Finishing Roughness Limits [106]

Specification		Class " S "	Class " I "	Units
ISO R484	(1966)	3	9	μm(PVA)
ISO R484/1	(1981)	3	6	μm Ra
ISO R484/2	(1981)	3	6	μm Ra

2.14.1 Static and Dynamic Balance of Marine Propellers

No criteria for the amount of unbalance to be considered tolerable for ship propellers has been established. An approach to a perfect balance is difficult and expensive obtain, and as propellers undoubtedly distort under load in a manner to change the condition of balance, attainment of absolute balance in the shop seems unnecessary [123].

After the industrial revolution, a technological improvement was accelerated and attack such an idea of the previous century and even a thousand years has changed relatively long ago, and static and dynamic balance measurements of ship propellers are limited to international standards beyond being an inevitable experience of factories. On the other hand, although many propeller assembly personnel can understand punched differences in weight values, especially on separately mounted blades, the final forming is still doing by expert workers in many propeller factories. As the diametrical size and weight increases, these studies take a long period, but the accuracy of the results are even higher than most of the automation machining process tool.

Nowadays, propellers manufacturers and classification societies are using a common standard for the manufacturing and control process on marine propellers. Moreover, It also a discussion on the hydrodynamic characteristics of a propeller, and the general impact of main propeller characteristics on performance. The overall objective of the matching propeller and ship is to maximize the propulsive efficiency of the vessel [124].

The main phenomenon to consider is thrust losses caused by axial water inflow, the speedup of the water going into the propeller. The basic lift theory for propeller blade is well known indeed, but hydrodynamic literature concentrates on iterative design solutions for the propeller itself in a steady-state and does not provide the type of dynamic model of thrust and torque that is needed for control [125].

As the most common advisory in shipbuilding practice points that the complete propeller shall be statically balanced in accordance with specified ISO 484 tolerance class (or equivalent) in presence of a surveyor. Dynamic balancing shall be carried out for propulsion propellers with tip speed exceeding 60 m/s. The manufacturer shall demonstrate that the assembled propeller shall be within the specified limits [126].

In addition to increased vibration and noise losses, propeller dynamic balancing causes the increase of cavitation and cavitation effects, but also the increase of propeller shaft bearing loads, the deterioration of the oil film, the increase of friction belts, the improper performance plan between the propeller and the hull. It can be effective in such a way as to cause many other effects such as decreasing the vector sensitivity, decreasing propeller efficiency or even destabilization in sensitive hull design form which react instantaneously.

A Marine shafting system will experience a set of significant out of balance forces and couples if either the propeller becomes damaged so as to alter the distribution of mass or the propeller has not balanced before its installation. Large propellers ISO 484/1 defines a

requirement for static balancing mass "m_b" at the tip of the propeller is governed by the equation:

$$m_b \pounds \ C \frac{M}{RN^2} \ kg \quad \text{or } KM \text{ kg whichever is the smaller} \tag{70}$$

where;

M : Mass of the propeller (kg)

R : Mip radius (m)

N : Shaft speed/propeller speed (rpm)

C and K– ISO balance coefficients

Table 2.14.1.1: ISO Dynamic Balance Limits [106]

ISO Class	S	I	II	III
C	15	25	40	75
K	0,0005	0,001	0,001	0,001

2.14.2 General Divergents of Propellers losses

Effectiveness of propeller technologies that may vary from ship to ship is trying to recover % 40 of energy loss portion of the propellers other than the total energy loss. Where thinking of the possible efficiency of the propellers with 60 %, frictional losses become 15 %. All other losses on propellers such as axial and rotational losses are 25 percent [127].

Manufacturers and operator engineers use extra definitions for further subject losses for a propeller. One of the well-known is the propeller slip that needs to be calculated for the propulsive efficiency even daily, onboard. Propeller slip, too known as prop slip, maybe a

critical measurement that specifically influences execution. The only way to clarify prop slip is to think of a screw. Each time a screw makes a total turn, it has completed a "pitch." Pitch is the separate screw traveled during one complete turn. A propeller turns in much the same way conjointly encompasses a pitch. The issue is that water produces drag against the watercraft and propeller, so the propeller never really comes to its full pitch. With other technical wording, the difference between ship's theoretical speed (calculated from propeller or engine revolutions and propeller pitch) and the actual speed of the ship is known "*propeller slip*" and is usually expressed as a percentage of the ship's theoretical speed [128]. This is a propulsive loss caused by the motional fatal reality for a propeller-hull combination.

Propeller Vibration loss is another subject, occurs in a ship due to exciting forces causing natural for forced vibrations of the hull and it's contents. The exciting forces may be divided into those which are periodic and those which are transient forces are associated with the existing sea-pattern and resultant unsteady motion of the ship. These forces can be of very high levels, the forces resulting when the hull "slams" into the heavy sea or when the propeller partly emerges from the water during rough conditions, being two examples.

The periodic forces are associated with either propeller or the machinery of the ship. Such forces have fundamental components having proportion to the operating speed of the propeller or the engine with higher harmonics that is equal to multiples of this frequency [129]. Harmonic or non-harmonic vibrational forces could caused by transmission system such as gearboxes, shaft bearing clearances, lubricating oil insufficiency, vibration damper penalties, axial bearing penalties, torque limiting failures, engine direct combustion failures, static propeller misalignments or dynamic balancing problems.

Propeller Noise causes of the problem of pressure pulses are of great importance when a high level of comfort onboard is requested. This is obviously a stringent requirement for passenger ships and yachts, for which very low levels of accelerations are admitted, leading,

therefore, to the necessity of very low-pressure pulses. The problem of propeller radiated noise has been related for many years almost only to naval ship's requirements. Only recently, the concern about the effects that underwater noise emissions may have on marine fauna and particularly on marine mammals has increased [130]. Propeller noise is also an energetic loss in a viscous environmental with the dynamic characteristic of a propeller and can be expressed as Propeller Noise Loss.

According to the plane hydrodynamic motion concept, the noise has a spreading effect through the boundary layer by the propeller and transferred to the water plane surface and partially emitted. On the other hand, sound diffusion lines will be screened by the layer of the water and reflect back to the propeller surface with another part. Such reflection may brake the propeller vortex axis and disruptive effect on water flow.

Hub vortex is one of the problems with propeller performance. With the emerging vortex on the propeller hub, it will reduce the speed and decrease the efficiency of the blades. Not only reduces the performance of the blades, but hub vortex also erodes the rudder. The interaction between rudder and propeller creates several problems such as cavitation caused by low velocity of the vessel, periodic impact due to rotation of the blades to ship structure or rudder, undefined natural side force due to hydrodynamic loads [131].

Propeller tip and hub vortex dynamics in the interaction with a rudder. Hub Vortex loss is a critical penalty that may be corrected during the design of the dynamic propulsion consensus. Propeller ducts or the propeller fins are well-known correction solutions in the literature. Many problems arise in ship propulsion systems that can affect propeller performance and result in fuel consumption. Some problems in propulsion are cavitation and vortex. The vortex hub causes thrust decrease by 3% to 5%, thrust in the hub decrease by 2% and in the blade decrease by 2% to 3%. [132] Propeller boss cap fins are one of the solutions to decrease that effects but, the configuration of divergent cap used in PBCF does not produce

87

an increase in efficiency but decreases efficiency while convergent cap can produce an increase in efficiency [133].

For conventional propellers increasing the circulation in the outer portion of the span tends to increase the strength of the tip vortex and therefore reduce the cavitation inception speed [134]. Many of the experiments result and experience us that propeller cavitational effects may result in a tip erosion on the conventional propellers. During the design of the propulsor, manufacturers may choose tip loaded propellers to enforced tip vortex radial and axial forces. But also there are experiences to decrease disk area once the effect discovered. Tip vortex erosion effect is a loss of the propeller in both the short and long term. In the short term, propeller vortex will break wake fraction estimations and emerged with cavitation but also in the long term there is a high risk of erosion (Disk area loss) occurrence.

A linear effective erosion may only lead a disk area loss with a result of decreasing propulsive efficiency but it may damage propulsion plant with unstable speed coupling of propulsor and prime movers. On the other hand, there is another risk of overload because of thrust deductions. In this case, the wake fraction is responsible for a horizontal shift between the thrust coefficient (or torque coefficient) diagrams of open-water and behind hull conditions, so-called thrust (torque) identity definitions.

The thrust deduction takes account for the increase in the hull resistance due to the propeller operation (suction force at the stem), for its determination a detailed knowledge of hull resistance at different speeds is required. The thrust deduction 'produces' a vertical shift in the mentioned thrust coefficient diagrams when thrust identity wake fraction has been already identified [135].

2.14.3 Propellers Cavitation

As the pressure on the back of a propeller falls lower and lower with the increase in a propeller's "*n*", the absolute pressure at the back of the propeller will eventually become low enough for the water to vaporize and local cavities form. This phenomenon is known as cavitation. ("*Pv*" the vapor pressure of water)
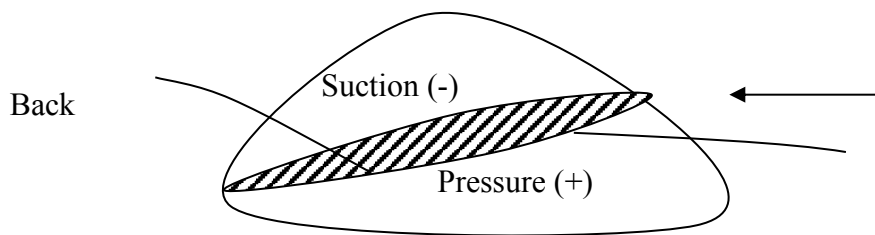
Figure 2.14.3.1 : Propeller Pressure Effective Directions [92]

The interaction between the propulsor and the hull, due to the irregular flow it is exposed to is a problem caused by the same or multiple variables. The cavitation occurs during radial movement with the increase of the propeller speed. The radial rotation pitch between the propeller and the hull or rudder, as well as the air bubbles formed by the differences between the suction and pressure surface columns of the propeller on a forward-moving ship, the pressure of the water in the condensation zone, pressure. Cavitation is seen much earlier. This is because microscopic particles and dissolved gases can also prepare the ground for cavitation.

In shipbuilding and operating practices, it is possible to cause damage to ship hull, propeller root, wing tips or rudder profiles as well as propeller-induced torque, momentary hydrodynamic thrust, vibration and noise losses, as well as affecting ship overall propulsive efficiency.

Cavitation effect in continuous flow, as a result of this abrasion, partial or complete of the propeller can be damaged but the attack caused by any single cavitation bubble can occur in very short time intervals by causing surface erosion. Although there are different methods

in the measurement theory, experimental methods such as acoustic measurement under water, trace surface simulation, propeller surface stain inking methods are also available. However, as the importance of separate and each of the propeller design theoretical parameters is important in the subject investigations, the cause-and-effect evaluation difficulty is inevitable due to the necessity to evaluate each ship hull design [92].

On the other hand, the hydrodynamics of the cavitation flow and the reaction of the material to the impact loading caused by the cavitation dispersion should also be considered. In a simple example, the final dispersion on one of the two extremes of cavitation recited in the propellers can be easily handled. For this point, there are pressure knocks and energy transfer to the material of the blade. Another extreme point is that the overall flow causes a severe disintegration. If this flow development is systematically understood, various cavitation formations can be diagnosed and prevented at an early stage. Cavitation on a propeller will lower the thrust of the propeller thus decrease its efficiency, cause vibration of hull and the propeller. Generates an uncomfortable noise, cause erosion of the propeller blade.

The cavitation is most likely to occur at the tips of blades where the relative velocity is the largest and the hydro-static pressure is the lowest when blades rotate to the highest position. It can also occur near the roots where blades join the boss of a propeller because the attack angle is the largest [55]. For better understanding such definition of "mean thrust loading coefficient" in viscous environment:

Mean thrust loading coefficient:

$$t_c = \frac{T}{\frac{1}{2} r V_R^2 A_p} \tag{71}$$

Where,

ρ : Density of the water

T : Thrust

A_p : Project blade area

V_R :The relative velocity at 0,7 R of a propeller and

$A_p / A_D = 1.067\text{-}0.229\ ^P/_D$

$$V_R^2 = V_A^2 + \left(2\rho \times 0.7 R \times n\right)^2 \tag{72}$$

However, the exposure of propeller surface geometric activity due to surface erosion caused by hydrodynamic principles in the way of movement of the hull. Other resistance factors associated with it may develop indefinitely in the direction of decreasing or increasing, while corrosion, electrolysis, component bio-fouling, such as kinetic changes, magnetic field, and component thermodynamics, is an effective element that can initiate or increase cavitation with the onset of surface-dependent form changes.

A cavitation bubble that will move from the surface of the propeller in dynamic motion due to the deteriorating surface geometry. On the others hand, bio-foulers may interfere with another bubble or other bubbles in a viscous volume or making a more effective bubble read by combining it, even if it is planned to defect, or it may move to another point. In consideration of very few propellers used in world maritime fleets are designed in such a way that cavitation does not affect the propeller disc. It is a fact that not all propellers will undergo cavitation wear. However, as described above, cavitation wear occurs when the bubbles circulate the wing as a result of passing through a fixed cavity or breaking directly from fixed cavitation. Correct abrasion from cavitation without semi-constant or constant changes in surface hydrodynamic geometry or carry it anywhere on the blade.

Propeller cavitation may usually be experinced on three major propeller location: The tip with the highest rotational speed is the region corresponding to the radius of 70% of the

radius where the load is maximum, and the blade roots where the wall thickness is high and the pressure distribution is affected due to the small gap between the blades [136].
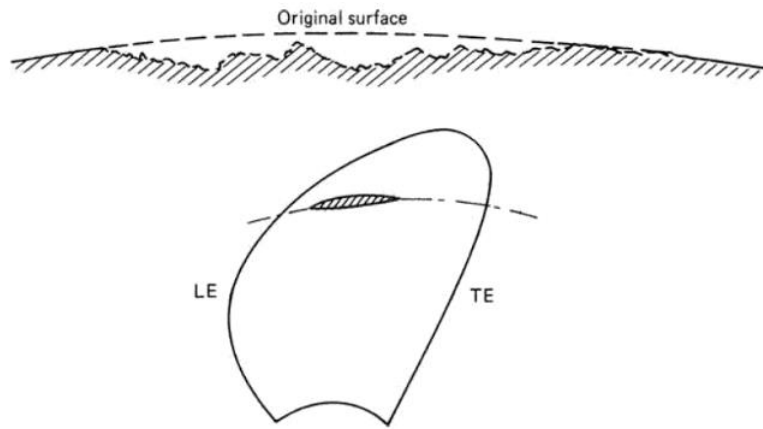
Figure 2.14.3.2 : Typical cavitation Damage Profile [92]

In this study, the micro-scale effect showing different propagation and density on the pieces placed at different depths can increase the cavitation effects easily if it is permanent at the point where it is in dynamic rotation. However, it may easily provide a protective surface in terms of surface damage at the points where the blade thickness is high, it can produce a facilitating effect in carrying the cavitational another effect to the blade tip on its region where the tension is high. The convective form in water cells may cause surface shapes that may cause unexpected breaks in the propeller's natural vortex or deletions in viscous vortex beams.

This hydrodynamic fact can increase the actual viscous resistance as well as alter the direction of the flow of the damped track resistance reflected from the hull. Although it is seen in the experiments and investigations that material surface erosions occur primarily at the points where the cavities explode, erosion does not usually effective at the starting points of the cavities. That is, a bubble and stain cavitation are more effective in material wear than sheet cavitation. Because the rate of formation of the wear varies, but in some exceptional cases serious material damage can occur within a few hours, while in other cases wear can occur in months or years.

Damages due to cavitation may be variable / circulating layer cavitation, stain-like vortex, scattered beam center, cavitation rotating to stain-type, vortexing from corners or ends, vortexing as stains, foamy root cavitation, stem vortex cavitation ending as a stain. Considering the change in surface geometry of the biofouling effects, foaming and foaming layer cavitations may occur, which may exhibit effects close to the descending edge, or may form layer cavitation near the rising edge, and may also form stains.

When the findings of many studies are reviewed, it is seen that the common point in the formation of cavitation is layer cavitations. It must be noted that the circulating layers are not always severely degraded, and the presence of circulating cavitation does not always seem to be a sufficient condition for various wear. In abrasion, of course, stain cavitations play a more important and dominant role. For example, some cavitations on the pressure side of the propeller are formed reliefs without damp. Since these cavitations are always considered harmful, it is imperative to carry out a full-scale, subject-ship and propeller-specific research to find actual answers.

Pressure fluctuations on the blades resulting from biofouling can vary greatly depending on the variable surface geometry. This may result in the need to increase the rounding radius of the rising corners, as well as the sudden change in load distribution. It may even be necessary to make changes to the shaft and / or curvature and to soften the agitated corners to correct the result after docking. Such phenomena, which may even require a change in the number of blades, should be handled in an extended manner for irregular surfaces as a safety factor in propeller designs [137].

Propeller cavitation can cause damage to the propeller's own structure or may develop due to layer cavitations on the rudder, partly due to the flow of the propeller and partly due to the irregular flow to which the rudder is exposed. Cavitation from the tip and hub vortex in the direction of the impeller flow is even more important. Interaction between hub cavitation and

pressure around the rudder is also important. Damage caused by abrasion occurs when small bubbles explode near the rudder as a result of vapor filling. Generally, the problem occurs in half-submerged rudders as gap and descending edge damage, which results in increased maintenance and repair costs. In rudders that have not been subjected to propeller cavitation, cavitation-related wear is usually associated with ± 5 ° angular movements during the course of the course, and the effects increase as ship speed increases.

Under normal conditions, different types of cavitation occur in rudders: bubbles, soles, cavities. In addition, there are cavitations caused by the propeller tip vortex, the biofouling, and the hub vortex. The cavitations of biofouling origin that are the subject of this study should be defined as a result of surface discontinuities themselves.

Evaluation theories of fluid mechanics for a potential cavitation factor can not be high-lighted in results of the experimental approaches. But Reynolds-averaged Navier-Stokes equations (RANS) are the most active analysis which may give effective and confident results for both in turbulent and non-turbulent flow applications except when the time average is not equal to zero and exposes calculations and equations by multiplying speed profiles. During biofouling increment, on surface movement points, newly created surface profiles in terms of deep and relatively shallow points in the vortex setup, the average velocity difference distorts the vortex effect which may also exhibit laminar behaviors according to the place, leading to the formation of the following vibration and noise echoes.

At this point, considering that eddy viscosity will also deteriorate, the effectiveness of RANS will increase even more. Because it converts viscous effects and vortex effects which are the source of irreversibility into a structure that can be expressed mathematically in terms of each other. It is evident that the turbulence density will significantly deteriorate with biofouling at the point where the diffusion rate and intensity factors of the turbulence are handled together.

Formulation of the equation [138] :

$$\frac{\partial \overline{U}_i}{\partial t} + \overline{U}_j \frac{\partial \overline{U}_i}{\partial x_j} = \frac{\partial \overline{P}}{\partial x_i} + \frac{\partial}{\partial x_j}\left[\frac{1}{R_e}\left(\frac{\partial \overline{U}_i}{\partial x_j} + \frac{\partial \overline{U}_j}{\partial x_i}\right)\right] + F_i \qquad (73)$$

Where F_i – body force

Vector components of the thrusting and swirling components of the body force:

$$F_i = \frac{f}{rU^2 / L} \qquad (74)$$

2.14.4 Fuel Economy and Propeller Roughness Penalty

In an assumption of the world, even as only a planet, has chosen nature to shield itself to meet the needs of the population and to survive, energy and fuels that are suffered at the intersection of rapidly depleting resources. It is noteworthy that the fossil fuel sources are depleted, as well as the reduction of its use due to the harmful consequences of consumption, as dinosaur tears of the desperate population. The reason of this idea may be evaluated that the countries use a sustainable relative energy sources produce the technology of these types of energy also. But these countries that produce and export the fossil fuel consumption technology products such as automotive products and marine diesel engines which is the largest engines as total fuel consumptions, since the first diesel engine of Rudolph Diesel [139].

Since the periodic changing of international raw materials and end product traffic, there are difficulties in access to resource, common strategic resource battles and weak character of shrinking economies. The biggest obstacles for ship operators to produce any strategy rather than change their strategies, it is important to sign a freight contract that satisfies the shipowners

95

existing situation and during this millennium, which they are trying to turn every option they can into an opportunity.

Under the pressure elements, any other business in the world is subject to operating criteria and the variability of the conditions which it is obliged to comply cannot be compared with the maritime sector. For example, it is normal to have research, development and adaptation processes to produce a new product in a factory established to produce a fixed product range. The adaptation of the ship's business to processes that change in seconds is a real challenge that requires strength and high flexibility because of unknown breakdowns, weather forecast changings or saving observations for fuel or time relatively.

It's better to clarify the situation with a recent example and in discussion of the impact of the 2008 financial crisis on the maritime sector as well as in the world's other markets. The well-known financial and economic crisis of 2008 had almost overnight suppressed the growth of the container-ships market. In fact, for the first time in the history of the maritime industry, growth has stopped and there is even a steady decline in the rate of containers shipped around the world. In the first six months of the year of the crisis alone, the shipping industry declined by close to 16% causing huge losses [140].

The crisis caused by the re-payment of ship owner's loans with their high interests taken to the newly building ships until 2008 and bankruptcy of stake-holder maritime companies coming to the point of the world have turned the vessels. It could have been many times more valuable than the value of the goods, into a consumption machine that produces valuable and daily expenses. The major risk factors for a shipping company's balance sheet are the value of its vessels on the asset side and its financing costs on the liability side. Where speaking of a 'crisis in shipping' when simultaneously observed an extreme asymmetric adverse movements

of both balance sheet risk factors, a sharp decline of freight rates and a strong increase in financing costs.

The dependence of these two factors is modeled by the main drivers of supply and demand for shipping services [141]. These are the world fleet and the world economy, respectively. For the aim of our study, it is important to note that only the supply of transportation services can be controlled by market players like shipping companies by ordering new vessels or scrapping old ones. Moreover, shipping investors can decide whether to lend money for new vessels or not and at which rate. These measures could have prevented the shipping crisis. Therefore, consideration of freight rates are suitable instrument to observe price risks in the shipping market [142].

The fuel consumption is the primary driver for operational expenditures, and it is directly linked to carbon dioxide emission, which is one of the greenhouse gases. Thus, in an optimization study, it is sought to select the engine of the least specific fuel consumption. Moreover, predicting the amount of fuel to be consumed in a journey is essential to design the fuel supply system. These are some of the reasons why the prediction of specific fuel consumption is relevant and addressed herein [143].

The total annual world's marine fuel demand is in excess of 400 million tons, with a projected 2020 demand exceeding 500 million tons. The larger containerships (4,000 TEU and greater) account for approximately 20 percent of all marine fuel demand. Fuel costs typically represent more than 50 percent of the total running costs for a ship and are increasingly becoming the focus for improvements in order to gain a market advantage [144].

World oil demand growth, 2018-2024

mb/d

● China   ● India   ● Middle East   ● Rest of the world

Marine bunkers product demand, 2015-2024

mb/d

IEA. All Rights Reserved

● Unscrubbed HSFO   ● Scrubbed HSFO   ● MGO   ● VLSFO
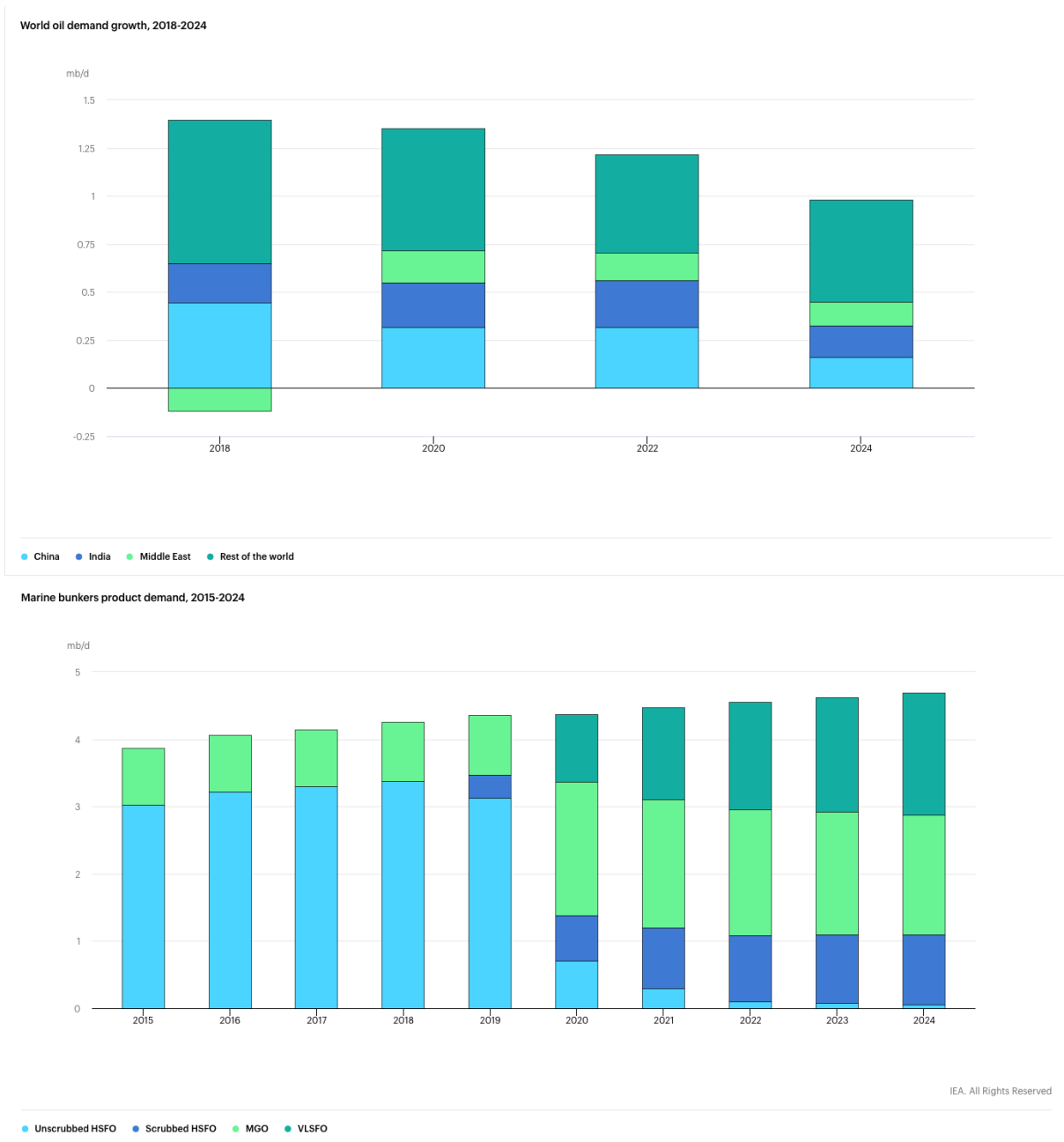
Figure 2.14.4.1 : World's Regional Oil Demand Growth Graph and Marine Bunker's Product Demand [145]

United Nations Conference on Trade and Development (UNCTAD) expects international maritime trade to expand at an average annual growth rate of 3.5 percent over the 2019–2024 period, driven in particular by growth in containerized, dry bulk and gas cargoes. However, uncertainty remains an overriding theme in the current maritime transport environment, with risks tilted to the downside [146].

Bunker prices in major bunkering hubs

USD per metric tonne

Prices are quoted on 18 December 2019
Source: BIMCO, Marine Bunker Exchange (MABUX)
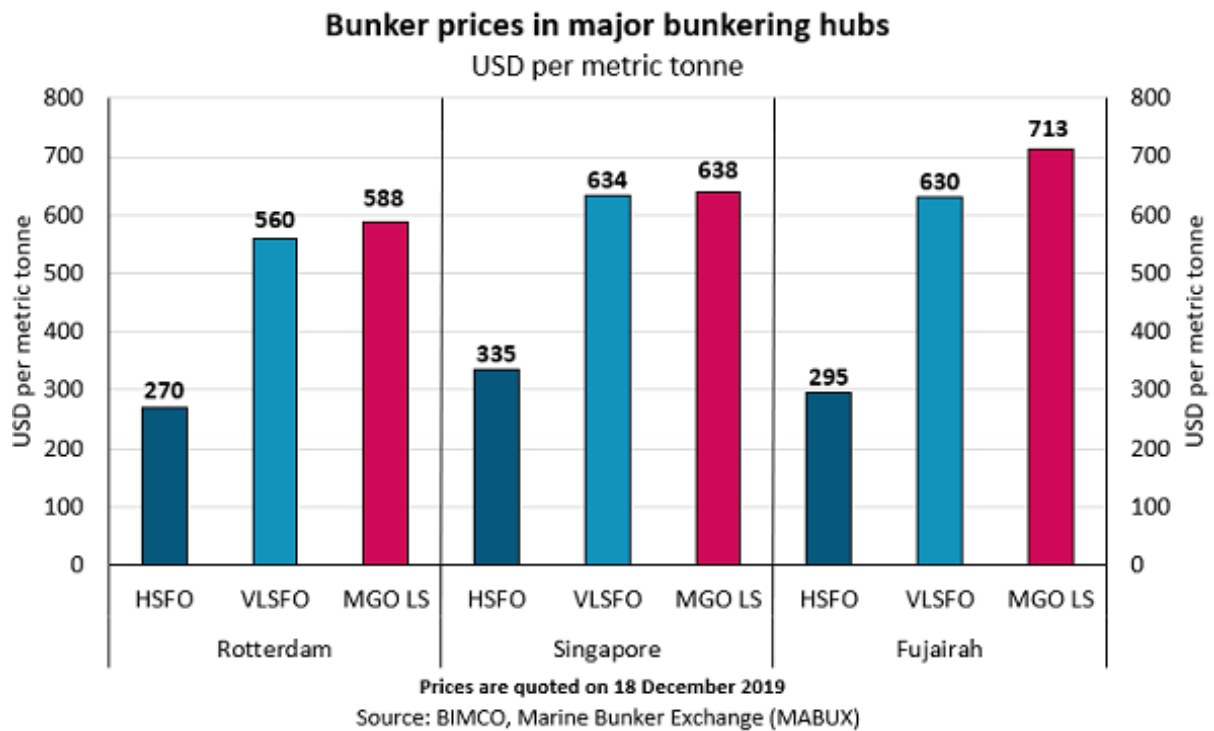
Figure 2.14.4.2 : Bunker Prices In Major Bunkering Hubs On The To Share Market Insights In Malaga,Spain and Amsterdam,Netherlands, World (BIMCO) [147]

At this point, the critical issue of marine trading's risky phenomenon will be the fuel costs and their surcharges in the close future in regard to these demands. Moreover, the section into the drive of the IMO 2020 control raises fresh challenges for the shipping industry. Potential issues may incorporate an increment in working fuel costs and cost instability, and a lessening in supply capacity and vessel accessibility. Any extra costs may have an effect on the cost to be paid by conclusion clients, as carriers will look to pass on expanded costs to shippers through different shapes, counting modern bunker surcharge formulation.

As a preface of marine diesel engines fuel consumption, in emission criteria TIER II-TIER III, it is mainly in a pattern of 140-185 g/kwh for 4 Stroke diesel engines according to ISO criteria. Credential, fuel consumption concept has relative indexes of efficiency factors of a propulsion system in the maritime sector. Therefore, the challenge is always inevitable. New regulations and their compliance and improvements in the sector brought different solutions to the engine manufacturers. Different makers are trying to decrease engine produced losses with

the removal of camshafts and similar attachments or using logical controllers for the fuel systems which is widely effective in use on fuel injection systems. On the other hand, improvement of the engine combustion volume is another credential with its narrow piston diameters but longer stroke lengths. On the other hand, improving the charge air efficiency is another method to decrease potential exhaust emissions but also engine power outputs. It's been known that speed controlled electro-turbines are in experimental product lines. Electrical propulsion systems are another improvement line that's a precession because of the alternative solution against cost-effective risks of International Maritime Organization (IMO) straight regulations which is applicable only to new buildings.

Not only in theory but also, in fact, the vessel's efficient propulsive energy utilization is under the effects of many different compulsory resistance factors which is expressed in previous sections of this study. In literature, the fuel consumption of an engine for a combustion engine described with the locution: Specific Fuel consumption (SFC). Specific fuel consumption definition was described with the general theory of thrust generation, the operation of any mechanical engine requires chemical energy to be converted into mechanical energy, typically by an intermediary conversion to thermal energy. In conventional piston and jet engines, the chemical energy stored in the fuel is consumed in an exothermic chemical reaction (via combustion) that adds considerable thermal energy to the air, rapidly increasing pressure or volume. The change in these states is then used to move the mechanical elements of the machine. It is a serious crucial for an engineering experience to compare the efficiency of different power plants by the definition of fuel consumptions as the quantity of fuel burned in a unit time (lbs/hr, kg/min, etc.). This is sometimes referred to as fuel flow determination. Definite specific fuel consumption *(SFC)* is as the quantity of fuel burned in unit time required to produce a given engine output. SFC is a technical figure of merit that indicates how efficiently the engine converts fuel into power [148].

The volumetric method of fuel consumption measurement was employed for fuel mass flow estimation according to the formula:

$$Vfc = \frac{V_p \cdot r_p}{t}$$

(75)

Where;

V_{fc} : Fuel mass flow [kg/s],

V_p : Fuel volume consumed during the measurement time [m3],

r_p: Fuel gravity in measurement condition [kg/m3],

t : Time of measurement [s]

For fuel mass flow estimation, the engine fuel oil system standard instruments were used - main engine fuel oil flow meter equipped with temperature gauge. Fuel oil analysis receipt will be utilized as the source of fuel oil basic data for further calculations. The fuel oil gravity temperature correction factor will be calculated accordingly. The specific fuel oil consumption of main engines calculated, based on the formula:

$$Sfc = \frac{Vfc}{P_{eff}}$$

(76)

Where;

Sfc : Specific fuel consumption [kg/kwh],

Vfc : Fuel mass flow [kg/hr],

$Peff$: Engine effective power [kw]

Recalculation for standard ISO condition will be provided according with the accepted standards (149).

According to reference datas' integration, manufacturers use standard corrections for related factors to calculate specific fuel-oil calculation which is based on a determination:

$$Sfoc = (Consumed\ fuel\ oil) - (leak\ oil)$$

where; *MGO quantity in supply line and other incidentials as leak oil.*

Correction factors are taken for ambient conditions such as ambient temperature, charge air temperature before cylinder, ambient pressure, lower calorific value (*LCV*), any attached pumps with their power consumption, exhaust gas back pressure by engine manufacturers. On the other hand a safety tolerance and extra correction factor for MGO because of ignition delay [150].

In a propulsion system, fuel consumption propulsive efficiency definitions are faced with a common point of view thrust. On engine side with the integrity of the propeller shaft energy-train mentioned via a torque (T_{tq}) . Relation between P*eff* and T_{tq} can be estimated as "kw" with in formula:

$$P_{eff} = \frac{T_{tq}.\rho.n}{30} \tag{77}$$

where;

T_{tq} : Mean measured torque [kNm],

n : Mean engine-propeller rotational speed [rpm]

In this study propeller shaft torque and propeller torque will be correlated in the equation below for an open water efficiency to reach propeller thrust and skin resistance with ignorance of stern-tube and shaft bearing's penalties:

$$T_{tq} = Q \tag{78}$$

$$Q = V_A(1 + a)A_0 \tag{79}$$

Background of the mathematical definitions for a propeller:

Propeller Froude number $\rightarrow F_r = \dfrac{V^2}{gD}$ (80)

Reynold's number $\rightarrow R_e = \dfrac{VD}{v}$ (81)

Propeller advance coefficienct $\rightarrow J = \dfrac{V}{nD}$ (82)

Thrust Coefficient $\rightarrow K_T = \dfrac{T}{rn^2D^4}$ (83)

Torque Coefficient $\rightarrow K_Q = \dfrac{Q}{rn^2D^5}$ (84)

Open Water Efficiency -> $h_0 = \dfrac{P_T}{P_D} = \dfrac{TV}{2\rho Qn} = \dfrac{K_T r n^2 D^4 V}{2\rho K_Q n^2 D^5 n} = \dfrac{K_T r D^3 R_e}{2\rho K_Q D^4 vn} = \dfrac{K_T r R_e}{2\rho K_Q Dvn}$

(85)

Specific fuel consumption - > $Sfc = \dfrac{Vfc}{P_{eff}} = \dfrac{30Vfc}{T_{tq}\rho n} = \dfrac{30Vfc}{Q\rho n}$

(86)

Where; $K_T = K_Q / D$

$$h_0 = \dfrac{K_T r R_e r n^2 D^5}{2\rho QDvn} = \dfrac{K_T r^2 R_e n D^4}{2\rho Qv} \triangleright Sfc = \dfrac{60Vfch_0 v}{TrR_e}$$

(87)

Where; $T = Q / D^2$

$$Sfc = \dfrac{60Vfch_0 v}{TrR_e} = \dfrac{60Vfch_0 vD^2}{QrR_e}$$

(88)

According to the equations' correlation between shaft torque (T_{tq}) and Specific fuel consumption (Sfc) in way of Propeller's Reynold's coefficient (R_e) and Open water efficiency (h_0) On the other hand, where propeller's Reynold's coefficient changed as ΔR_e, an estimated specific fuel oil consumption and open water efficiency will also change. When the propeller's R_e is a coefficient is directly related to propeller's roughness certainly, expected specific fuel consumption (Sfc) should change in a different status. Finally, a statement where the propeller frictional coefficient with relatively, Reynold's coefficient changed a ship can not consume the same quantity of the fuel for the same distance or same distance can not be complete with the same quantity of fuel.

2.14.5 Exhaust Gas Emission Limits And EEDI In Related Propeller Roughness

Diesel fuels commonly used in marine engines are a form of residual fuel, also known as dregs or heavy fuel oil (HFO). They are cheaper than marine distillate fuels but contain a higher amount of nitrogen, sulfur and ash content. This significantly increases the NOx and SOx in the exhaust gas emission. The diesel engine combustion process almost always leaves by-products of oxides of nitrogen, unburned hydrocarbons, carbon monoxides and particulate matter [151].

According to current estimates presented in this Third IMO GHG Study 2014, international shipping emitted 796 million tonnes of CO_2 in 2012, which accounts for no more than about 2,2% of the total emission volume for that year. By contrast, in 2007, before the world's economic downturn, international shipping is estimated to have emitted 885 million tonnes of CO_2, which represented 2.8% of the world's emissions of CO_2 for that year. These percentages are all the more significant when considering that shipping is the principal carrier of world trade, carrying as much as 90% by volume and therefore providing a vital service to global economic development and prosperity. In 2011, IMO adopted a suite of technical and operational measures that together provide an energy efficiency framework for ships. These mandatory measures entered into force as a 'package' on 1 January 2013, under Annex VI of the International Convention for the Prevention of Pollution from Ships (the MARPOL Convention). These measures address ship types responsible for approximately 85% of CO_2 emissions from international shipping and, together, they represent the first-ever, mandatory global regime for CO_2 emission reduction in an entire industry sector [152].

The entry into force of several world's environmental instruments and voluntary standards being adopted in the sector has also had an impact on shipbuilding and shipyards, as they are responsible for incorporating new standards into the design and construction of ships. Pressure on the industry to develop cleaner and energy-efficient vessels is increasing.

Certification schemes are being introduced, and considerable investment is going into the development of better hydrodynamics, more energy-efficient engines and low-carbon fuels for ships.

In an explanation with an example, trade and development price differences between natural gas and low-sulfur fuel oil suggest that an economic advantage may favor the use of natural gas. In addition, natural gas infrastructure has been growing, rendering ships fed by natural gas more plausible [153].

The new IMO 2020 regulation, bringing the sulfur cap in fuel oil for ships down from 3,50 percent to 0,50 percent, is expected to bring significant benefits for human health and the environment. Related regulation has entered into force at the date of 1 January 2020. Enforcement, compliance with and monitoring of the new sulfur limit is the responsibility of states party to the International Convention for the Prevention of Pollution from Ships (MARPOL), 1973, as modified by the Protocol of 1978 (MARPOL 73/78), annex VI. Ships found to be not in compliance may be detained by port State control inspectors, and/or sanctions may be imposed for violations. An additional amendment to MARPOL 73/78 is going to enter into force on 1 March 2020. The amendment will prohibit not only the use but also the carriage of non-compliant fuel oil for combustion purposes for propulsion or operation on board for a ship unless it is fitted with a scrubber, which is an exhaust-gas cleaning system. [146].

In detail of IMO Criterias based on Greenhouse Gas (GHG) protocol defines other factors to be mentioned in the revised target settings. Definition of the emission factors of IMO criteria can be expressed in a group of oscillation as complete pollutants: Fuel based CO_2, fossil fuel CH_4 ingredient, combustion fuel output N_2O, cooling refrigerants HFC, Fire-fighting foam-based aqua film-forming foam PFC, not-expected gradient of compressed gas cylinder contaminations SF_6, Combustional compound of nitrogens in the environment NO_x,

106

non-methane volatile organic compounds of unburned fuels NMVOC, an emission global constant fort he incomplete combustion CO, particulate matter of incomplete combustion PM, mainly petroleum-derived combustion sulfur SO2 and other sulfur compound SOx.

On the other hand, researchers, designers, and manufacturers have targetted their applicable rehabilitation for further emission factors at the output. In theory, alternative energy source discoveries and bio-fuel consumption were assessed for the conventional trading vessels. All available rehabilitation resulted in the spread last ten years. In shipping practices, applicable rehabilitation are engine modifications or new designs, propeller upgrades, speed reductions, optimization of water flow and weather routing and other energy efficiency applications such as lighting and rotatable equipment optimization are the major potential applications. On the other hand, ship owners and the operators may have very limited but preferential critical options such as hull cleaning, coating, and propeller polishing.
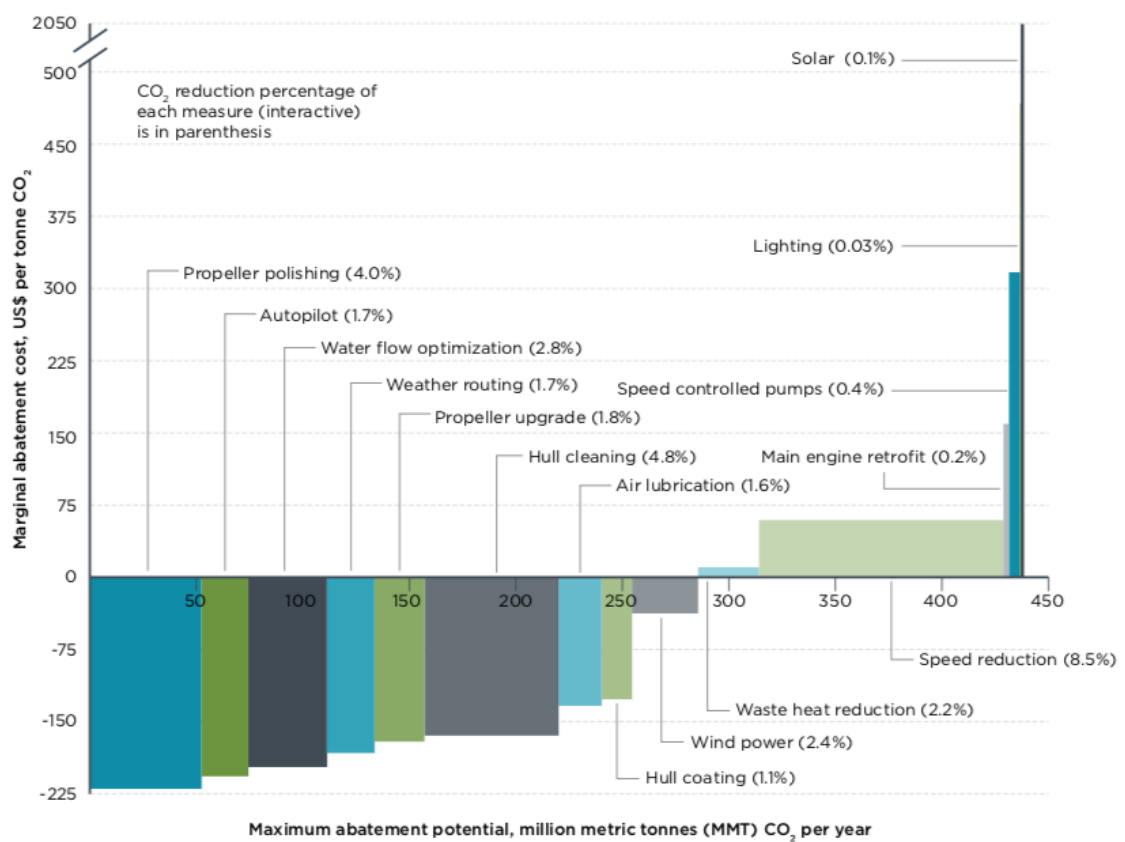
Figure 2.14.5.1: Marginal CO_2 abatement costs of analyzed technologies [154]

On the other hand, in a comparison of potential improvements with their cost-effective intentions, goals are still limited. Because of the purpose differences of the trading mechanism of the world's fleet and their resistance and operational criteria have different outputs to reach certain targets. For instance, speed reduction and weather routing are not an option for a cruise vessel because of it's trading mental. In another preface, relatively fast vessels as operations such as container vessels and tankers, propeller upgrading methods do not efficient as they are for general cargo vessels or bulkers because of their sensitive propeller born-design objectives.
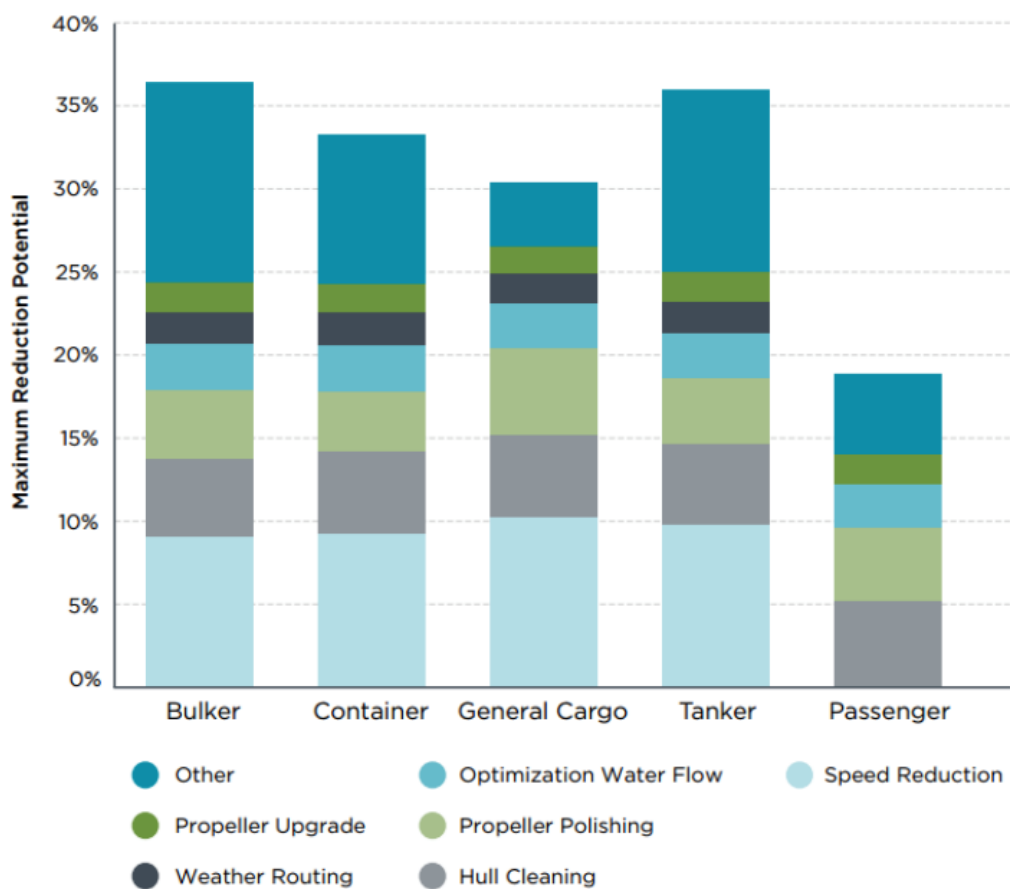
Figure 2.14.5.2 : CO_2 Reductions of technical and operational measures by ship types. [154]

The projection of the future emissions of maritime shipping requires the projection of future developments in the fuel efficiency of the fleet. In the period up to 2030, recognition between market-driven efficiency changes and changes required by regulation, i.e. energy efficiency design index (EEDI) and ship energy efficiency management plan (SEEMP).

according to resolution MEPC.203[62] and document MEPC 66/WP.10/add.1, the attained EEDI of new ships built after 1 January 2013 must be at or below the required EEDI for that ship. the required EEDI is calculated as a percentage of a reference line that is specific to ship type and size. the reference line is the best fit of the estimated index values (a simplified EEDI which is calculated using default factors for specific fuel consumption and auxiliary engines and does not take ice class or fuel-saving technologies into account).

Overtime, the distance to the reference line must increase. Implementation of the regulation is now applied to the world's fleet as the first two of the phases according to the plan until the deadline of 31 of Dec.2019 [155].

Since the 1930s, diesel engines were invariably 4-stroke and ran on distillate fuels rather than residual fuels. Nowadays, very big 2-strokes diesel engines with their better power-to-weight ratio are in use for large vessels. Mostly high-speed 4-stroke diesel engines are rarely met on conventional trading ships are regularly used for propulsion but increasing. On the other hand, dual-fuel engines are in use rarely and tri-fuel engines are in trial stages. It's a fact that the major subject of the greenhouse gas emission concern is combustion based pollutants and their reductions as a synthesis. On the other hand, it should be noted that marine gas oils have higher specific energy implying lower specific fuel consumption when using them [156].

Exceptionally, decreasing fuel consumption may only tolerate emissions effectively in an existing situation or in the period of implementation to use other conventional energy sources on board vessels. With the same approach of specific fuel consumption decreasing methods, it is also possible to reach an estimation of emission deductions on propulsion engines. Consumption perspectives and estimations of the regulatory bodies are mostly quantitative methods of consumed territorial or sectoral divergence for reaching a final output.

Because, fuel type, ship's operational activity mode, Engine age and use of emission reduction technologies should be in consideration and categorized. But technically, statement of a relation between specific fuel consumption based on consumed fuel flow and characterized emission output. According to studied estimations, specific fuel consumption is related to roughness an assumption in the formulation:

$$\text{Specific fuel consumption} \rightarrow Sfc = \frac{Vfc}{P_{eff}} = \frac{30Vfc}{T_{tq}\rho n} = \frac{30Vfc}{Q\rho n} \tag{89}$$

Where ; $T = Q / D^2$

$$Sfc = \frac{60Vfc\eta_0 v}{Tr R_e} = \frac{60Vfc\eta_0 vD^2}{Qr R_e} \tag{90}$$

The definition of the stated results will be deteriorated will be compared with the emission factors with the engine power approach. [157]

Table 2.14.5.1: [157]-Emission factors based on Engine Power and Consumption

Gas Component	HFO (ME)	MDO (AE)
CO_2	620	690
CO	0.5	0.8
SO_x	9	1.7
NO_x	18.1	11.8
PM	1.3	0.4

Emission factors gas compund/Engine Power approach g/kWh

Gas Component	HFO (ME)	HFO (AE)	MDO (AE)
CO_2	3179	3179	3179
CO	2.545	5.727	3.687
SO_x	46	46	8
NO_x	87.136	52.673	54.182
PM	6.667	2.203	1.843

Emission factors gas compound /Consumption approach kg/tonfuel

2.15 STATEMENT OF THE PROBLEM

Ship resistance is a very broad concept that includes many active physical resistances. It is a concept index that requires relative approaches with its problems requiring solutions from almost all areas of engineering sciences. Although the loss coefficients seem the same as all other engineering losses because of the massive energy consumption volume, the problems that need to be solved also require relative perspectives due to the variable nature and environments. MARPOL Annex VI regulation has been implemented and amended 3 times since 1997. On 2020, that is as the end of 3th phase, sulphur content limit of ships' fuel oil is 3.50% m/m was finalized and 0.50% m/m limit is on due after 1 January 2020. Today, major subjects of rehabilitation is taking serious actions and solutions to decrease these penalties and prevent these losses. In this study, one of the very complicated but also critical consensuses of ship resistance concept will be examined and evaluated in an experimental approach to find answers to the subjects below:

i-) In the period of long anchorage biofouling process grow in the port limits in shallow waters aggressively. Definitives of this effect in port of Kyrenia is the first subject to be addressed.

ii-) Effects of biofouling on ship's hull is a subject, well-known by the researchers, scientists and sector population. However, propulsion effects are needed to be determined with more experimental approaches.

iii-) Propeller resistance due to biofouling should be well studied because of direct effect to the prime movers and their consumptions.

iv-) Bio-fouling and emission subjects should be cross-evaluated for the ships anymore. Visible anecdotes should be open to discussion.

v-) Bio-fouling effect is not only the subject of operators and ship owners but also authorities and governments indeed.

3. MATERIALS & METHODS

3.1 MATERIALS

The choice of materials in all engineering branches in the production stages is always a fundamental issue and brings it many problems. In particular, the requirements for surface shaping and subsequent re-formations extend the repertoire in material selection. Considering the effects of such subsequent operations on the economic life of the material and the economic operational requirements that are the most important instrument of the repertoire.

"It is been stated that there are 40.000 to 80.000 different material option in the field of engineering. Improvement of new generated international standards precession tries to reduce this number. On the other hand, new materials are inventions" [159].

3.1.1 Tested Propeller Material and Composition

Because of corrosion resistance, erosion effect, cavitation, abrasion, high surface strength, surface sensitivity requirement, material weight limitations can only be satisfied using a wide range of alloys based on steel, nickel, aluminium, bronze and stainless steel in all aspects with high using rate. Single casting, semi-casting and welded joints are in use of products as well as bolted jointing techniques for the controllable pitch propellers (CPP)There is a material selection amplitude that expands as the size decreases from elastomers to reinforced polycarbonates or even compressed waste materials.

Even there are solutions with low hydrodynamic friction and high propulsive efficiency on new generation propellers, in this study, it has been used one of the most common material composition according to spectrometric analysis 22.May.2018 @ manufacturer lab. Metaller Dünyası San.ve Tic.ltd.Şti and material were graded according to German Standards DIN En1982 2 1502CuSn12.

Table: 3.1.1 Spectrometric analysis applied with PMI Master – Pro (Calibration cert. No: 118926)

	Cu	Zn	Pb	Sn	P	Mn	Fe	Ni
Average	87	0,31	0,657	11,6	0,662	<0,0030	0,0139	0,28
	Si	Cr	Al	As	Ag	Bi	Sb	
Average	0,0099	<0,0020	<0,0020	<0,0200	0,0429	<0,0100	<0,0500	%

Physical and mechanical properties of the material in the DIN Norm:

Density: Approx. 8600 kg/m^3

Melting Point: 830-1000 °C

The specific heat at room temperature: 355 kg.grad

Thermal conductivity coefficient at room temperature: 54 grad

The thermal expansion coefficient at room temperature: -18

The limit of tensile strength: 360 Mpa

Tensile elongation : % 7

Brinell Hardness: < 81

This material is a hard material with high abrasion resistance, suitable for high wear rates. It is corrosion resistant in seawater and is resistant to surface pressures as well as impacts. It is especially suitable for parts subject to friction wear and is resistant to cavitation according to the closest international standards are the EN1982, ASTM B505 C90700 and DIN 1705 CuSn12 According to surface finishing requirement of the manufacturer's workshop, part's are N1-N2 according to (ISO) Class roughness details with the limit Ra = 0,025-0,2 (where 0,02 < N < 0,30)

3.1.2 Tested Material Size And Areas

Table : 3.1.2.1 Dimensional Details Of The Test Material
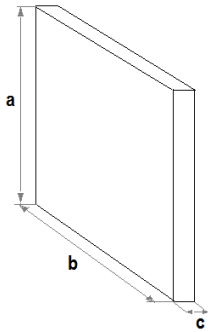
	Dimension in "mm"			Area (without c)	
	a	b	c	mm2	m2
Part ID No:1	145.2	140	11	20328	0.2033
Part ID No:2	146	140	11	20440	0.2044
Part ID No:3	145.2	140.8	11	20444	0.2044
Part ID No:4	145	140.3	11	20344	0.2034
Part ID No:5	145	139.6	11	20242	0.2024
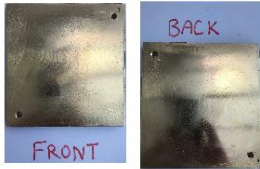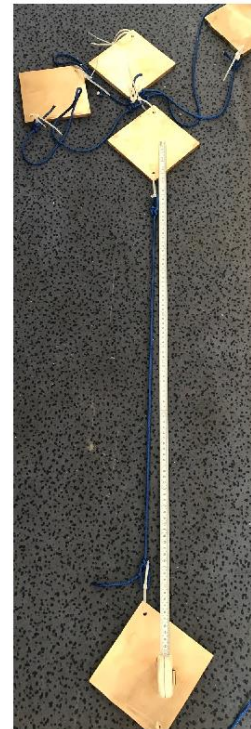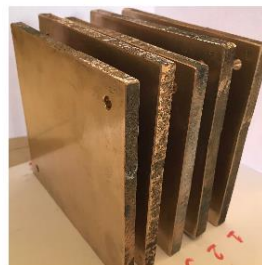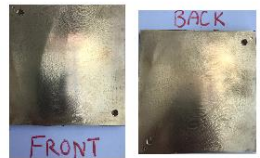
Figure 3.1.2.1 : Materials were used in the experiment before installation

3.2 METHODOLOGY

3.2.1 Methodologic Flow Chart
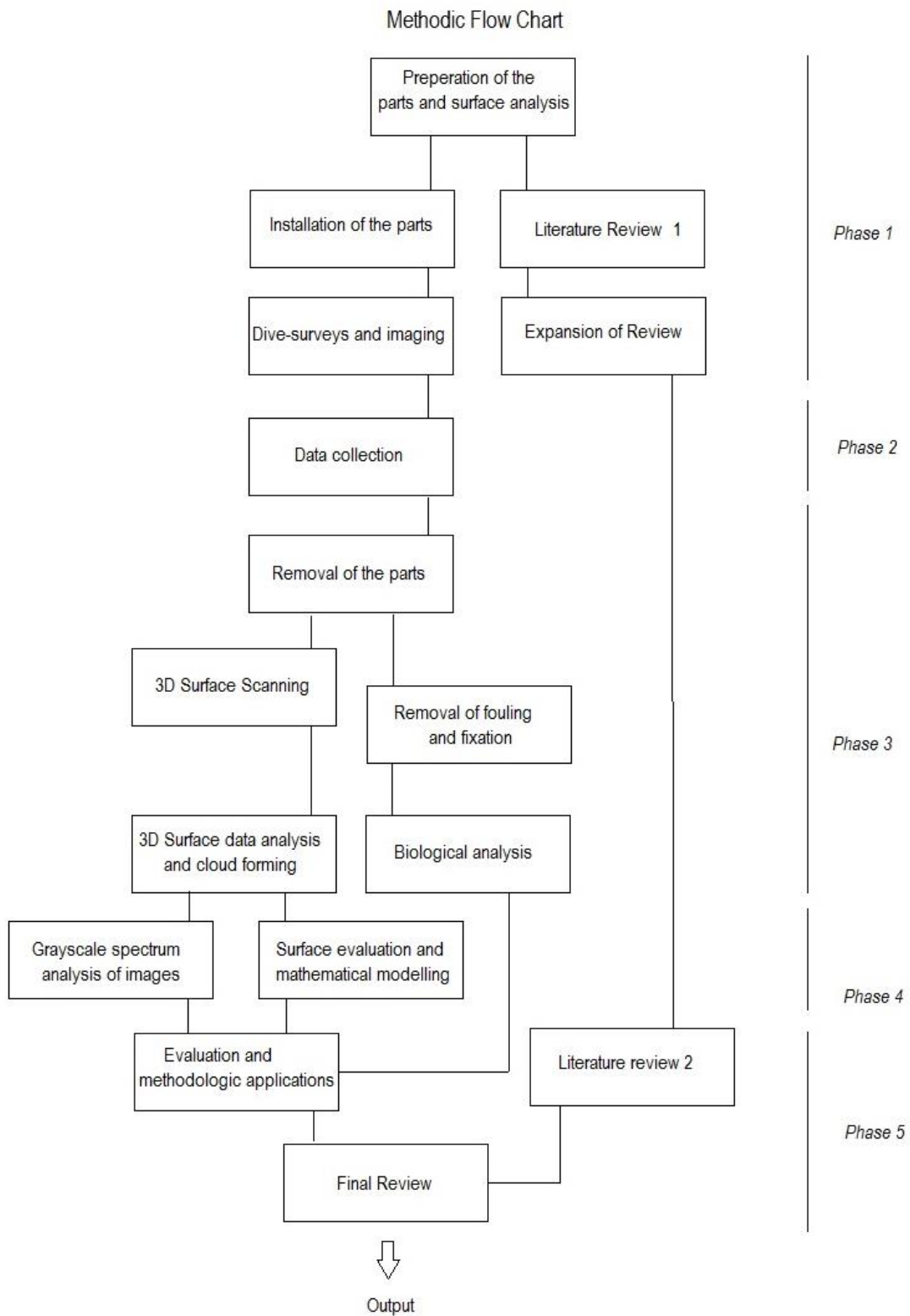
Figure 3.2.1 : Methodic Flow Chart Of The Study

3.2.2 Qualitative Methods

A qualitative research method is defined as the general limits, reactive feedback is questioned by the external evaluator within the limit values, which can be evaluated as a standard deviation out of the limit values, efficiency and feedback between the general use of a stream of methods to use more efficient arrangement. The scientific approach does not contain boundary lines or content numerical values but can produce numerical transformations in the analysis phase of the activity audit. If the efficiency of the limit values increases, the standard deviation is relative and the research may have to change the structure in an approach or may lead to the explanation of the results with the usual principles. However, the effectiveness of the assessment as well as the efficiency can be present and the rational expression of the result is a scientific method of evidence even for complex subjects to determine.

This study contains technical but non-numeric quantitative methods of time series approaches of image collections and data collected during repeated surveys underwater. Preliminary assessment of these data trans-progress to another elective approach by the way of algorithmic-based computer technologies. The final assessment contains supportive quantitative other approaches to reach certain determinations.

3.2.3 Photographic Undetermined Time Series Analysis

Normally, undetermined time series apply to very long experimental applications to conduct another determinative approach. Feedbacks of the method are substantially nonlinear. Models are mostly used in social sciences in literature. Linearity testing and estimation of nonlinear models, both parametric and nonparametric, are considered as well as post-estimation

model evaluation. Data-based nonlinear model building is illustrated with an empirical example [160].

In this study, non-regular control periods of the surfaces applied and data collected for photographic qualitative evaluations during the experimental period.

3.2.4 Photographic spectrum analysis /Digital Grayscale Spectrum Analysis

Based on Newton's prism experiment in 1666, colour spectrometry has enabled the development of doppler and sonar technologies [161]. The colour ranges between black and white trans-changed to the visual colour definition and it's super-changed to the pixel level extremely thru surface quality identification. Due to possibilities of imaging in thousands of meters to deep seas to photometric surface sensitivity measurement, now this technique enables the measurement of surface area for enlarged differences in the shades of grayscale by placing in pixels.

As is known, digital images can be saved as grayscale images that even contain grayscale formations in colour images. This is because each pixel has brightness regardless of its colour. Brightness may also be defined as brightness or density, which can be measured on a scale from zero density black to full density white. In this way, most visual file formats support $2 \wedge 8$ or 256 brightness levels per pixel and a minimum of 8 bits of grayscale. Moreover higher pixel formations may contain a spectrum of more than 65000 levels of luminance [162].

In this study, digital grayscale spectrum analysis used to generate a visual define accuracy of areal biofouling engagement in time series. In the experimental flow process, the grayscale transformations of the underwater images that are taken during the visual control period were compared with the surface areas of these test pieces. This control method does not force a conclusive idea in terms of topographic elevation and possible friction connection on the surface in terms of diffusion and propagation velocity in the two-dimensional space on the

surface of the test parts but expresses that the surface is transforming from the previous plane area to another field structure.

Adobe Photoshop is one of the more effective devices accessible to researchers nowadays. It is crucial within the planning of advanced pictures of examples for estimation, particularly for isolating important highlights from foundation detail. Logical Imaging with Photoshop is the definitive direct to the utilize of Photoshop in logical investigate, with an extraordinary accentuation on the moral repercussions of the utilize of an image-enhancement computer program to extricate information from computerized pictures. "In the fall of 1987, Thomas Knoll, a doctoral candidate in computer vision, was trying to write–as a diversion from his doctoral–computer code to display grayscale images on a black-white bitmap monitor." The existing release was improved and adopted with his brother John Knoll [163].

3.2.5 Fuzzy Logic-Based Histogram Equalization

The theory of histogram modification of continuous real-valued pictures is developed. It is shown that the transformation of grey levels taking a picture's histogram to the desired histogram is unique under the constraint that the transformation is monotonic increasing. Algorithms for implementing this solution on digital pictures are discussed. A grey-level transformation is useful for increasing visual contrast but may destroy some of the information content. It is shown that solutions to the problem of minimizing the sum of the information loss and the histogram discrepancy are solutions to certain differential equations, which can be solved numerically [164].

Fuzzy logic-based histogram equalization (FHE) is proposed for image contrast enhancement. The FHE consists of two stages. First, a fuzzy histogram is computed based on fuzzy set theory to handle the inexactness of grey level values in a better way compared to

classical crisp histograms. In the second stage, the fuzzy histogram is divided into two sub-histograms based on the median value of the original image and then equalizes them independently to preserve image brightness. The qualitative and quantitative analyses of proposed FHE algorithm are evaluated using two well-known parameters like average information contents (AIC) and natural image quality evaluator (NIQE) index for various images. From the qualitative and quantitative measures, it is interesting to see that this proposed method provides optimum results by giving better contrast enhancement and preserving the local information of the original image.

The experimental result shows that the proposed method can effectively and significantly eliminate washed-out appearance and adverse artefacts induced by several existing methods. The proposed method has been tested using several images and gives better visual quality as compared to the conventional methods [165].

In this study, histogram modification technique has been used to the generic definition of the biofouling spread on the studied surfaces. Underwater imaging is a difficult technique to use as a quantitative method because of environmental variables such as shadows, daylight contrast, motional foaming effect, underwater currents, digital imaging shuttering and optical focusing difficulties. But grey-scale histogram is a modification on the image to eliminate factors of the combined effects. On the other hand, it's a transfer method of photographic spectrum analysis qualitative method to assessable quantitative method normally. In most of the cases, accessible transfer output has been extensive other proofs to reach certainty. The subject study improves predictions with another qualitative definition inside the biological analysis.

3.3 Quantitative Methods

Quantitative methods have a huge scope of different numerical based data collecting and analysis approaches. It's applicable both data collection or data analysis is possible with wide ranges and convertible feedbacks and outputs. Due to the wide range of data collection and comparison function, these scientific methods are accurate, reliable, suitable for forecasting and basis on a visible causality. Complex numeric data analysis and regular or irregular data processing is applicable and compatible with other computerized methods or easily integrate other models and repeatable verification option exist.

In this study, it's inevitable to apply these methods because of complex data uncertainty. Applicable data needs to be transferred to other analysis of methodic substances.

3.3.1 Hybrid geometric measurement with a non-contact method

3D laser scanning developed during the last half of the 20th century in an attempt to accurately recreate the surfaces of various objects and places. The technology is especially helpful in fields of research and design. The first 3D scanning technology was created in the 1960s. The early scanners used lights, cameras and projectors to perform this task. Due to limitations of the equipment, it often took a lot of time and effort to scan objects accurately. After 1985, they were replaced with scanners that could use white light, lasers and shadowing to capture a given surface. Next is a brief history of the 3D scanning development.[166]

One of the first applications was capturing humans for the animation industry. By the mid-nineties, they had developed into a full-body scanner. In 1994, 3D Scanners launched REPLICA - which allowed fast, highly accurate scanning of very detailed objects. Meanwhile, Cyberware were developing their high detail scanners, some of which were able to capture object colour too, but despite this progress, true three-dimensional scanning - with these

degrees of speed and accuracy - remained elusive. While these optical scanners were expensive, Immersion and Faro Technologies introduced low-cost manually operated digitisers. These could indeed produce complete models, but they were slow, particularly when the model was detailed. The solution was accurate, fast, truly three dimensional, capable of capturing colour and realistically priced [167].

In this study, Faro ATM EDGE 9FT 7 axis model:14000 was used to scan fouled experimental materials in the Gunsel production facility in Near East University Campus. Submerged material carried to facility uninterrupted seawater contact to keep possible biofouling activity and surface profile as same as in the viscous environment. Removal of each part from the sea-water and surface scanning were a continuous process. After the scanning process, all surfaces were scraped carefully and obtained contaminations fixed separately with alcohol 99% purity in 5 different, disinfected bottles to deliver biological laboratories of Institute of Marine Sciences of Middle East Technical University/Turkey.

3.3.2 Photometric modelling, computer-aided of 3D measurement

Rhinoceros is a 3D imaging and modelling program developed by Robert McNeel & Associates based on non-uniform rational B-spline (NURBS) mathematics and supporting the many kinds of file format including the *STL format. Another major advantage of the Rhinoceros program, which is used in many areas such as reverse engineering, is that many plugins can be used in computerized rhinoceros functional path. Rapid prototyping and some animational reproductions and visualization applications that use faceted approximation instead of NURBS surfaces to represent 3D free form objects, Rhino also provides a set of polygon mesh tools.In this study mesh units were not used for improved numbers of points cloud.

Making NURBS surfaces usually requires a set of curve frameworks. Therefore, Rhino has a set of curve tools. To enable modification and improvisation of surface models, Rhino incorporates a comprehensive set of editing, transformation, and analysis tools. Apart from that, it has tools for outputting 2D engineering drawings and highly photorealistic rendered images and animations [168].

In this study, 4.3.31 version of mesh2surface, which is a reverse engineering add-on for rhinoceros 5 and rhinoceros 5, was used. The reason for using this version is that the segmentation is easier for deviation analysis and this version is more stable. Because the scanned files are detailed, the average file size is around 1.70GB. The used computer was boosted by overclocking due to the freezing of the computer when doing analysis of large files and the log analysis process. The processor lock (CPU warning temperature setting in the bios) is fixed to 95°C to prevent the physical damages during overclocking, taking into account the voltage and T-junction bond. At the same time, the maximum operating frequency of 3.50 GHz is taken into consideration while the processor is boosted.

The part to be analyzed has been imported into rhinoceros program in *STL format. The file of the imported is placed on a plane in the segmentation section which is under the mesh2surface plugin, and this plane is created into Rhino. The maximum peak point and minimum pit point were found with the deviation analyzer under the Mesh2surface plugin. The length between the maximum and minimum points was determined by the dimension property in the rhino program.

3.3.3 Computed Mathematical Model, Linear And Non-Linear Equations, Closure Approximations

The majority of interacting structures in the actual world is distant too intricate to a mannequin in their entirety. Hence the first phase of compromise is to become aware of the most essential components of the system. These will be covered in the model, the relaxation will be excluded. The 2nd stage of compromise issues the quantity of mathematical manipulation which is worthwhile. Although arithmetic has the attainable to show universal results, these outcomes rely severely on the structure of equations used. Small modifications in the shape of equations may additionally require vast adjustments in the mathematical methods. Using computer systems to deal with the mannequin equations may additionally by no means lead to stylish results, however, it is plenty greater sturdy towards alterations.

A model which makes use of a giant quantity of theoretical facts commonly describes what occurs at one stage in the hierarchy through thinking about approaches at decrease tiers these are referred to as mechanistic models, due to the fact they take account of the mechanisms thru which modifications occur. In empirical models, no account is taken of the mechanism by means of which adjustments to the device occur. Instead, it is only cited that they do occur, and the mannequin tries to account quantitatively for modifications related to extraordinary prerequisites. Both math and their algorithms are the definite parts of the world's population's simple subjective necessities and inevitable objective of science millennium.

In this study, due to critical point of the sensitive engineering measurement on surface metrology is an essential part of the project and underwater surface composite which can't be kept for a long period at the out of the surface should only be examined by ordinary differential equations and eigenvalue problem solutions. Tolerance of the surface shape could only be regenerated on computerized advances. Measurement and physical analysis of approaches are only possible with complex equations to realize their effects, understanding of regenerative and

suggestive optimized solutions to the core problems. Computerized equations and analitic model will be based on Microsoft Office Professional Plus Excel (2016)

3.3.4 Biological Taxonomic Group Analysis and Quantification

Taxonomy in biology is the method of inserting organisms into comparable groups based totally on particular criteria. A taxonomic analysis is consequently an analytical process that effects in a set-up of classes and that describes their relationships. In a taxonomic analysis, the centre of attention is on figuring out the relationship between wholes and components. Determining priorities for taxonomic lookup and improvement of the approach will facilitate bridging the clearances amongst compilers, further researchers and implementers of taxonomic information, and streamline the taxonomy-conservation obstacle.

In this study, taxonomic group analysis is only used to pre-identify the groups of organisms concerning the biofouling as technically. But on the other hand, Cypriot fauna is at the middle of significant geographical positions, as a part of the East Mediterranean Sea is in a between Atlantic Ocean, Black Sea and the Red Sea. On the other hand, Levantine Basin between Cyprus and Turkey has been one of the widest continental shelf areas along the Eastern Mediterranean [169]. So that experimental results of this project is feasible to re-apply or open for improvements. Because Cypriot underwater species are in circulation in different geographic currents and oceanic seasonal re-circulations.

In the period of the experiment, aggressive biological growth as a dominant mechanism may consist of different other variables and results in different periods or locations around of Cyprus.

4. RESEARCH RESULTS AND EVALUATION

4.1 Application of The Experiment

In the following sections a study has been applied according to the planned methodic flow chart: Figure 3.2.1.

4.1.1 Periodical Diving Surveys, Output and Fouling Spread Rating of Analysis

During experimental period, it has been applied 5 control and underwater imaging dive conducted at the dates of: 14.6.2018/ 26.6.2018 /9.7.2018 /24.7.2018 /9.8.2018. There are applied more dives for general conditional control and experimental safety. These images were taken via GoPro Hero4.

On these dives, it's been used a diving computer Suunto D4i with integrated temperature sensor. Last approved manufacturer maintenance date was 26.04.2018/Turkey.

Table 4.1.1.1: Photometric Dive Control Day Details

Diving Date	Time	Depth of Temp.(m)	Temp.(^0C)
14.6.2018	16:14	4,9	28
26.6.2018	16:10	4,6	28
9.7.2018	15:57	5,0	28
24.7.2018	14:27	4,7	29
9.8.2018	11:37	4,9	29

		ACTIVITY	DIVE MODE	DIVE TIME	MAX DEPTH	MAX DEPTH TEMP.
6 Time	0,7 m Depth		Nitrox	0:07'32	4,9 m	28 °C
-- No dec time	28 °C Temperature					
-- Ceiling	Nx 21 Mix					

Tissue Saturation ■ N₂ ■ He

Fast   Slow

		ACTIVITY	DIVE MODE	DIVE TIME	MAX DEPTH	MAX DEPTH TEMP.
15 Time	1,3 m Depth		Air	0:09'16	4,6 m	28 °C
-- No dec time	27 °C Temperature					
4,6 m Max depth	-- Ceiling					

Tissue Saturation ■ N₂ ■ He

Fast   Slow

		ACTIVITY	DIVE MODE	DIVE TIME	MAX DEPTH	MAX DEPTH TEMP.
10 Time	1,9 m Depth		Air	0:08'27	5,0 m	28 °C
-- No dec time	28 °C Temperature					
5,0 m Max depth	-- Ceiling					

Tissue Saturation ■ N₂ ■ He

Fast   Slow

		ACTIVITY	DIVE MODE	DIVE TIME	MAX DEPTH	MAX DEPTH TEMP.
6 Time	1,3 m Depth		Air	0:06'01	4,7 m	29 °C
-- No dec time	29 °C Temperature					
4,6 m Max depth	-- Ceiling					

Tissue Saturation ■ N₂ ■ He

Fast   Slow

		ACTIVITY	DIVE MODE	DIVE TIME	MAX DEPTH	MAX DEPTH TEMP.
0 Time	1,4 m Depth		Free	0:03'48	4,9 m	29 °C
31 °C Temperature	1,4 m Max depth					

Figure: 4.1.1.1 Dive-days Poscture

4.1.2 Photographic Spectrum Analysis/Digital Grayscale Spectrum Analysis of the Surfaces
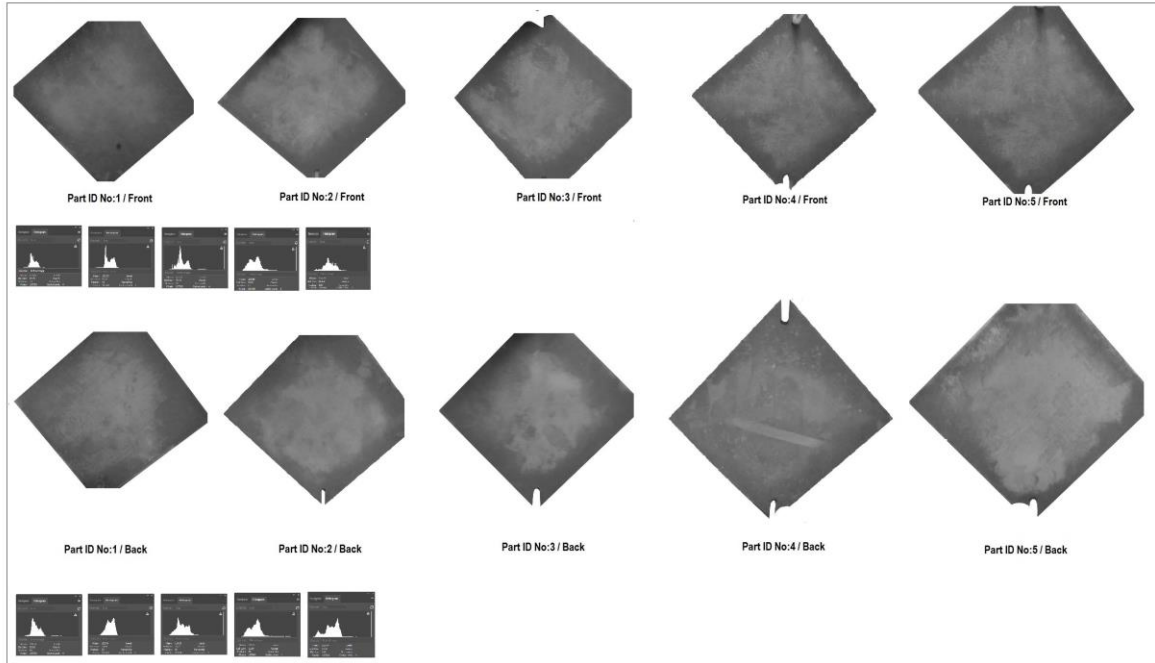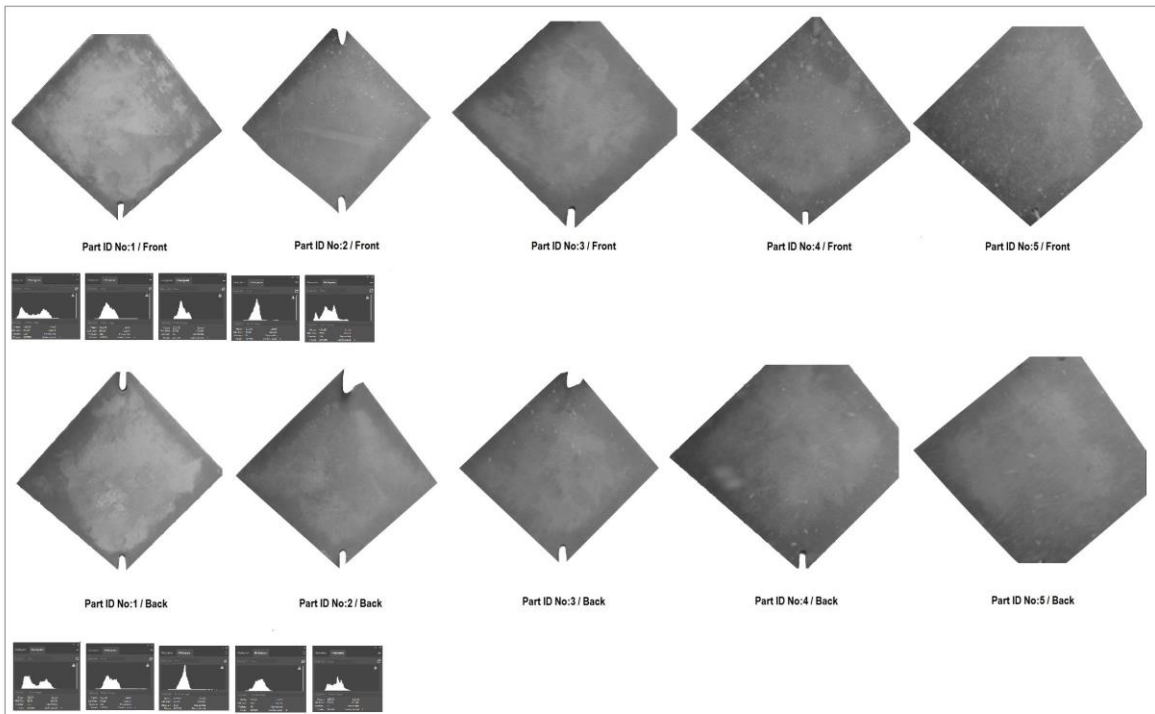
Figure 4.1.2.1 : Dive Date Images and Spectrum Analysis 26.06.2018 and 9.7.2018

DIVE 24.7.2018

Part ID No:1 / Front   Part ID No:2 / Front   Part ID No:3 / Front   Part ID No:4 / Front   Part ID No:5 / Front

Part ID No:1 / Back   Part ID No:2 / Back   Part ID No:3 / Back   Part ID No:4 / Back   Part ID No:5 / Back

DIVE 9.8.2018

Part ID No:1 / Front   Part ID No:2 / Front   Part ID No:3 / Front   Part ID No:4 / Front   Part ID No:5 / Front

Part ID No:1 / Back   Part ID No:2 / Back   Part ID No:3 / Back   Part ID No:4 / Back   Part ID No:5 / Back
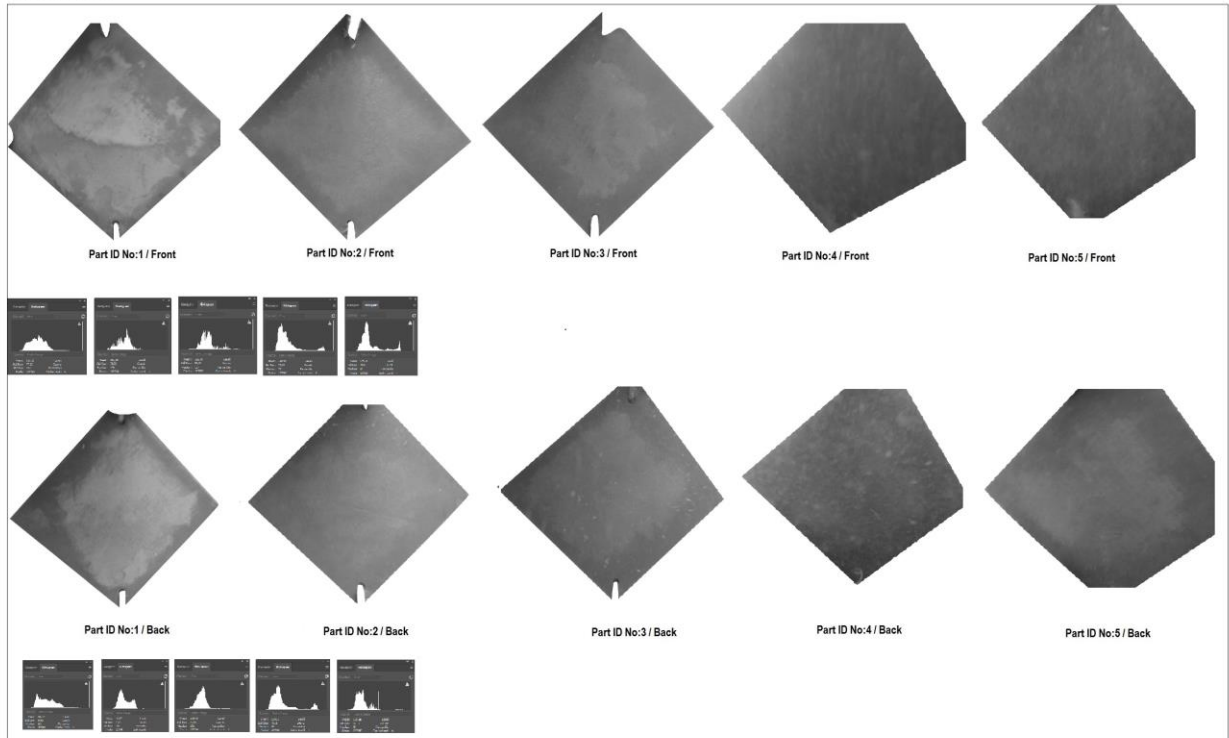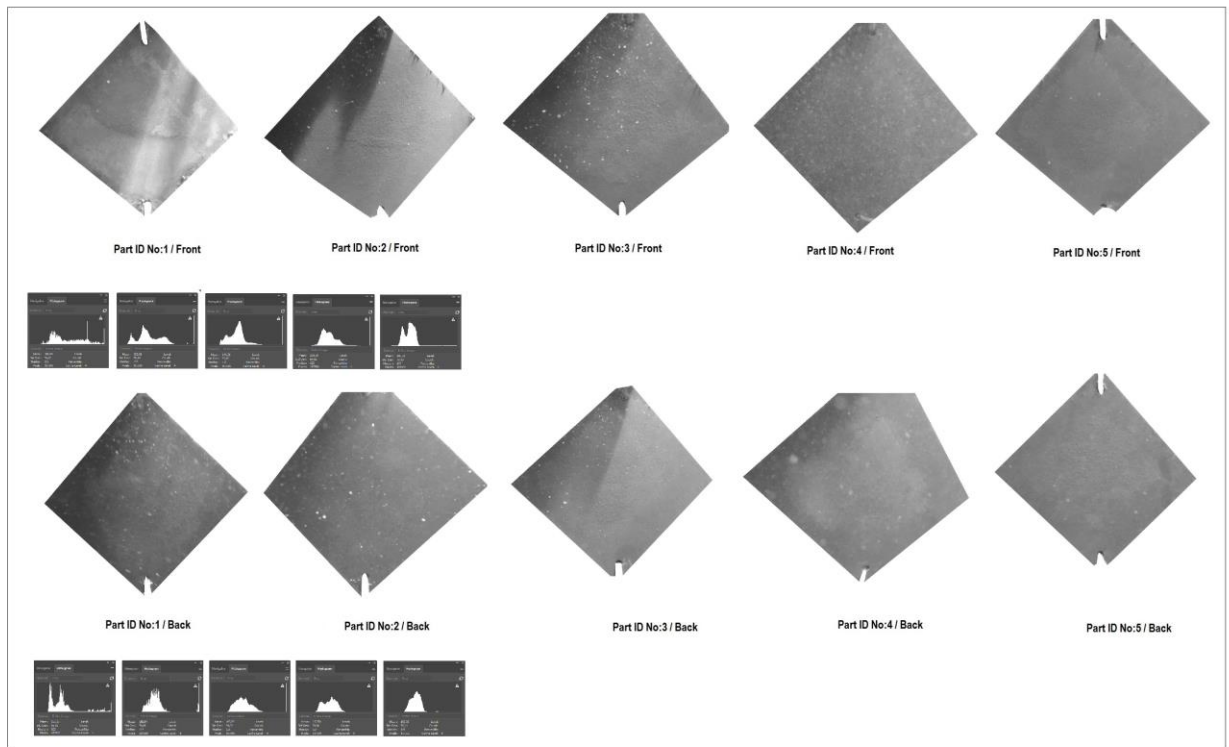
Figure 4.1.2.2 : Dive Date Images and Spectrum Analysis 24.07.2018 and 9.8.2018

128

DIVE 12.9.2018

Part ID No:1 / Front   Part ID No:2 / Front   Part ID No:3 / Front   Part ID No:4 / Front   Part ID No:5 / Front

Part ID No:1 / Back   Part ID No:2 / Back   Part ID No:3 / Back   Part ID No:4 / Back   Part ID No:5 / Back

Figure 4.1.2.3 : Dive Date Images and Spectrum Analysis 24.09.2018

4.1.3 Photographic Time Series Analysis
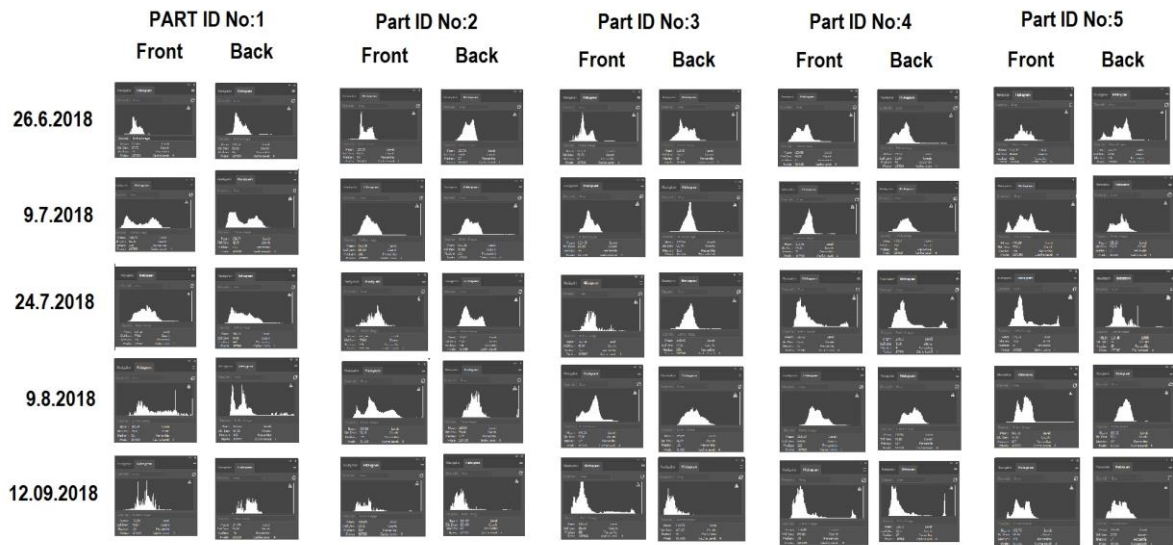
Figure 4.1.3 : Grayscale Spectrum Analysis in Dive Dates

4.1.4 Grayscale spectrum analysis result evaluation

Possible determinations determinations and propositions on Grayscale spectra are as follows:

1) It is most possible reason of shadow area high scale formation on surface reflections that surface light immersion and lighting position difference. However, the shaded areas created by relatively deep surface points due to the location of the photograph taken will represent the hollow points behind the higher points. From this view, it can be said that the trough-peaks in each part increase in quantity. It can be assumed that this situation is especially noticeable in the first and fourth dive imaging, from which is the first one-month process may be the main stage of corrosion and subsequent biofilm formation.

2) Looking at the date intervals, the spectrum of the base spread is seen to be widening in almost every image, and it can also be assumed that the differences in reflection on surfaces reflect spectral amplitude from the closer to the edge rather than the midpoint of the parts. Howev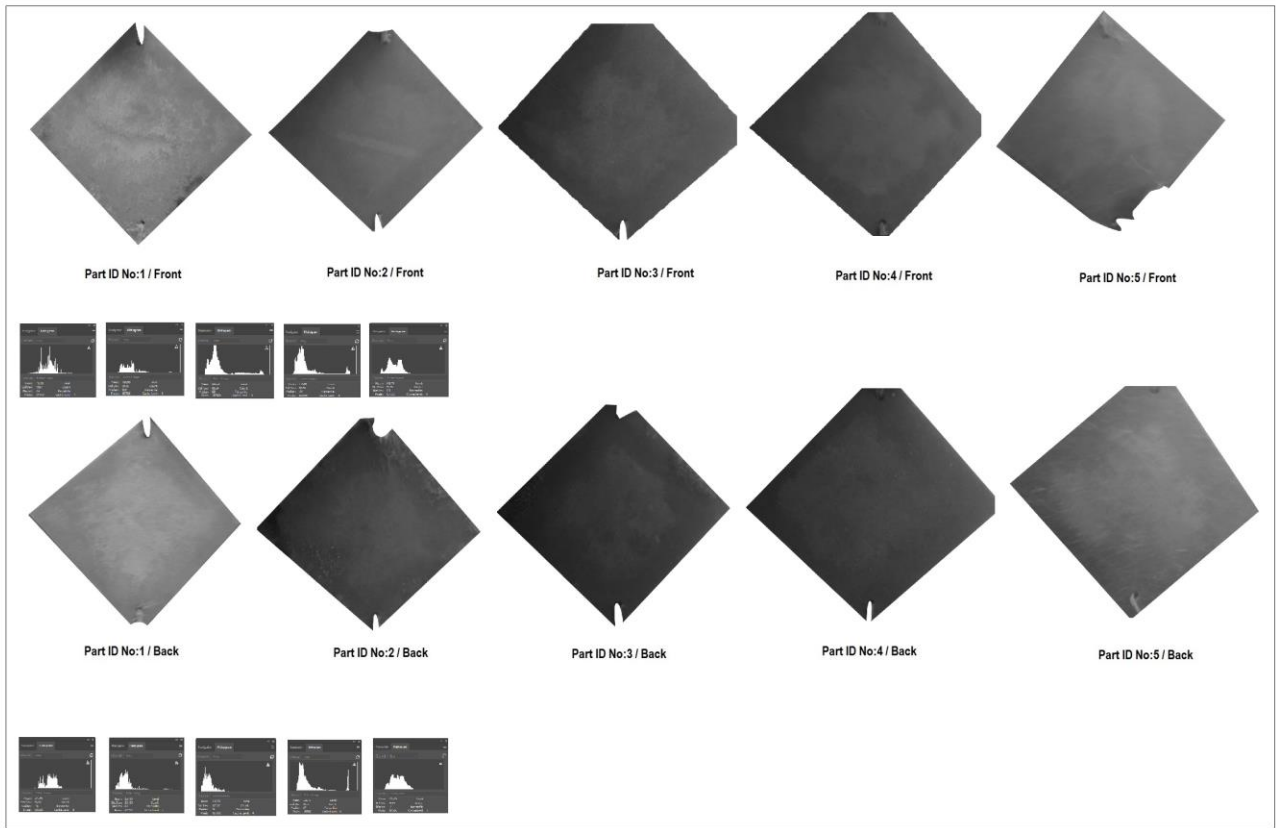er, this will not be sufficient to prove that the origin of corrosion or biofilm formation takes place from the middle or edge.

3) It is thought that the reflections on the surface decrease as the depth increases and this may be due to the decrease of the light coming from the sea surface. It is observed that the same reflective activity continues on the surface which is expected to have changed relatively in comparison with the reflections from its surface in the spectrum time interval of the Part ID No:5 standing at the bottom of the experiment.

4) It may be assumed that the matured fouling surface may have formed a less reflecting surface at the stage of the process. In the same way, it is not wrong to assume that the maturing fouling may be less rough as new layers are formed as a focal point of the spectrum analysis. In order to make this situation more meaningful, the application of a technology that can

perform underwater 3D scanning at different time intervals stands as the only solution. The output of the 3D scanner is usually in the form of a point cloud, i.e. a large set of sampled 3D points. This point cloud often requires additional processing to be visualized appropriately [172].

5) The fact that the reflection efficiency is more pronounced in the second and third parts, means Part ID No:2 and Part Id No:3,positioned in the 1.5 meter and 2.5 meter, leads to the assumption that this level of fouling may have been more effective. The most important criterion that can support this assumption is that biodiversity will also indicate the presence of a quantitatively more intense activity in the samples identified in these samples.

4.2 An Overview of Biological Determination Of Experimental Fouling

In this study taxonomic and biological determinations were used to compare, elucidate and describe roughness relations with surface realization by avoiding an exponential definition without biologist's final progressive experiments and their presence.

As a result, the highest number of individuals was determined in the sample bottle 2 which is scratched from Part ID No:2. The total number of individuals in the colony forming groups cannot be determined exactly and suffering detailed survey by the specialist However, it is seen that the colonies are mostly found in sample bottles 2 and 3, respectively.

4.2.1 General Classification of Experimental Surface Species

Biological process outcome shows us in taxonomic classification in 12 groups of the species as relatives of the experimental bio-fouling environment.

Hydroid colonies: There are generally fragmented forms. Intertwined structures were observed in the form of a cage. In some of them, Hydrotheca and Gonotheca sections can be clearly seen in hyroids.

Phytoplankton-Epiphytic diatoms(Licmophora spp.) colony: Diatoms were seen as colonies attached to hyroids. Especially in the sample bottle number 2, it was abundantly observed.

Benthic Foraminifera(Miliolida): This group of species s were embedded in biofilm. In the entire sample, it was buried in this mud-like structure. When these muds are separated and separated, Miliolid foraminifera were detected.

Benthic Foraminifera(Rotaliida): Unlike other foraminifera, these creatures were found only in sample bottle number 2 in the free generative form.

Harpacticoid copepod: It was observed in individuals belonging to 3 different species in both adult and early (copepoid) stages.

Gastropoda: The size of the individuals belonging to this group is small and individuals were identified in the larval period.

Amphipoda juvenile+Amphipoda adult (In similarity of Gammaridae): Individuals belonging to 2 different species were found. However, they couldn't be specified whether it is a benthic form or a pelagic form.

Bivalvia veliger: Individuals belonging to planktonic larval period were found.

Cirripedia larvae(Cyprid stage): An individual was found in the larval period belonging to the Barnacle group.

Nematoda: Individuals of different sizes were encountered buried in the biofilm. Especially in sample bottle 2, it was found abundantly

Unknown organisms: Generally, it has a yellow structure in cocon's structure and has an oval shape. It is thought to belong to one species.
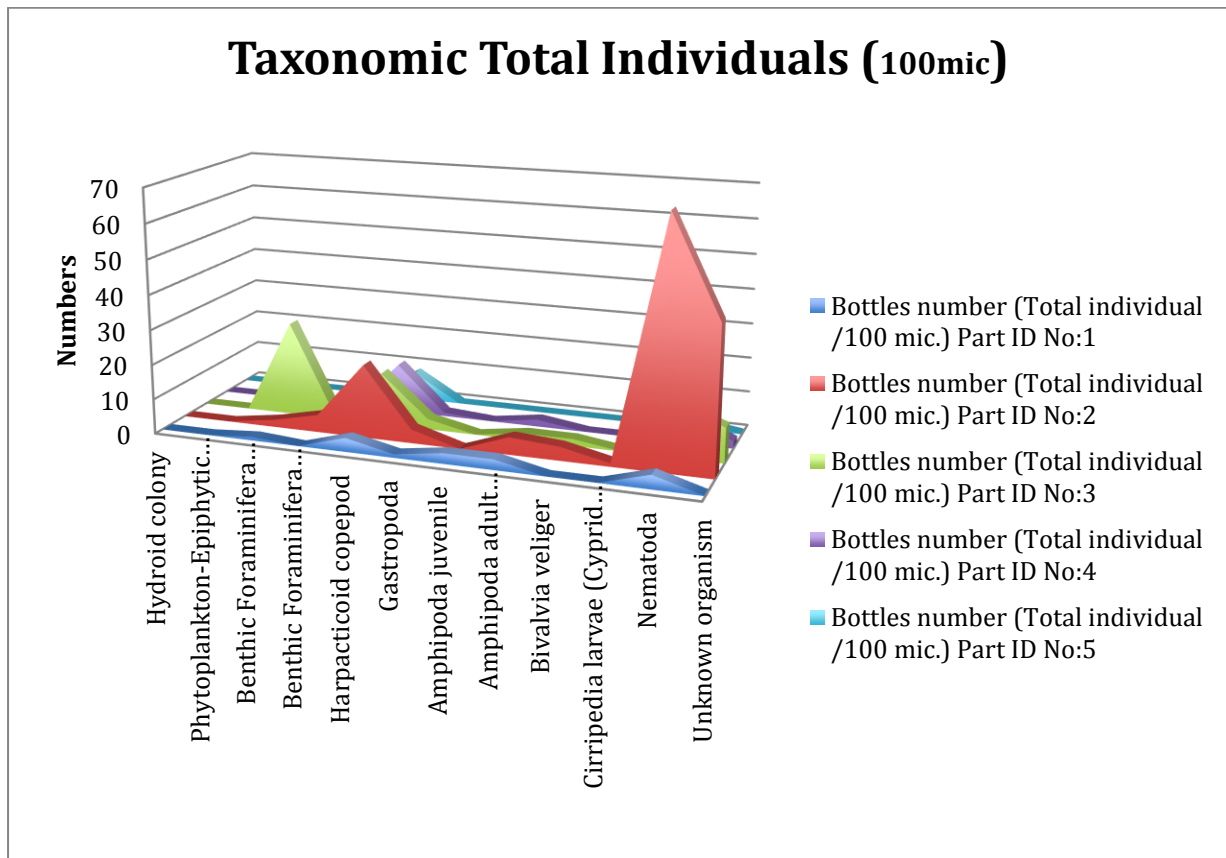
Figure 4.2.1.1: Taxonomic Total Individuals of Experimental Parts (100 mic)

4.2.2 General Characteristics of classified Experimental Species

Here below, bio-fouled species with their general definitions in combination according to their size-weight and general geometric forms.

Hydroid colony (Polips)

The polyps, also known as Hydrozoa, contain over 3800 different species that's a predatory taxonomic class of colonies, with very small sizes typically lives in saltwater with live form of singular or colonial called hydroids.[174] Hydroids, like many colonial animals, often encrust surfaces in the sea. They grow by the elongation and lateral branching of stolons [175]. Rough surfaces, rather than the work on glass surfaces, such as very low roughness values of 10: 25μm width and depth are observed in forms that can grow easily.
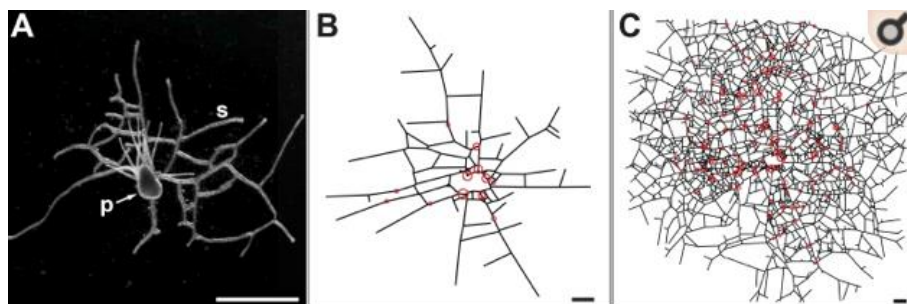
Figure 4.2.2.1 : One of the example Hydroid colony growth *Podocoryna carnea* (A) Top view of a young colony bearing a single polyp (p) and a ramifying hydrorhizal network of stolons (s). (B) Digitized image of a colony after 20 days growth. Circle denote locations of polyps, straight-line segments denote stolons. (C) Digitized image of the same colony after 58 days growth. Scale bar: 1 mm [176]
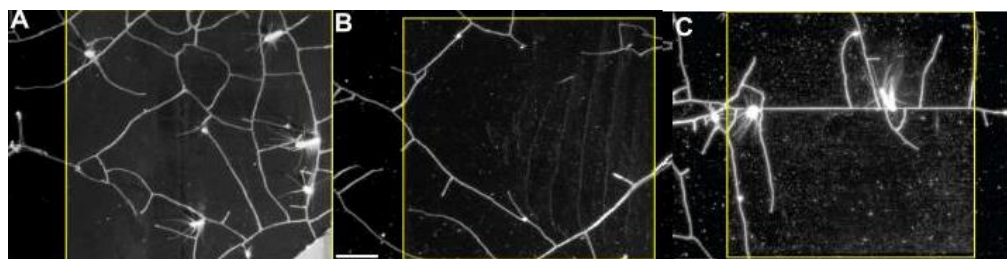
Figure 4.2.2.2 : Podororyna carnea Shallow, narrow grooves. Groves run horizontally. Width:Depth (A) 5:5 μm, (B) 10:10 μm, (C) 25:25 μm. Regions of the wafer internal to the yellow bounding boxes were etched with grooves, regions outside the box were not etched. Scale bar = 1 mm [176]

Phytoplankton-Epiphytic diatoms /(Licmophora)

Planktonic variations corresponded to oscillations in climate, hydrography, and weather, which determine water column stability in the fjord. The tychopelagic species, Paralia sulcata, was more abundant in unlaminated sections of the core, indicating preference for a vertically mixed water column. No direct effects of increased nutrient loading on the plankton could be established. Epiphytic diatoms show a period of decline from the 1950s to 1990s. This trend probably follows a shift in the macroalgal community to less-suitable host species [177].

Epiphytic algae are an important constituent of the autotrophic community of a macrophyte-oriented aquatic ecosystem [178]. Even though epiphytic algae are very important components of the pelagic-benthic part of lentic ecosystems for both nutrient cycles and food-webs, their ecology has been subject to relatively little investigation [179].

Licmophora is a genus of benthic diatom. It is an epiphyte, which means it must perch on another organism or object for structural stability. Typically, licmophora are distinctly triangular and form a striking fan shape around a central stalk. They are usually a yellow or brown in color, not green, despite being photosynthetic [180].

Single-celled algae that possess a distinct nucleus (eukaryotic) .Divided into two major groups based on the structure and shape of the valves: Centrics (Order: Biddulphiales) and Pennates (Order: Bacillariales) They are plant-like and meet their nutritional needs through photosynthesis The presence of chlorophyll and accessory pigments, especially fucoxanthin, give them a golden color and serves to harvest light energy from the sun. Cells are encased in a transparent glass-like silica frustule that resembles a petri-dish. Frustules can be ornate and very beautiful, and due to the strength of silica, they form an important part of the fossil record.Cells may form chains or colonies.Up to 100,000 species of diatoms have been recorded world-wide.
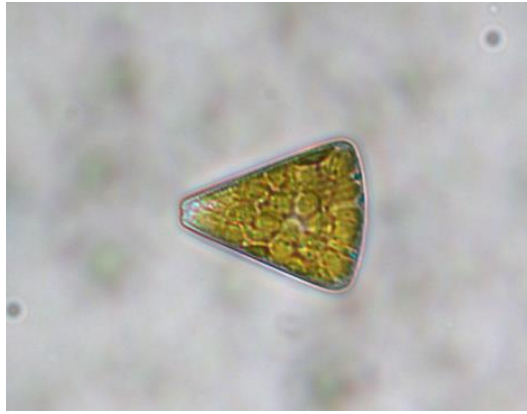
Figure 4.2.2.3 : Phytoplankton-Epiphytic diatoms - (Licmophora) [181]

Epiphytic diatom, cells grow on a common stalk that is attached to rocks or algae. Often found in low numbers in shallow or turbid environments, both marine and freshwater.
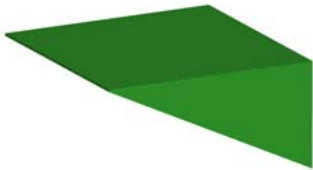
Species	Licmophora
Division	CHRYSOPHYTA (HETEROKONTOPHYTA)
Class	Diatomophyceae (Bacillariophyceae)
Order	BACILLARIALES (PENNALES)
Trophy	AU
Geometric shape	Half parallelepiped
Formula	l*w*h/2

Size class	1	2	3	4
Unit	cell	cell	cell	cell
Size range	45x55-65	10x20-30	15x30	7x20
Length(l1), µm	60.0	25.0	30.0	20.0
Width(w), µm	45	10	15	7
Height(h), µm	20.0	6.0	8.0	7.0
No. of cells/counting unit	1	1	1	1
Calculated volume, µm3	27 000	750	1 800	490
Calculated Carbon pg/counting unit	1 130	62	126	44

Figure 4.2.2.4 : Distinct triangular or fan-shaped cells. Liomophora/Computerized Geometry [182]

Benthic Foraminifera (Miliolida)

From the Triassic onwards abundance and diversity markedly increased to make this order one of the most important in the Foraminifera. They are particularly useful in stratigraphical studies because they range down to the present day and dominate shallow, warm water, micro faunal assemblages [183]. Miliolids, which range from the Carboniferous to recent, are benthic Foraminifera abundant in shallow waters such as in estuaries and along coastlines, though they also include deepwater oceanic forms [184].

Foraminifers are single-celled organisms, usually some 100μm in size,but larger specimens may be several centimeters in size [185].
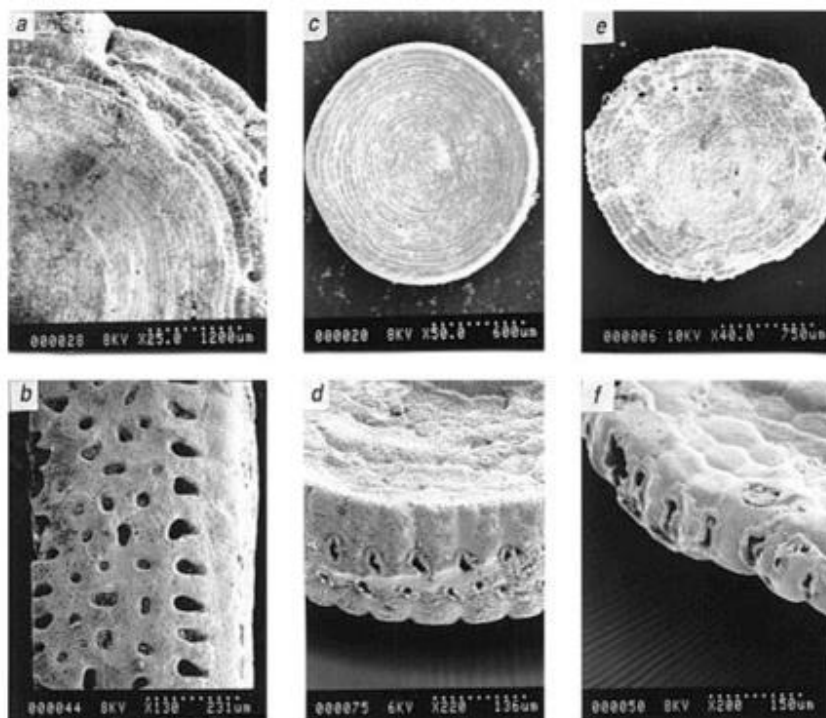
Figure : 4.2.2.5 Marginopora vertebralis, Under electron Microscoph a) surface view b) Apentural view: Amphirous hemprichii c) Surface view: apentural view: Sorites orbiculus e)Surface view f) apertural view: Magnification and scale bar are shown at the bottom view of each photo [186]

Foraminifers are characterised by a multi chambered skeleton,featuring perforations from chich fine strands.The milliolida (Caboniferous until present) have two or multi-chambered non-porous casing (imperforate).The casings are agglutinated or composed of

calcite.The randomly oriented calcite crystals ferlact light in all directions – the casing thus have a porcelain-like appearance [186].

Benthic Foraminifera (Rotallida)

The Rotaliida are the most abundant order in numbers of genera, penetrating most marine environments but especially characteristic of shelf seas. Although mainly trochoid they show the greatest range of coiling modes with many specially adapted for a fixed life on hard, current-swept substrates, including the assumption of arborescent growth resembling that of bryozoans together with bright colours [183].

The rotalliida (Jurassic until present) posses multi-chambered hyaline calcite casing. The coiled Nummultidae are of cellular plasma emerge. Nummultidae are large foraminifers that can reach several censimeters in diameter,with largest species growing to around 15 cm.size. They live in shallow marine benthic habitats and in symbiosis with photosynthetic endosyymbionts (often diatoms with out-casing) [186].

Figure 4.2.2.6 : Benthic forms, Taken with a Leica DFC 490 camera mounted on a Leica M205C binocular microscope. Collected in 2011 at 51°42′32.88″N 2°27′3.98″E on the edge of the Belgian part of the North Sea. Diameter = ~600 μm [187]

Harpacticoid Copepod

There are 10 Taxonomic orders of copepods, of which 9 have marine representatives. Of these the most important marine orders are the Calanoida, Cylclopoida and Harpacticoida. Calanoid copepods are primarily pelagic, 75 % of the known species are marine and some are bentholpelagic or commensal [188]. Copepods are useful as food for marine fish densities.However, their benthic nature also makes mass culture difficult, since large surface areas must be provided [189].

Copepods vary considerably, but can typically be 1 to 2 mm (0.04 to 0.08 in) long, with a teardrop-shaped body and large antennae. Like other crustaceans, they have an armoured exoskeleton, but they are so small that in most species, this thin armour and the entire body is almost totally transparent [190].

Some polar copepods reach 1 cm (0.39 in). Most copepods have a single median compound eye, usually bright red and in the centre of the transparent head; subterranean species may be eyeless. Like other crustaceans, copepods possess two pairs of antennae; the first pair is often long and conspicuous. Copepodes were represented by Rhinodiaptomus indicus, Mesocyclops leuckartii, Tropocyclops prasinus and Nauplius larvae. Copepods contributing 29% of the total net zooplankton. Density of R.indicus fluctuated between 10 org/l and 48 org/l. Mesocyclops sps ranged from 18 org/l (April) to 48 org/l (Jan).Tropocyclops prasinus fluctuated between 28 org/l (March) to 68 org/l (August). Seasonally they were abundantlyobserved in winter season [191].

The size of copepods depends on the species as well as on the ontogenetic stage. Various copepod sizes are used for specific larviculture applications, assuring an efficient uptake by the target predator at any time during its larval rearing.

The harpacticoid Tisbe holothuriae grows from a nauplius size of 55 µm to an adult size of more than 180 µm, Schizopera elatensis from 50 to 500 µm, and Tisbentra elongata from 150 to more than 750 µm. Sizes for Eurytemora sp. (Calanoidea) are on an average 220 µm, 490 µm, and 790 µm for nauplii, copepodites, and adults, respectively [192].
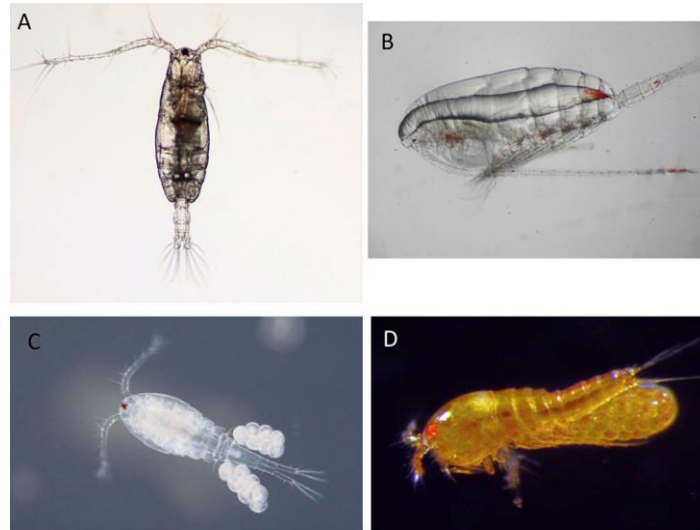
Figure 4.2.2.7 : Copepods In Close Exposure [193]

Gastropoda

Slugs and snails (phylum Mollusca: class Gastropoda) are soft-bodied, non-segmented invertebrates with the body composed of three regions: head, foot and visceral mass. The last-mentioned is covered by a layer of epithelial cells, called the mantle; this secretes a shell of calcium carbonate and encloses a mantle cavity. The mouth usually contains a rasping tongue or radula, armed with thousands of minute chitinous teeth. Most molluscs, such as clams, cuttlefish, octopuses, oysters, sea-slugs and squids, are marine animals; several species live in freshwater habitats but only certain slugs and snails in the order Pulmonata are able to survive on land [194].

During first four weeks, measurements of the size (height and diameter of shell), total weight, and the oxygen consumption rate were carried out two times a week, and thereafter, once a week. Linear sizes were measured using binocular adjustment with an eyepiece micrometer if the shell height was up to 5 mm, otherwise we used a using vernier caliper accurate to within 0.1 mm. Animals with a weight up to 250 mg were weighedusing a torsion balance accurate within 1 mg. If the weight of an individual specimen was less than 3 mg, all mollusks from the group were weighed, then the specimen weight was calculated. The total weight of animals of large sizes was measured using a rough balance accurate within 10 mg [195].
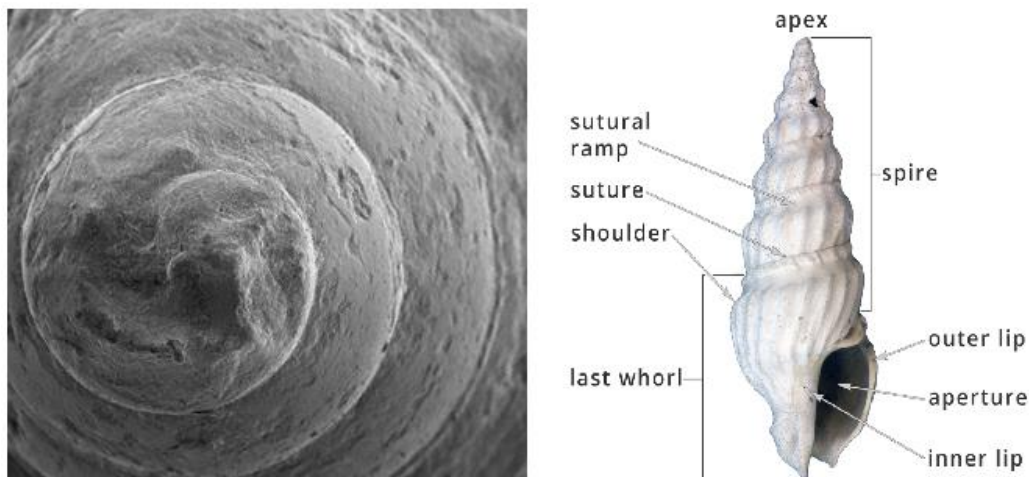
Figure 4.2.2.8 : Gastropoda, [196]

Amphioda Juvenile and Amphioda adult (Gammaridae)

Amphipods are important components of many aquatic ecosystems, especially in Temperate Zones where they are often the most abundant macroinvertebrates in alkaline springs, spring-fed streams, and subterranean waters. Their generalized feeding habits and high food quality contribute to the major ecological impact that they make in habitats where they are abundant [197].

141

The smallest known amphipods are less than 1 millimetre long [198]. However, There are more detailed researches was available in literature. In seasonal investigations, there are 0 to ± 2 mm from measured lengths. ead capsule length-body length/weight relationships for these amphipods are seasonally robust, and may be estimated from single collections provided all size classes are obtained [199].
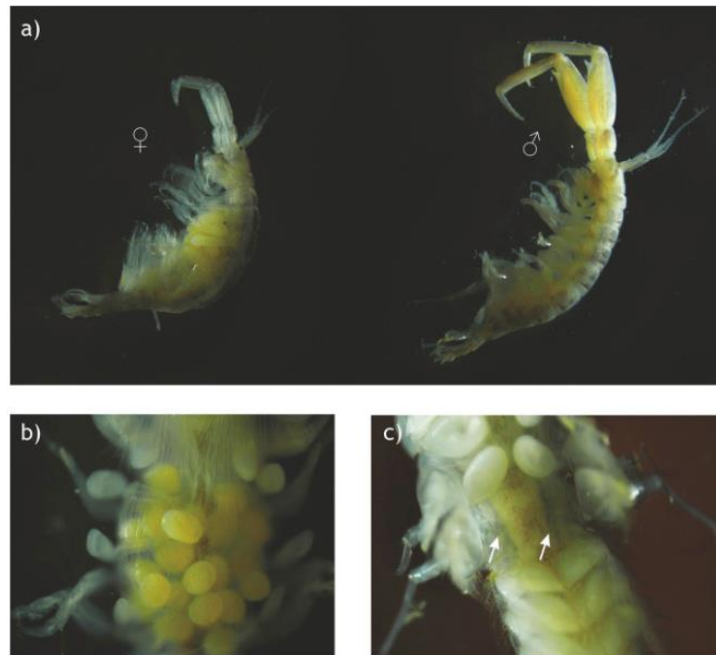
Figure 4.2.2.9. Amphiodas (a) *Corophium volutator* female and male; (b) Adult female –Marsupium , clearly visible oostegites with developed setae holding eggs; (c) Adult male, arrows point to genital papillae (photos made by W. Podlesińska during the study of *C. volutator* from the Puck Bay) [200]

Bivalvia Veliger

Bivalve, any of more than 15000 species of lams of clams, oysters, mussels, scallops and other members of the Phylum Mollusca characterized by a shell that divided from front to back in to left and right valves. The valves are connected to one another at a hinge. Primitive bivalves ingest sediment; however, in most species the respiratory gills have become modified into organs of filtration called ctenidia. In keeping with a largely sedentary and deposit-feeding or suspension-feeding lifestyle, bivalves have lost the head and the radular rasping organ typical of most mollusks [201].

Bivalves in larval period, 0,10 µg to 0,39 µg for the smalllest weight class as *bivalves* and *gastropod veligers*.Their weights may reach 51,20 – 102,39 µg on c*ladocerans* [202]. Bivalves range in size from about 1 mm. in length to the giant clam of South Pacific coral reefs, which may be more than 137 centimetres in length and weigh 264 kilograms Such an animal may have a life span of about 40 years [201].

The miscroscobic features of a molluscan shell record certain pysiological conditions of the organism at the time the shell is formed.Carbonate minerals within a molluscan shell crystallize and grow under physicochemical conditions controlled by the physiology of the organism [203].
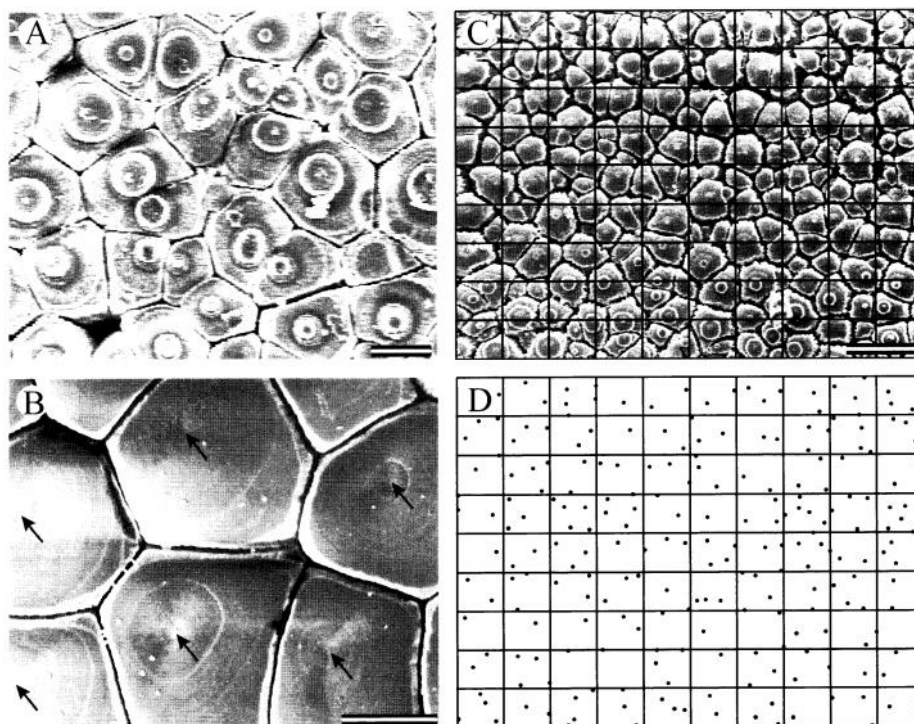
Figure 4.2.2.10: Geometry of Bivalve prismatic shell *A.* SEM Photograph of the outer shell surface of the vertical composite prismatic shell layer in A.woodiana (SUM-HM-B0027) showing clear growth increments wihtin individual prism, Scale : 20µm. *B.*The simple prismatic layer in pinctada maculata (SUM-HM-B0015) Arrows indicate nucleation sites,scale : 20µm *C.*The SEM image of A.woodiana subdivided in to squares, scale: 50µm *D.*Distribution of nucleation sites prisms in C [204]

Fractures through the prodissoconch of Ostrea edulis reveal a more complex structure than previously reported in bivalve larvae and demonstrate a gradual change in shell microstructure from the earliest portion of prodissoconch I to the end of prodissoconch II.

1- The outer layer, which underlies the periostracum, is generally about 0.7 / *mm* in thickness in the early prodissoconch I but thins toward the prodissoconch-I margin and appears to be absent over the greater portion of prodissoconch II. The layer consists of exceedingly fine, irregular prisms that in the inner part of the layer vary from 0.05 to 0.1 / *mm* in diameter. Next to the periostracum, the prisms attenuate into the fine needles described above.

2- The inner layer, which forms the inner surface of the larval shell except at the free margins of the valves, is distinctly prismatic in structure. In scanning electron micrographs, the prisms appear to be uniform in texture rather than granularas in the outer layer. They are also coarser than the outer prisms, reaching diameters of about 0.3 / *mm*. In fully developed prodissoconchs, the inner layer is thickest in the umbonal region, beneath the prodissoconch-I portion of the shell, where it may exceed 3 / *mm* in thickness.

3- Beneath the pitted zone of prodissoconch I a third, middle layer is little more than a discontinuity between the inner and outer prismatic layers. This discontinuity thickens beneath the early portion of the stellate-radial zone and becomes a layer of randomly arrayed granules, a fabric that is generally referred to as "homogeneous" [205].
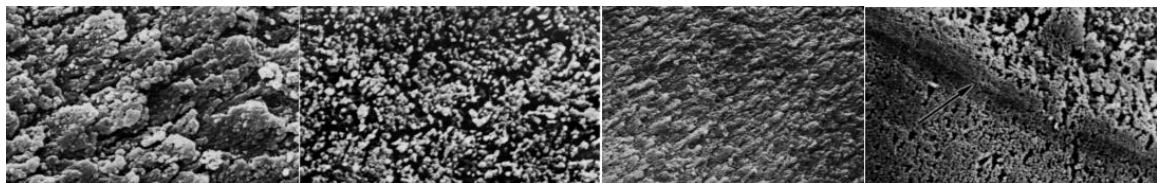
Figure 4.2.2.11 Example Formation Of Ostrea Edulis From Veliger , Pitted zone (2 *mm* to 5 *mm*) [205]

144

Cirriperida Larvae (Cyprid Stage)

The identification of balanomorph larvae plays an important role in ecological study and for protection against biofouling. However, it is difficult to identify species of cyprids (settling larvae) of balanomorph barnacles, as they show remarkably similar morphology [206]. But there are many clear identifications to highlight this specie to be mentioned in barnacle literature.For example, stalked and acorn barnacles (Cirripedia Thoracica) are important members of marine communities from the rocky intertidal zone to offshore specialized habitats such as coral reefs [207]. Regions of the developing cuticle and the patchy material itself stained for reactive oxygen species. Bacteria were absent until the cyprid was firmly attached, but populations died as barnacle development progressed. The oxidative environment may contribute to the cytotoxicity observed for bacteria and has the potential for oxidative crosslinking of cuticle and proteinaceous materials at the interface [208].

Cyprid populations may come to be different in size from more than one possible cause.The populations may represent different races, that is , be gentypic origin.In view of extensive mixing of the cyprids in the surface waters during planktonic phase and their ultimate distribution over the whole intertidal zone in B. *Balonoides,*together with necessity for cross-fertilization, it seems unlikely that distinct races of adults giving rise to populations of different-sized cyprids would be developed [209].

There are many different cultures are in literature but common culture is widely effected by the temperature for the species' growth. For example: Larval development from stage a cyprid larvae was taken for 20 days at 21±2ºC to 28C±2ºC and 13 days at 28±2ºC continuously and results are shown in the table:

Stage	n	Total length (μm)		Shield width (μm)		Shield length (μm)	
		Mean ± SD	Range	Mean ± SD	Range	Mean ± SD	Range
I	20	241 ± 6	230–260	119 ± 5	110–130		
II	20	282 ± 9	265–300	184 ± 8	175–205		
III	20	321 ± 9	310–345	210 ± 6	200–215		
IV	20	344 ± 16	320–365	246 ± 14	230–275	242 ± 12	230–265
V	20	408 ± 11	385–420	284 ± 9	275–310	282 ± 10	260–305
VI	20	464 ± 13	445–485	326 ± 10	315–340	318 ± 10	310–340
Cyprid	20	408 ± 9	390–420	190 ± 5	185–195		
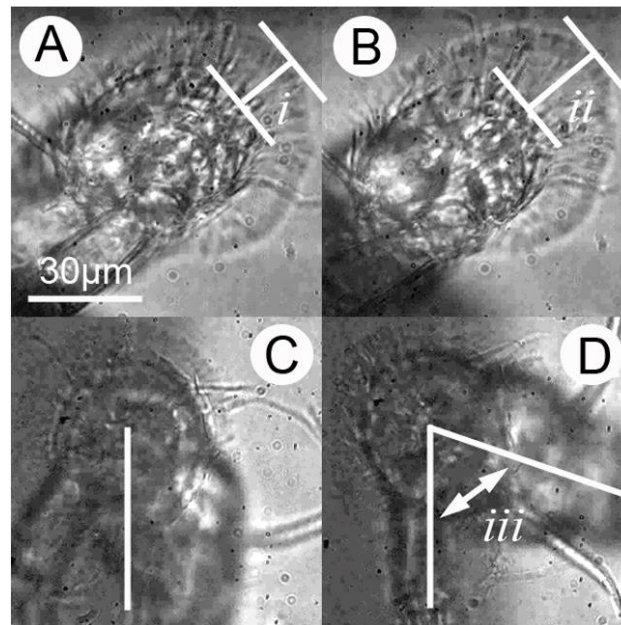
Figure 4.2.2.12 Illustration of changes at an adhesive interface under stress.of Cyprid A) The cyprid antennule viewed from below, with adhesive disc attached to the polystyrene surface and cuticular villi (i) in the resting state. B) As stress is applied to the system, the cuticular villi elongate and draw parallel to the surface (ii). When torsion forces are experienced, the antennule twists around the pivot point of the attached disc C) before detachment is initiated D) at around 70° from the resting position (iii) [211]

Nematoda

Nematodes were once classified with a very large and heterogeneous cluster of animals grouped together on the basis of their overall worm-like appearance, simple structure of an internal body cavity called a pseudocoelom, and the lack of features such as cilia and a well-defined head that are found in most animals. This group, variously known as Aschelminths or Pseudocoelomata, is today no longer recognized as a natural one. It is quite likely that the simple body plan of these organisms has resulted from reduction and simplification from more

than one group of ancestral organisms, and so the pseudocoelom is neither a uniquely derived nor useful character [212].

Nematode length was also affected by grain size, where shallow-water coarse sediments were inhabited by longer nematodes. Nematodes from the oligotrophic Aegean Sea were characterised by low length values and high width values, probably as an adaptation to sediments poor in organic matter. These observations suggest that local factors can also be very important for shaping the morphometric landscape of the nematode communities [213].
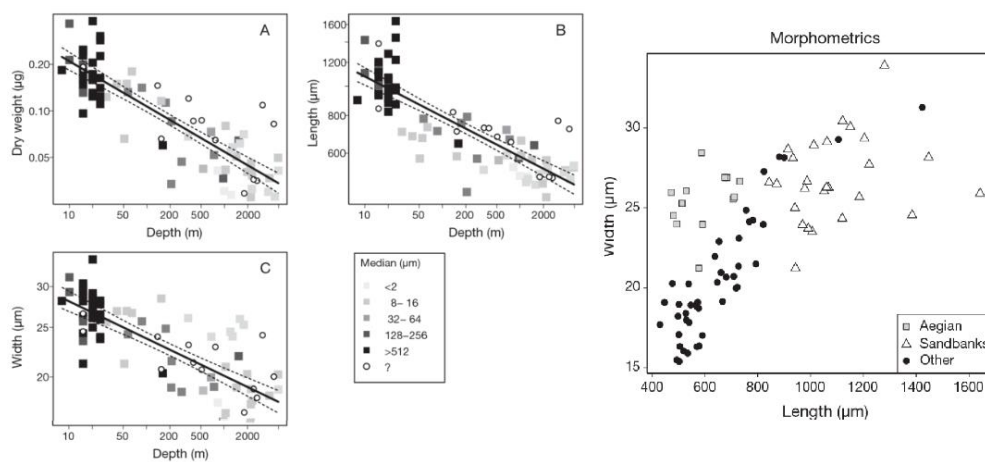
Figure 4.2.2.13 Side/left: Relationship of mean nematode (A) dry weight (µg), (B) length (µm) and (C) width (µm) per station versus water depth (m). Coloration is a function of sediment median grain size (µm) Side/Right: Nematode length (µm) versus width (µm). Data are station means for the Aegean Sea, sand banks and other stations [213]

The body of a nematode is long and narrow, resembling a tiny thread in many cases, and this is the origin of the group's name. The word "nematode" comes from a Greek word nema that means "thread". The epidermis (skin) of a nematode is highly unusual; it is not composed of cells like other animals, but instead is a mass of cellular material and nuclei without separate membranes. This epidermis secretes a thick outer cuticle which is both tough and flexible. The cuticle is a feature shared with arthropods and other ecdysozoans. As in those other groups, the cuticle is periodically shed during the life of a nematode as it grows, usually four times before reaching the adult stage. The cuticle is the closest thing a roundworm has to

a skeleton, and in fact the worm uses its cuticle as a support and leverage point for movement. Long muscles lie just underneath the epidermis. These muscles are all aligned longitudinally along the inside of the body, so the nematode can only bend its body from side to side, not crawl or lift itself. A free-swimming roundworm thus looks rather like it is thrashing about aimlessly [214].
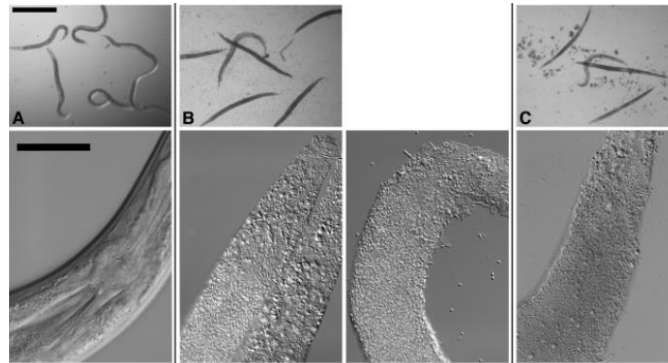
Figure 4.2.2.14: Top row: Dissecting microscope view of nematodes cultured under various conditions. Scale bar of all images in top row is 500 µm. Bottom row: Compound microscope view of nematodes cultured under various conditions. For all images in the bottom row, anterior of the worm is top right and scale bar is 50 µm. (A) C. elegans cultured in a well with B. thuringiensis without Cry5B. Top row: None of the six nematodes are infected. All are healthy. The blur associated with some of the worms in the top row is due to their movement in the well. Bottom row: The internal structures of C. elegans fed B. thuringiensis without Cry5B, including the pharynx and intestine, are all intact. (B) C. elegans cultured in a well with B. thuringiensis and Cry5B. Top row: Five of the six worms are completely infected (rigid, lack of internal structures and normal coloration); one is not. Bottom row: Infected animals show complete or near complete digestion of internal structures by the bacteria. Vegetative and sporulated bacteria can be seen in these lethally infected animals. (C) Similar images as in (B) except the bacterium cultured with the nematodes is Bacillus anthracis. [215]

4.3 Virtual Surface Model Of Experiment Materials

Experimental parts's removal applied on the date of 12.09.2018 and parts were scanned with the laser 3D surface scanner to apply surface metrology process via hybrid geometric measurement with non-contact method.

As a part of the study, due to application process of biological analysis method, test pieces were installed in to a container fully filled with seawater. Pieces were hanged from their ropes to avoid any contact to each other or any non-viscous surface other than the seawater. 3D scanning process was applied to each part one by one and during a scan period, next pieces kept in the seawater.All process completed in 22 minutes. Fouling material were softly scratched from the surfaces and taken in to disinfected containers filled with % 99 purity alcohol for fixation till to final destination of biological test center.

All, five test pieces have been scanned for surface measurement definition of metrological form to an independent and messy point cloud as in most applications require an automatic processing of the point clouds to extract information on the shape of the recorded objects. This processing often involves the recognition of specific geometric shapes or more general smooth surfaces [173].

Measured data packages were taken in to 10 different folders for each scanned parts in compressed data file about 9,30GB in total folder with more than 2,3 billion points of the cloud. Each part cloud was taken in to an accelerated computer for rendering to state a solid parts again from the cloud by Rhinoceros 5.Because of the solid data losses of raw cloud surface effectiveness, data couldn't been used and solid meshes were broken. On the second trial point clouds were stated to a plain sectional fraction to decrease cloud size other than the surface in depth of 2 mm.New generated surface clouds have been examined in metrology process in different tolerances and surface roughness calculated for each surfaces.

4.4 3D Scanning Of Bio-fouled Materials
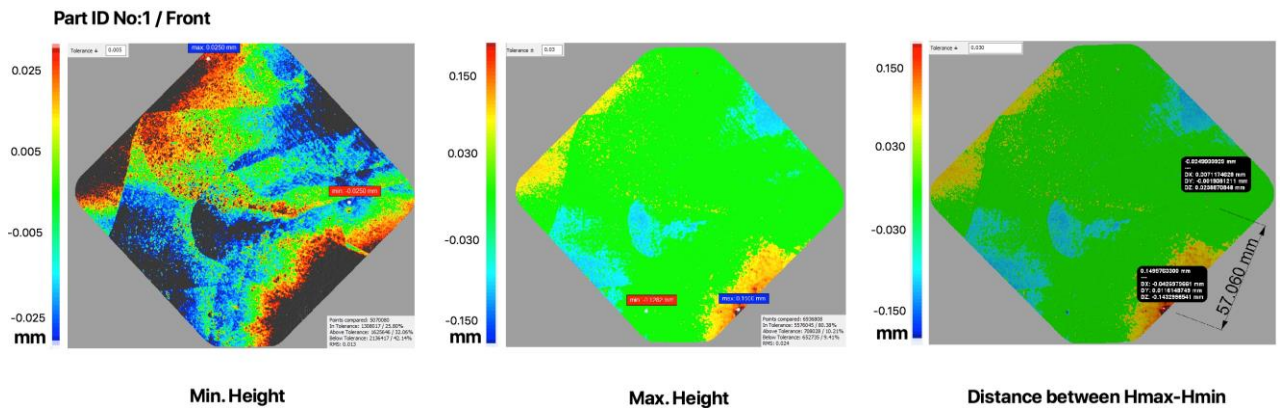
Figure 4.4.1.1 : Part ID No:1Front View Point Cloud Image and Min.and Max. Heights With Distance
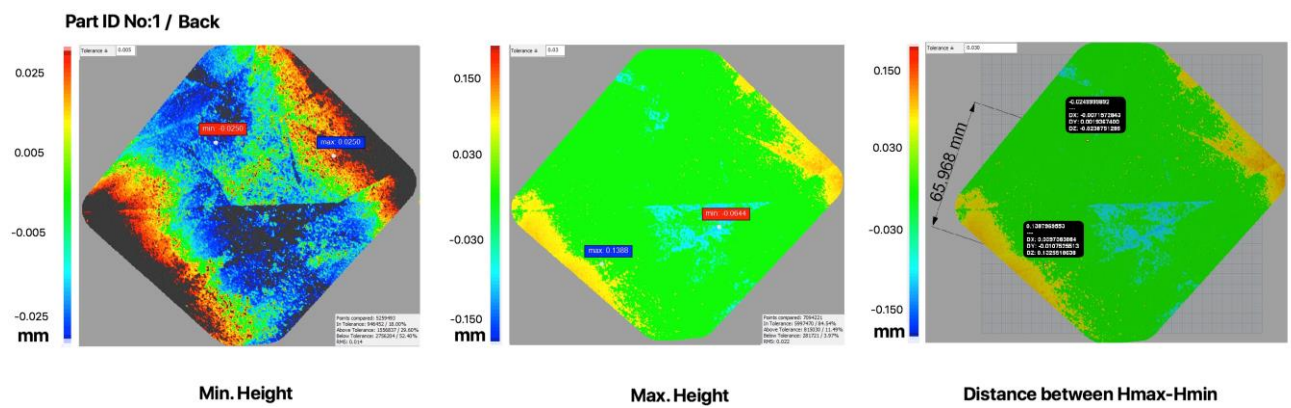
Figure 4.4.1.2 : Part ID No:1 Back View Point Cloud Image and Min.and Max. Heights With Distance
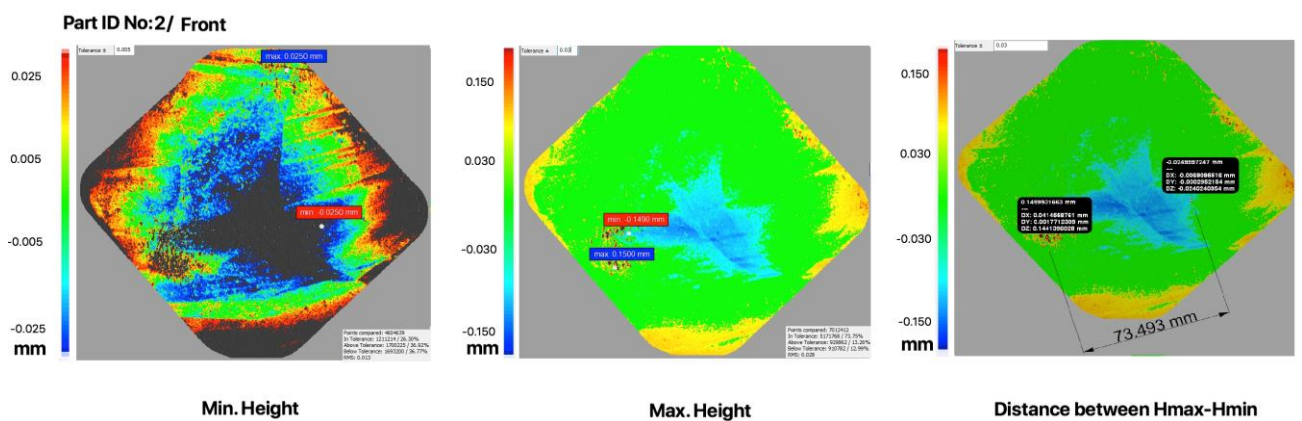
Figure 4.4.1.3 : Part ID No2 Front View Point Cloud Image and Min. and Max. Heights With Distance
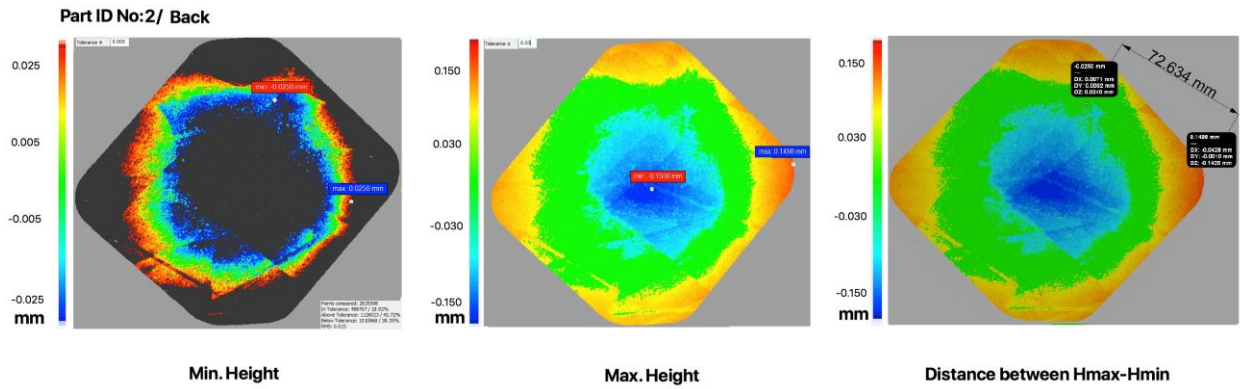
Figure 4.4.1.4 : Part ID No2 Back View Point Cloud Image and Min. and Max. Heights With Distance
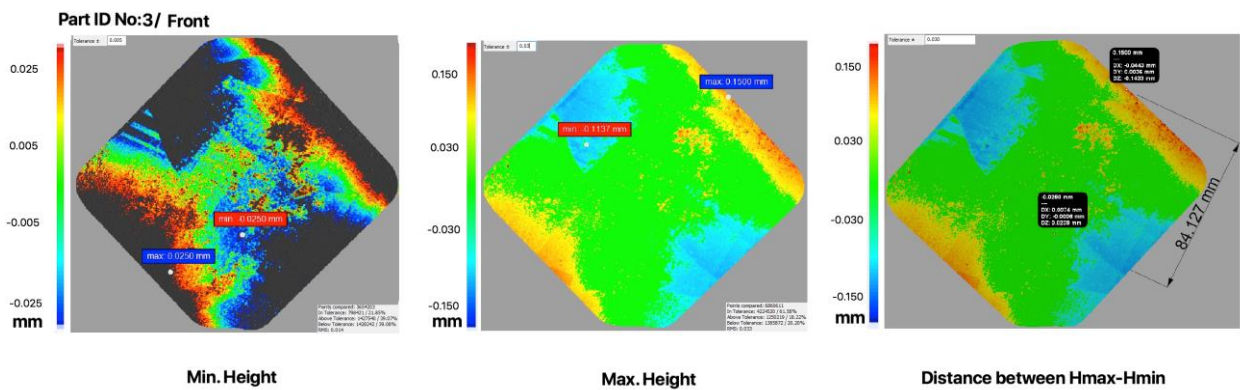
Figure 4.4.1.5 : Part ID No3 Front View Point Cloud Image and Min. and Max. Heights With Distance
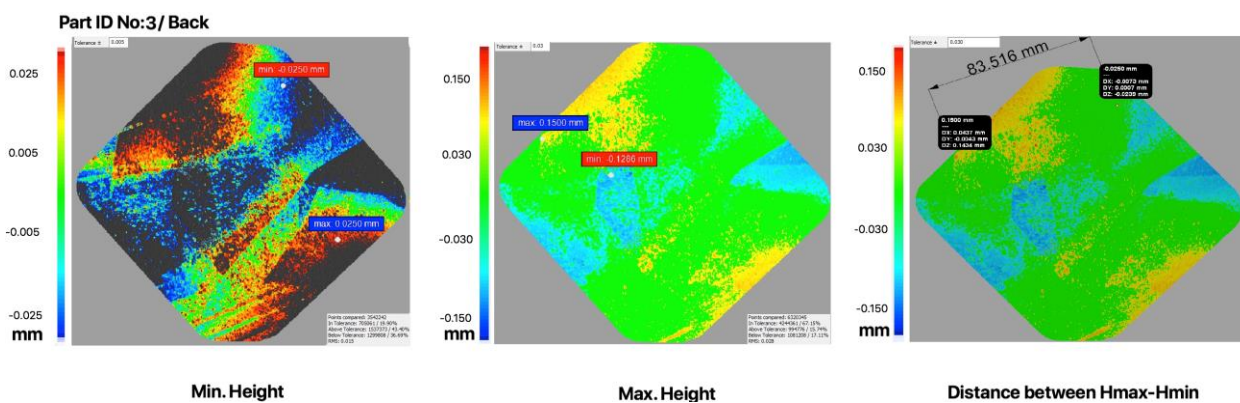
Figure 4.4.1.6 : Part ID No3 BackView Point Cloud Image and Min. and Max. Heights With Distance

Min. Height   **Max. Height**   **Distance between Hmax-Hmin**
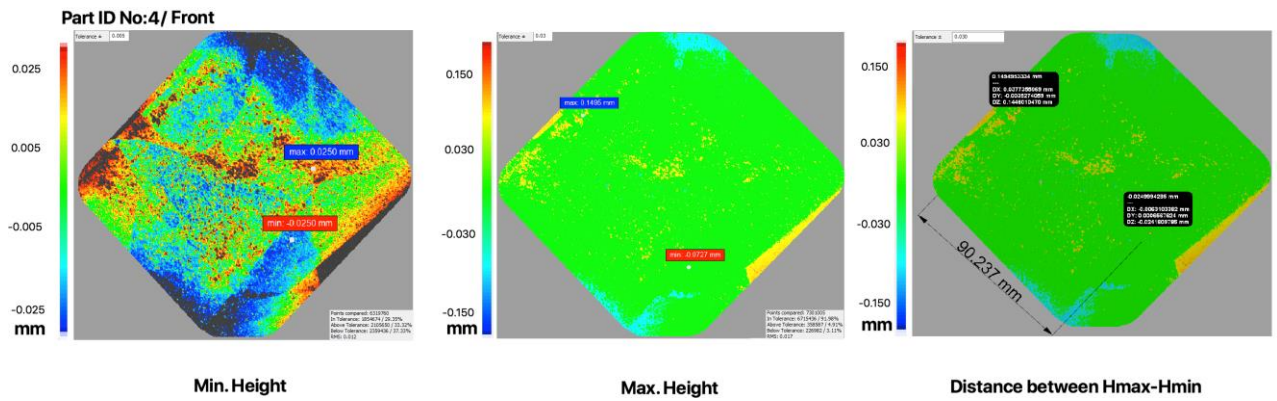
Figure 4.4.1.7 : Part ID No4 Front View Point Cloud Image and Min. and Max. Heights With Distance

Min. Height   **Max. Height**   **Distance between Hmax-Hmin**
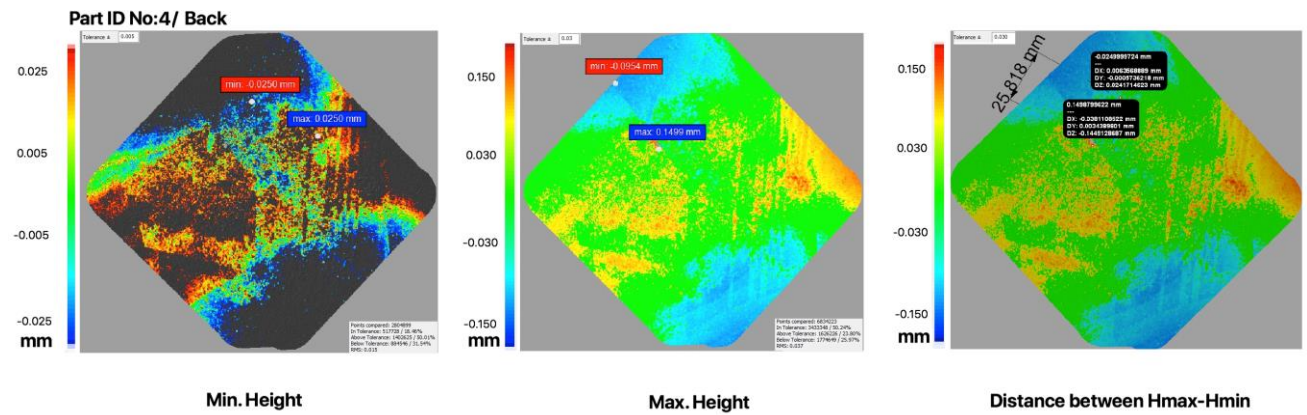
Figure 4.4.1.8 : Part ID No4 Back View Point Cloud Image and Min. and Max. Heights With Distance

Min. Height   **Max. Height**   **Distance between Hmax-Hmin**
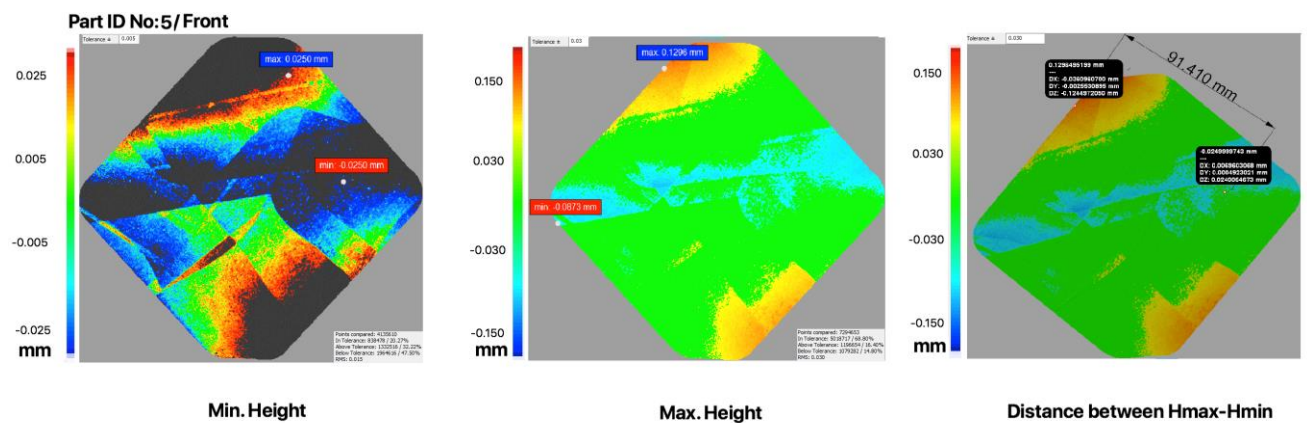
Figure 4.4.1.9 : Part ID No5 Front View Point Cloud Image and Min. and Max. Heights With Distance

152
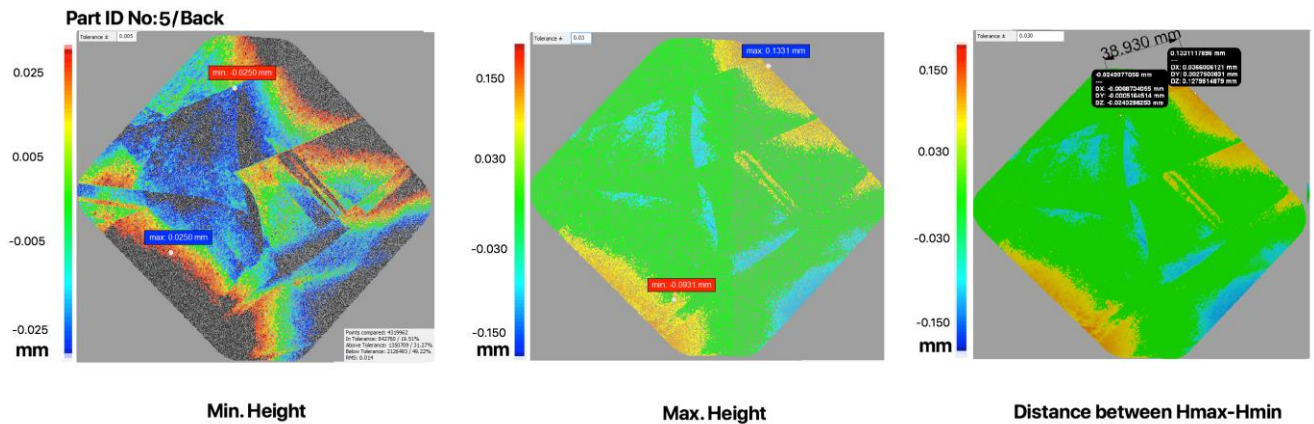
Figure 4.4.1.10:Part ID No5 Back View Point Cloud Image and Min. and Max. Heights With Distance

Note: Abovementioned Figure numbers can be visible with details in Table 4.4.1.

In literature there are three different definitional approaches are available according to the flow regimes that may be explained in relate with Reynolds number "*Re*". Laminar flow is the fluids sliding on the lamination surfaces according to the relative neighbor state where flow motion is infinite. Flow inside the straight pipe matches with this definition. A Propeller installed in to a fixed duct also partially may be an example for this according to the conditioned flow regime. $Re < 10^6$ is the certain assumption for such a flow regime.

Turbulent flow character has different velocity on all of the surfaces without a certain frequency on all flow fields. $Re > 10^8$ is the basic acceptance. Transitional flow regime is a mixed flow model has a Reynolds number between both stated flow regimes. $10^6 < Re < 10^8$

In this study, a test plate was in use to define a frictional surface specification. Therefore, a flow regime as turbulent may be calculated by Schoenherr (1947) or ITTC (1957) formulations according to the stated Reynolds number. But our surface average $8,15x10^4$ is far-wider than mentioned Reynolds numbers.. So that both regime definitive are irregular for this pattern to explain frictional description. Taylor-Couette (1923) formulation simplification

based on a wall function for the combination of smooth boundary layers and fully rough boundary layers formulation will be used in combination [170] :

$$C_F) = \frac{0,455}{\ln^2(0,06\,\mathrm{Re}_x)}$$

(91)

First of all acceptance of these estimations taken $30 < y^+ < 0.1\delta+(x)$ and fully rough condition for our plate means: $k^+ = k_{u\tau}/v + > 15$

$$\frac{d}{x} \gg \frac{0,37}{R_E^{1/5}}$$

(92)

Thus ;

$$C_F = \left[2,87 + 1,58\log(\frac{x}{k_s}) \right]^{-2,5}$$

(93)

Where, X is the plate length and taken 140 mm. for our experimental parts and k_s from the max. height of our points cloud in certain tolerance to define roughness.

4.5 Estimational Evaluation of Experimental Results in Fuel Economy

The roughness of the propeller surfaces is approximated by propeller technologies and scientific studies. Most of the studies performed on the unit surface for determining the surface quality are then evaluated for the total surface, and the surface quality is determined with the help of the obtained data and various scales.

In this study, studies were carried out on Rubert Scaling, Musker Profile and ISO grade number, and the effects of the fouled propeller were determined with Musker Profile [216] which is based on the eddy viscosity concept [217]. Calculated datas are to be compared with the Musker's Characteristics Roughness of Rubert Gauge Surfaces on Table: 2.12.1

Ra: The arithmetic mean of the absolute value of the roughness deviations from the base line defined for the roughness profile, i.e. the arithmetric average of the absolute values of the pit points and the absolute values of the peaks.

$$R_a = \frac{1}{L} \int_0^L |Z(x)| \, dx \qquad (94)$$

Rq (Rms) : Root mean square of surface roughness other wording deviation of roughness profile.

$$R_q = \sqrt{\frac{1}{L} \int_0^L Z(x)^2 \, dx} \qquad (95)$$

Where;

$$R_a = \sqrt{\frac{2}{\pi}} R_q = 0.8 R_q \qquad (96)$$

Rq (RMS) values of the test pieces were determined by deviation analysis with computerized plugin. The Ra values of the parts with Rq values are determined by equation (96); The surface quality of the parts with Rubert Scale and New ISO Scale (N) scaling are specified in Table 4.4.1 below.

Table 4.5.1: Surface Profile Determination Of The Experimental parts

Part ID	Part Side	Tolerance	Rq(RMS)	Ra(μm)	Rubert Scale	New ISO Scale Number (N)
I	Front	0.005	1.3	1.04	A4	6-7
		0.010	2.1	1.68	B1-B2	7-8
		0.020	2.3	1.84	B2-C1	7-8
		0.025	2.4	1.92	B2-C1	7-8
		0.030	2.4	1.92	B2-C1	7-8
	Back	0.005	1.4	1.12	A4-B1	6-7
		0.010	2.1	1.68	B1-B2	7-8
		0.020	2.2	1.76	B2-C1	7-8
		0.025	2.2	1.76	B2-C1	7-8
		0.030	2.2	1.76	B2-C1	7-8
II	Front	0.005	1.3	1.04	A4	6-7
		0.010	2.2	1.76	B2-C1	7-8
		0.020	2.8	2.24	B2-C1	7-8
		0.025	2.8	2.24	B2-C1	7-8
		0.030	2.8	2.24	B2-C1	7-8
	Back	0.005	1.5	1.20	A4-B1	6-7
		0.010	2.8	2.24	B2-C1	7-8
		0.020	4.3	3.44	B2-C1	8-9
		0.025	4.7	3.76	B2-C1	8-9
		0.030	1.8	1.44	B1-B2	6-7
III	Front	0.005	1.4	1.12	A4-B1	6-7
		0.010	2.5	2.00	B2-C1	7-8
		0.020	3.3	2.64	B2-C1	7-8
		0.025	3.3	2.64	B2-C1	7-8
		0.030	3.3	2.64	B2-C1	7-8
	Back	0.005	1.5	1.20	A4-B1	6-7
		0.010	2.5	2.00	B2-C1	7-8
		0.020	2.8	2.24	B2-C1	7-8
		0.025	2.8	2.24	B2-C1	7-8
		0.030	2.8	2.24	B2-C1	7-8
IV	Front	0.005	1.2	0.96	A3-A4	6-7
		0.010	1.6	1.28	A4-B1	6-7
		0.020	1.7	1.36	B1-B2	6-7
		0.025	1.7	1.36	B1-B2	6-7
		0.030	1.7	1.36	B1-B2	6-7
	Back	0.005	1.5	1.20	A4-B1	6-7
		0.010	2.8	2.24	B2-C1	7-8
		0.020	3.7	2.96	B2-C1	7-8
		0.025	3.7	2.96	B2-C1	7-8
		0.030	3.7	2.96	B2-C1	7-8
V	Front	0.005	1.5	1.20	A4-B1	6-7
		0.010	2.4	1.92	B2-C1	7-8
		0.020	3.0	2.40	B2-C1	7-8
		0.025	3.0	2.40	B2-C1	7-8
		0.030	3.0	2.40	B2-C1	7-8
	Back	0.005	1.4	1.12	A4-B1	6-7
		0.010	2.2	1.76	B2-C1	7-8
		0.020	2.5	2.00	B2-C1	7-8
		0.025	2.5	2.00	B2-C1	7-8
		0.030	2.5	2.00	B2-C1	7-8
Average			2.4	1.94	B2-C1	7-8

All Scaling based on Ra

156

Surface points clouds of experimental parts had very huge number of quantities.Because of that, parts were separated and decreased as numbers from the 3 mm. in depth of each part surfaces to eliminate raw data which will not be examined. At that moment, available new points clouds size was approx. 6.Mionumers/pc. After the separation rendering experimental part' " *h'* " (roughness parameter) calculated for each surfaces. By The way of deviation analysis ,10 different roughness parameter found and average toleransında bulunan peak height recorded 145,064μm in 0,030 mm tolerance.

Table 4.5.2: Average Roughness Parametry Calculation

Part ID	Max. Heights(mm)	Min. Heights(mm)	Distance (mm)
No:1 Front	0,1499760300	-0,0249999929	57,060
No:1 Back	0,1387969553	-0,0249999892	65,968
No:2 Front	0,1499931663	-0,0249997247	73,493
No:2 Back	0,1497641355	-0,0249987952	72,634
No:3 Front	0,1499953419	-0,0249999724	84,127
No:3 Back	0,1499811709	-0,0249999929	83,516
No:4 Front	0,1494953334	-0,0249994285	90,237
No:4 Back	0,1498799622	-0,0249999724	25,818
No:5 Front	0,1296495199	-0,0249999743	91,410
No:5 Back	0,1331117898	-0,0249977056	38,930
Avarage(μm)	145,0643405	-24,9995548100	68.319

According to the defined h' =145,064 compared with the [97] Rubert scale and identified between grade D and E.

Calculation of the specific fuel consumption increase based on [97] experiment vessel data with an estimate estimated fuel consumption: 171 g / kWh which is applicable fort he size according ISO standards and advanced coefficient was taken J = 0.4 was accepted since there is no information about fuel consumption for the model ship.

Table 4.5.3: Characteristics of The Experimental Model of [97]

Main Ship Particular			Machinery	6 Cylinder Sulzer 2SA
Overall Length	163,150 m		Max. output	8952 KW
Length B. P.	155,000 m		Design output 85% MCR	7610 KW
Breadth	22,860 m			
Depth	13,420 m		Propeller Characteristics	
Max. Summer Draught	9,727 m			
DWT at Max. Summer Draught	9015,000 tonnes		Diameter (D)	5,5 m
Block Coefficient	0,71		Pitch 0.7R (P)	4,758 m
Wetted Surface Area (at T=9.727)	5079,000 m		Pitch Ratio (P/D)	0,865
Design Speed	16,75 knot		Developed Blade Area Ratio (BAR)	0,66
Taylor Wake	0,38		Number of Blades (Z)	4
Thrust Deduction	0,195		t/c 0.7R	0,04
Relative Rotative Efficiency	1,03		RPM	122 rpm

Figure (5.3) Effect of Propeller Roughness upon K_T, K_Q and η_o
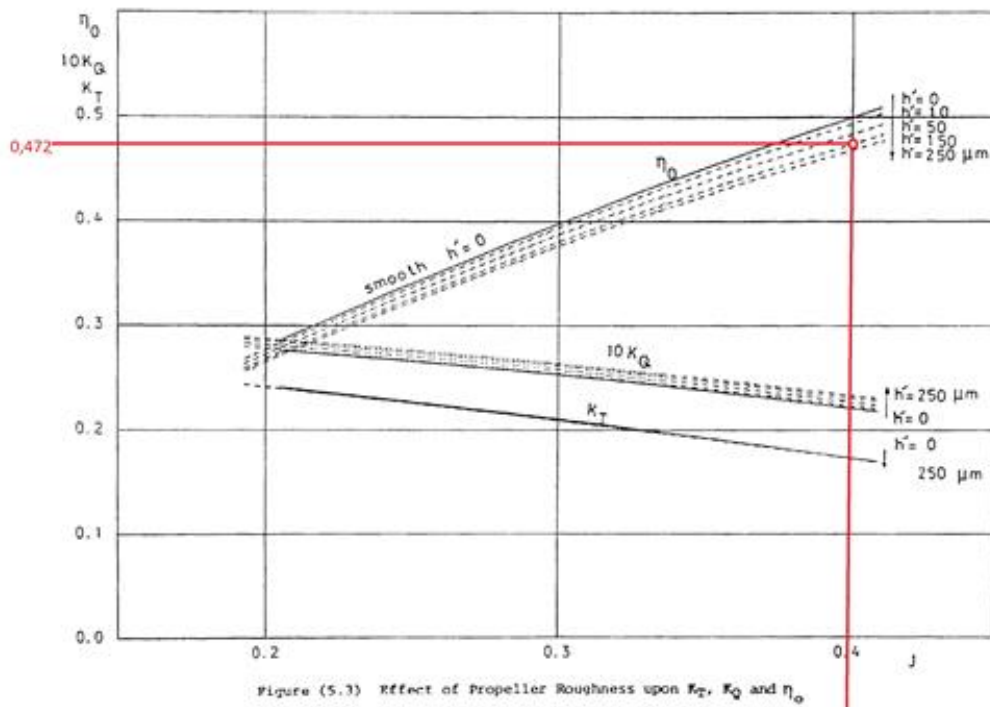
Figure 4.5.1: Effect of Propeller Roughness on Open Water Efficiency [97]

158

Further more, K_T, K_Q and η_0 graph of the same experiment used to define Open Water Propeller Efficieny, $\eta_{0=}$ 0,472 and estimated specific fuel consumption was calculated.

$$Sfc_n = \frac{171x4.72}{1000} \cong 0.81\frac{g}{kWh} + 171\frac{g}{kWh} = 171.81\frac{g}{kWh}$$

(97)

$$\Delta Sfc = (171.81x8952) - (171x8952)/1000 = 7.161\text{kg/kwh}$$

According to the equation mentioned above, hourly extra fuel consumption of this rough ship with 100 % rated power (8952kw) found 7,161kg/h.

As a result, an estimation of such a vessel fuel consumption, in an economical power rating (85%) 146,084 kgs/day may be higher than previous after a month of anchorage where applicable. Daily and monthly cost of the extra fuel consumption for an operator in related with differenet fuel types, in terms of 2019 prices according to Figure 2.14.4.2 will be:

For a consumption of HSHFO: 43, 8252 $/day -- > 1314,756 $/month

For a consumption of VLSFO 88, 819072 $/day -- > 2664,572 $/month

For a consumption of LSMGO 94, 4140892 $/day -- > 2832,423 $/month

4.6 Estimational Evaluation of Experimental Results With Actual Emission Criterias

Calculations of the specific fuel consumption increase, it's been correlated comparison applied according to Roughness effect of Open Water Propeller Efficiency table of [97]

In this case Specific Fuel Consumption was found 0,81 g/kwh at the J= 0,4 and η_0 characteristics and new prediction found as η_0 = 4,72.

At the final calculational predictions of the specific fuel consumption increase compared and added to EU Commission emission criterias for the vessels on "sailing condition

emission" penalties and expressed as a increase of emissions in the table 4.5.1 for different fuel types which is still in use.

Table 4.6.1 : Emission Penalty of Biofouled Propeller Condition in comparison EU Commission predictions.[218]

Engine Type	Fuel Type	Actual NOx	NOx	Actual SO2	SO2	Actual CO2	CO2	Actual HC	HC	Actual Specific Fuel Consumtion	Specific Fuel Consumption
Slow speed Diesel	MGO	30,77	17	1,629	0,9	1064,28	588	1,09	0,6	334,85	185
	MDO	30,77	17	6,697	3,7	1064,28	588	1,086	0,6	334,85	185
	HFO	32,761	18,1	19,005	10,5	1122,2	620	1,086	0,6	352,95	195
Medium Speed Diesel	MGO	23,89	13,2	1,81	1	1167,45	645	0,91	0,5	367,43	203
	MDO	23,892	13,2	7,421	4,1	1167,45	645	0,905	0,5	367,43	203
	HFO	25,34	14	20,815	11,5	1225,37	677	0,905	0,5	385,53	213
High Speed Diesel	MGO	21,72	12	1,81	1	1167,45	645	0,36	0,2	367,43	203
	MDO	21,72	12	7,421	4,1	1167,45	645	0,362	0,2	367,43	203
	HFO	22,987	12,7	20,815	11,5	1225,37	677	0,362	0,2	385,53	213
Gas Turbine	MGO	10,32	5,7	2,72	1,5	1668,82	922	0,18	0,1	524,9	290
	MDO	10,317	5,7	10,498	5,8	1668,82	922	0,181	0,1	524,9	290
	HFO	11,041	6,1	29,865	16,5	1755,7	970	0,181	0,1	552,05	305
Steam Turbine	MGO	3,62	2	2,715	1,5	1668,82	922	0,181	0,1	524,9	290
	MDO	3,62	2	10,498	5,8	1668,82	922	0,181	0,1	524,9	290
	HFO	3,80	2,1	29,87	16,5	1755,70	970	0,18	0,1	552,05	305
										Emissions Units	g/kWh
										Extra Fuel Consumption (g/kWh)	0,81

4.7 Dynamic Balance and Cavitation Acceptance

In this study, scaling effect of bio-fouling and related dynamic balance and cavitation effects couldn't be quantified. Because test plates were just a parts of a vital propeller material which doesn't' comply and reflect a real propulsor. Therefore dynamic balancing and cavitation extent approach was taken in to the study for sharing to form an idea with simulated numbers for estimation.
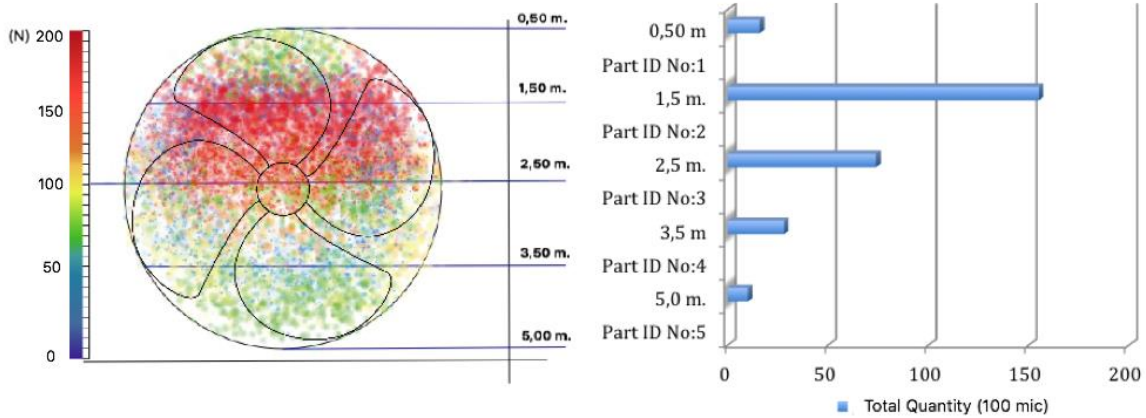
Figure 4.7.1: Spread illustration of Biofouling and Total Quantities in 100 mic.

Table 4.7.1 Counted number of the species biofoulers on different depths

Part ID No:1	Part ID No:2	Part ID No:3	Part ID No:4	Part ID No:5
0,50 m	1,5 m.	2,5 m.	3,5 m	5,0 m.
16 pcs.	155 pcs.	74 pcs.	28 pcs.	10 pcs.

.

If the propeller wheel disc dynamic balance correlation applied to the different submerged patterns of the propeller, where applicable of exclution of other large colonies, an assumption may be expressed as below:

Number of the counted species of the biofouling equally spread to the surface with depth basis:

Part 1 + Part 2 = 171 pcs.

Part 4 + Part 5 = 38 pcs.

Part 3 divided equally - - > 37 pcs. to each side of the propeller.

And

Part 1 + Part 2 = 208 pcs.

Part 4 + Part 5 = 75 pcs.

161

Where ; Each 1 gram of each piece of these foulers:

208-75 = 133 grams differences between two patterns on the propulsor surface. It's clearly

state that there may be a dynamic balancing difference will occur on a propulsor with

unknown results.

A Ship propeller may have different effects where bio-fouling occurred. It's been

expressed such as results in our literature review part and named those results as cavitation and

erosion. It's very limited data which is not even applicable to understand resultant factors on a

ship propeller but, finally their effect may arise fast and seriously defective when they

prolonged on the surface. Only for a critic understanding example here below for a propulsor

which may have cavitation with bio-fouling penalty.

According to the 2D partially cavitating foil linearized theory [220] a lift cavitation

formulation for partial scaling can be written here:

$$C_L = pa(1 + \frac{1}{\sin b})$$
(98)

$$l_{CAV} = \cos^2 b$$
(99)

$$\frac{a}{s} = \frac{1}{2} \tan b \frac{1 - \sin b}{1 + \sin b}$$
(100)

$$\sigma = P - P_{vap}/0.5\rho V^2$$
(101)

$$V_{CAV} = \frac{pa}{16} \cot b(1 + 4\sin b - \sin^2 - 4\sin^3 b)$$
(102)

Where,

α : Geometric angel of propeller pitch and inflow angle difference/Attack angle

l : Where cavitation length

β : Improper cavitation extension as angle (effected by maneuvering characteristics)

σ : Cavitation number

V_{CAV} : Volume of the foil bubble

P: Pressure of arize of wheel disk

Choosen characteristics are calculated for random given numbers:

$\alpha = 15°$

$P - P_{vap} = 0,10 \text{ g/mm}^2$

$P = 0,001015 \text{ g/mm3 (seawater - 1,025 g/cm}^3)$

$\beta = 16° \text{ (which is nearest with attack angle)}°$

The following results were found in the mathematical calculations.

$C_L = 217.98$

$l_{CAV} = 0.92 \text{ mm}$

$\sigma = 196.80$

$V = 1.00 \text{ mm}^2$

$V_{CAV} = 19.85 \text{ mm}^3$

It is obviously clear that even $1°$ changing of attack angle gives us a result of cavitation bubble. Such a result may arise extra vibration and noise losses as illustrated below:
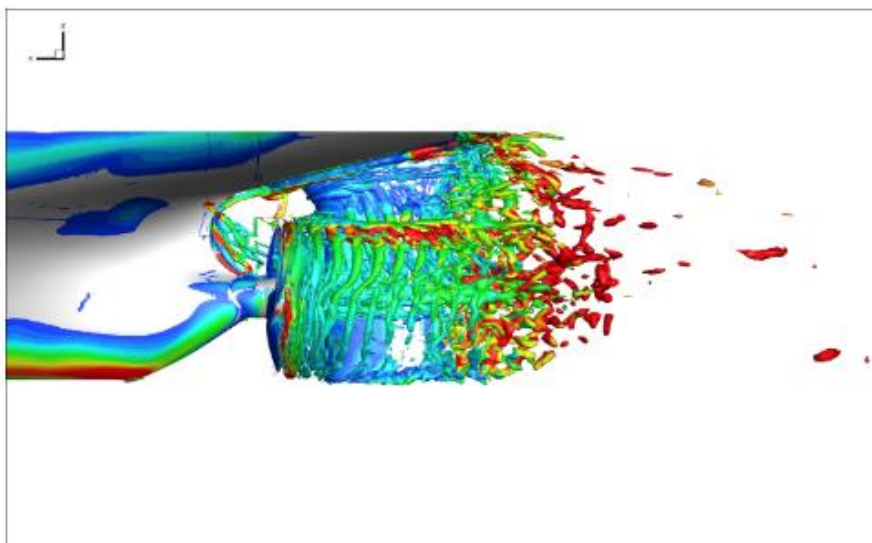

Figure 4.7.2 : Example of A Noise Spread of Propeller in Cavitation D.Li, J.Hallender, R.Karlsson (2015)

5. DISCUSSIONS

It is been calcluated that the estimated surface roughness increase expectation of fuel consumption which seems to be relatively low, may be significant in terms of specific fuel consumption in an effective biological process that may continue until a propeller cleaning or polishing activities may renew surface roughness to relatively better condition. On the other hand, it should be kept in consideration that the consumption found via a group of reference numerical values may give completely different results in another ship or propeller. For this reason, it is a definite necessity to carry out other studies for the results of lower roughness points in theoretical calculations.

The effectiveness and importance of the first one month process, which is the period of rapid spreading, which is perhaps the highest phase of bio-fouling on the propellers, has been able to form a new discussion point in terms of evaluations in this study. Basis of this discussion as a first phase, the inevitability of a compulsory limitation that may have to be brought to the maximum duration on anchorage in the safe anchorage positions within the harbor borders, taking into account the depths where some biological species which may sustain their vital activities suspended in the sea water and may pass the active spreading process.

In the high-lights of the evaluation of analysis results, in the region of first 1.5-2.5 meters from the sea surface, the biological formation observed in depth is in a linear harmony with the numerical excess in the three-dimensional (3D) surface analysis. Thus, it may necessitate evaluation of the underwater locations of the ships in a way that reduces the possibility of bio-fouling due to the characteristics of the geographical location. For example, a strategy may be observed for a ship that will stay in a safe anchorage for a long period, should always wait in full-ballast condition or perhaps, with condition with an optimized draft,

exceeding 1.5-2.5 meters in the shallow waters anchorage positions.There could be a chance of keeping clean of it's propulsor for a longer period as a polished surface.

It's obviously arise a viscous resistance whether it is relatively effctive. Propeller resistance calculations are mostly based on predictions and scenarios as similar as in this study. Propeller torque requirement will most probably increase as oppositely as the thrust forces'deduction and ship's relative speed. But it's unclear appoint a derivative any approach because of the nature of multi-factorial divergents. There should be a specific method how to evaluate ship's total resistance increase in together with propeller condition as well as hull performance a fixed anymore. Because separated approaches most probably violate and keep results in a shadow. From this point of view, similar studies of existing one here, can be widely used in shallow water anchorage areas where biodiversity is relatively more active and can lead to improvements that may point effective results considering the local scope of emission criterias.

According to obtained data in this experimental analysis, depending on the fact that the bio-film roughness at different depths may change in open water characteristics as well as the turbulence penalites, cavitation, erosion or other propeller-based resistants where the propeller can independently be fixed in different depth layers and it is possible that the effectiveness of biofouling is different and caused a different surface roughness. In a situation where accepted this as a premise, examination of the situation of five different propellers, which will be another open path for a new discussion topic. As if, considering each other independently, the proposal may be generated for five different ships or it is evaluated for the same ship propulsor it should be known that an effect in terms of dynamic balance and its results will be natural when it is handled just like in this study.

In the initial stage of Bio-fouling, the main chemical activity of bio-film formation is an important issue in terms of the another importance of the studies that can be done in terms of preventing the onset of corrosion, increasing the effectiveness of anti-fouling coatings, mostly due to the propellers that are moving with the bare surface or immobilized due to the dynamic condition

Corrosion is the main initial chemical activity of bio-film formation at the initial stage of bio-fouling. It should be a common decisional aspect of another activity that is as important as increasing the effectiveness of anti-fouling coatings in order to prevent corrosion in the ship's hull is that it can be prevented from corrosion of naked propellers that in motion in sea-water due to their physical nature or that stay without motion for a period. The activities of anode placement or electrolysis cathodic protection systems seem to be re-considered in more detail in terms of the stationary state of the ship and the location of the propeller.

It is possible to assume that the parts placed underwater for the experiment seem to move relatively free in the water, but in reality these parts retained their positions in direction due to the their fixing arrangement. In this case, the roughness equivalence of the front and back surfaces shows only a little deviation. In this case, there is no impression that the position of the parts relative to sunlight is subject to the effects of the pier or a similar shade position. However, in an ignorance of ship's berthed condition to a pier and take consideration of free positioning under the wind relative, it should be evaluated of biofouling effect in a different lookout in safe anchoareg areas.

In this study, calculated fuel consumption formulation was based on a correlation arising from torque deduction of the propulsion system. Emission assumption was integrated and compared with the International Maritime Organization (IMO) criterias whieh normally defined and described basis of environmental factors. But it's been known that these criterias

should include optimized and active investigational method with multi-functioned formulations due to physical conditions of the engine rooms where as the place of consumption by the main engines. Such an optimization process should also separately be examined as a factor in related how the propeller can be affected by variable phenomena such as the biofouled species' activities in a volume that is close to engine room and under effect of engine room temperature which is relatively hot even if the propulsor in active motion inside the water but in contiquity with engine rooms.

When the results are evaluated, it is always possible to evaluate very economically, indicate thrust losses which may be calculated from engine thrust bearings or to handle the instantaneous torque losses in the power and efficiency relation in order to define active the propeller resistance indication under the instant surveillance, as similar as relatively expensive dynamometers, where the shaft power is measured. It may be another possible economic applications which can make enough precise measurement from axial bearing lubricating oil pressure, axial bearing instant resistive forces or acoustic methods to compare and digitally expressed with an output in terms of biofouling efficiency where applicable. It is thought that the axial bearing clearance indicators used by 2-Stroke engine manufacturers in particular can create sufficient motion examples for this type of solution at the initial stage.

Since the cases produced with empirical formulas during the study produced results in the light of comparisons with the inevitable simulation techniques, they are excluded from the classification of mechanical engineering fields with surface sensitivity. The absence of a standard that classifies the Bio-fouling phenomenon, while establishing rules for the largest transport area in the world in the field of sustainability, stands as an obstacle to establishing a premise in terms of comparing further determinations in the field. In other words, perhaps international norms such as ISO should transform biological surface impurities into class

definitions and categories accepted in the context of surface roughness and coefficient of friction for shipping industry.

Total estimated cost of increased fuel consumption for operators in this study are worthwhile to discuss in terms of a possible propeller polishing cost but also, should be compared with the acceptional rehabilitation cost for the technological energy efficiency improvements for different type of vessels that may be spent in the further next drydocking period.

REFERENCES:

[1] Max Jammer, (2012) Concept of Force, Open web-pdf. of the book, ISBN: 9780486150567

[2] I.B. Cohen, A. Whitman (1999) A new translation of *The Principia*, Isaac Newton, Translated by, University of California press, Berkeley.

[3] Third translation of *The Principia*, Isaac Newton, Translated by Andrew Motte, Gresham College1729

[4] John Nicholas Newman& Paul Sclavounos(1978), The Unified Theory of Ship motions Department of Ocean Engineering, Massachusetts Institute of Technology. OCLC 9127059 Re-printed and presented at Naval Hydrodynamics in Tokyo, 1980.

[5] William Froude, English engineer, hydrodynamicist and naval architect lived between 1810-1879.

[6] Deniz Ünsalan, (1992) The Effects of Hull and Propeller Roughness and Fouling on Ship Performance, Ph.D.Thesis, Istanbul Technical University.

[7] Xueting Wang, Stefan Moller Olsen, Eduardo Andres, Kenneth Norager, Soren Kiil (2018) Drag resistance of ship hulls: Effects of surface roughness of newly applied fouling control coatings, coating water absorbtion, and welding seams. @ Journal of Coatings Technology, and Reserach, pp 1- 13 2018

[8] Principle of Naval Architecture ,2nd revision by Edward Lewis, Page 7, 1988 Printed by The Society of Naval Architects and Marine Engineers, ISBN No. 0-939773-01-5

[9] Jean Le Rond D'Almbert, French mathematician and physicist, lived between 1717-1783, From the Biography,wroted   byJ.J. O'Connor and E. F. Robertson,1988 @ School of Mathematics and Statics University of St.Andrews,Scotland.

[10] George Gabriel Stokes ,Irish Physicist and mathematician.Lived between 1819-1903. Author of "On the theories of the internal friction of fluids in motion" 1845. From the Biography,wroted by J.J. O'Connor and E. F. Robertson,1988 @ School of Mathematics and Statics University of St.Andrews, Scotland.

[11] Claude Luis Navier French Physicist and engineer. Lived between 1785-1836.From the Biography,wroted by J.J. O'Connor and E. F. Robertson,1988 @ School of Mathematics and Statics University of St.Andrews, Scotland.

[12] Osborne Reynolds, Irish Physicist and engineer

[13] Sanjay Kumar Thakur, R. Gopal Krishnan,(2011) Advances in Applied Surface Engineering', Research Publishing Services, Singapore, , ISBN 978-981-08-7922-8.

[14] François Blateyron, (2013) The Areal Field Parameters DOI 10.1007/978-3-642-36458-7_2 @ Springer.

[15] Michael W.Sayers, Steven.M.Karamihas, (1998) The Little Book Of Profiling,Basic Information About Measuring And Interpreting Road Profiles. University of Michigan Transportation Research Institute. Retrieved 2010.

[16] Bharat Bhushan, (2013)Principles and Applications of Tribology , Printed ISBN: 9781119944546 Online ISBN: 9781118403020

[17] Jean Frêne , (2003) La Tribologie De L'antiquite A Nos Jours The Annals Of Universıty "Dunărea De Jos" Of Galaţi Fascicle VIII, Tribology , @ ROTRIB'03 National Tribology Conference, ISSN 1221-4590

[18] Hakan Kaleli, (2011), lecture notes of Prof. Dr. Hakan Kaleli &Triboloji Prensipleri ve Uygulama Örnekleri [online], Yıldız Teknik Üniversitesi, (Ziyaret Tarihi - 19.7.2018/Etik ref. Onay tarihi: 20.7.2018) http://www.yildiz.edu.tr/~kaleli/ Triboloji Prensipleri ve Uyg. pdf

[19] David j. House,(2007) Ship Handling Theory and Practice, ISBN: 978-0-7506-8530-6

[20] E. Eugene Larrabee, (July 1980), The Screw Propeller, Vol. 243, No. 1, pp. 134-149

[21] Francesco Baldi, Hannes Johnson, Cecilia Gabrielii, Karin Andersson, (2015) Energy and Exergy Analysis of Ship Energy Systems – The Case study of a Chemical Tanker - International Journal of Thermodynamics (IJoT) Vol. 18 (No. 2), pp. 82-93, 2015 ISSN 1301-9724 / e-ISSN 2146-1511 doi: 10.5541 / ijot.70299

[22] Masataka Yoshimura,(2010) System design optimization for product manufacturing , ISBN 978-1-84996-008-3

[23] Buhaug, Ø., Corbett, J.J., Endresen, Ø., Eyring, V., Faber, J., Hanayama, S., Lee, D.S., Lee, D., Lindstad, H., Markowska, A.Z., Mjelde, A., Nelissen, D., Nilsen, J., Pålsson, C., Winebrake, J.J., Wu, W., Yoshida, K. April (2009), Second IMO GHG Study 2009, International Maritime Organization (IMO) London, UK.

[24] Anthony F. Molland & Stephen R. Turnock & Dominic A. Hudson, (2011), Ship Resistance and Propulsion, Cambridge University Press, USA, ISBN 978-0-521-76052-2

[25] Toshifumi Fujiwara & Michio Ueno & Yoshiho Ikeda, May 28-June 2, (2006) @ Proceedings of the Sixteenth International Offshore and Polar Engineering Conference, International Society of Offshore and Polar Engineers, USA, ISBN 1-880653-66-4 , ISSN 1098-6189

[26] Svend Aage Harvald, (1983) Resistance and Propulsion of Ships, John Wiley & Sons Press, USA, ISBN 0-471-06353-3

[27] John Travis Hunsucker (2011) Quantification Of Frictional Drag Due To Biofouling On In-Service Ships , PhD Thesis.

[28] Anthony F. Molland,Stephan R.Turnock,Dominic A. Hudson (2011) Ship Resistance and Propulsion: Practical Estimation of Propulsive PowerISBN-13: 978-1107008014.

[29] J.H.Michell (1898) Wave resistance of a Ship Philosophical Magazine, vol. 45, Sec. 5, pp. 106–123.

[30] A.Gotman (2002) Study Of Michell's Integral And Influence Of Viscosity And Ship Hull Form On Wave Resistance, Oceanic Engineering International, Vol. 6, No. 2, 2002, pp. 74-115.

[31] Pijush K. Kundu, Ira M. Cohen and David R Dowlin, (2011) Fluid Mechanics, 5th editionISBN:978-0123821003.

[32] Stephen B. Pope, (2000) Turbulent Flows, ISBN: 978-0521598866.

[33] J. Longo, J. Shao, M. Irvine, F.Stern (2007) Phase-averaged PIV for thenominal wake of a surface ship in regular head waves, ASME J.Fluids Eng. 129 (2007) 524–540.

[34] Zixuan Yanga, Zuo Cuia, Shizhao Wanga, (2019) A New Numerical Framework For Large-Eddy Simulation Of Waves Generated By Objects Piercing Water Surface, Theoretical & Applied Mechanics Letters 9, 79-83.

[35] Shiju John, Md. Kareem Khan, P C Praveen, Manu Korulla and P K Panigrahi (2012) Ship Hull Appendages: A Case Study International Journal of İnnovative research & Development Volume 1, issue 10 (Special issue) ISSN: 2278-0211 (online).

[36] ITTC Recommended Procedures (2002) Testing and Extrapolation Methods High Speed Marine Vehicles Resistance Test , 7.5-02-05-01 Page 14 of 17.

[37] J. Zhang (2006) – Open source- Lecture notes Chapter-5, part 2, United Sates Naval Academy.

[38] J.S.Carlton (2018) Marine Propellers and Propulsion, 4th Edition ISBN: 9780081003664.

[39] Joseph Holtrop (1984) Statistical re-analysis of resistance and propulsion data. International Shipbuilding Progress, 31(363), 272–276.

[40] Daniel Savitsky (2003) On The Subject Of High-Speed Monohulls , available video-slight www.sname.org

[41] Solas, (1974) is a convention expressed by IMO (International maritime Organization) to declared and agreed publication for express minimum criterias for Safety Of Life At Sea.

[42] M. Debbou, M. Pietrzak-David, (2015) "An Optimal Control Strategy for Innovative Electric Naval Propulsion System", in Proc. EVER 2015 Conf., Monte Carlo, Mar.,

[43] R.Reid (1978) Improvement of Ship Steering Control for Merchant Ships - Phase II, Technical Report, NMRC-KP-188,Chapter V.

[44] Henry Havelock (1922) The effect of shallow water on wave resistance Volume 100,Issue 706, ISSN: 0950-1207.

[45] Hoyte C. Raven (2012) A computational study of shallow-water effects on ship viscous resistance, Proceedings of the 29th Symposium on Naval Hydrodynamics Gothenburg.

[46] Florin Pacuraru and Leonard Domnisoru (2017)Numerical investigation of shallow water effect on a barge ship resistance , IOP Conf. Ser.Volume 227.Conference 1: Mater. Sci. Eng. 227 012088.

[47] Takao Inui, Kogakushi (1954), Wave-Making Resistance in Shallow Sea and in Restricted Water, with Special Referenceto its Discontinuities.

[48] Masao Kinoshita,Kogakushi (1954) , On The Restricted Water effect On Ship Resistance.

[49] Michael Leer-Andersen, Lars Larsson (2003) An experimental/numerical approach for evaluating skin friction on full-scale ships with surface roughness', Journal of Marine Science and Technology,Volume 8, Issue 1.

[50] Townsin,R. L., Byrne, D. ,Svensen, T. E., Milne, A., (1989) Estimating the Technical and Economic Penalties of Hull and Propeller Roughness, Trans. SNAME, 89, pp. 295–318, 1981.

[51] International Towing Tank Conference (ITTC), 2008 'Proceedings of 25th ITTC-Volume II', Fukuoka, Japan,

[52] B.S.Bowden,N.J.Davison (1974) "Resistance Increments Due to Hull Roughness.

[53] Onur Usta, Emin Korkut (2013) A Study For The Effect Of Surface Roughness On Resistance Characteristics Of Flat Plates ,The Royal Institution of Naval Architects,Marine coatings.

[54] Tom R. Thomas, (1999), Rough Surfaces, Second Edition, Imperial College Press, ISBN: 978-1-86094-100-9.

[55] Eric.C. Tupper (2013) Introduction to Naval Architecture, 5'th edition ISBN: 978-0-08-098237-3

[56] Boud Van Rompay (2012) Hydrex Underwater Technology, Quarterly Journal ofShip HullPerformance, Volume 2, issue 2 Chapter IV.

[57] Wojciech Jurczak, (2016) A Study of The Corrosion resistance of Ship Aluminium Alloys, Scientific Journal of Polish Naval Academy, 2016 LVII, 2 (206) DOI: 10.5604/0860889X.1224745.

[58] K.Shiotani, I. Samusawa, S. Tachibana, T. Komori, (2012)Proc. ICSOT, Ambon, Indonesia, The Royal Institution of Naval Architects, p. 27.

[59] Kazuhiko Shiotani, Masayoshi Nakamura (2015) Coating Deterioration and Corrosion Behaviorof Ship Using Corrosion Resistant Steel for Ballast Tank "JFE-SIPTM-BT", JFE Technical report No:20.

[60] Dogancan Uzun, Yansheng Zhang,Yiğit kemal Demirel,Osman Turan (2017) Experimental Determination Of Added Resistance Due To Barnacle Fouling On Ships By Using 3D Printed Barnacles,Conference Paper of 5th International Conference on Advanced Model Measurement Technology for The Maritime Industry, At Glasgow.

[61] Simone Dürr, Jeremy C. Thomason (2009) Biofouling , Page 397 ISBN: 9781444315479

[62] Yiğit Kemal Demirel (2015). Modelling the roughness effects of marine coatings and biofouling on ship frictional resistance. (PhD Thesis), University of Strathclyde

[63] Schultz, M. P. (2004). Frictional resistance of antifouling coating systems. Journal of Fluids Engineering, 126(6), 1039-1047.

[64] ITTC. (2011). Fresh Water and Seawater Properties. International Towing Test Conference (ITTC) Recommended Procedures and Guidelines, Procedure 7.5-02-01-03, Revision 02. Retrieved from

[65] Alexander I. Railkin (2004), Marine Biofouling—Colonization Processes and Defenses. CRC Press, Boca Raton, USA (hbk), 300 pp., ISBN: 0-8493-1419-4.

[66] Diego Yebra, Torben Munk, Daniel Kane (2009) The effects of corrosion and fouling on the performance of ocean-going vessels: a naval architectural perspective @ Woodhead Publishing Series in Metals and Surface Engineering 2009, Pages 148-176.

[67] Michael P. Schultz, Geoffrey Swain ,John Finlay,Maureen Callow, J.A Callow Adhesion Strength of Settled Spores of the Green Alga Enteromorpha Pages 251-256 | Published online: 09 Sep 2010.

[68] Diego Meseguer Yebra, Søren Kiil∗, Kim Dam-Johansen (2003) Antifouling technology—past, present and future steps towards efficient and environmentally friendly

antifouling coatings Technical University of Denmar @ Progress in Organic Coatings 50 (2004) 75–104.

[69] Melo L. F., Bott T. R.& Bernardo C. A. (1988) Fouling science and technology. Dordrecht, The Netherlands: Kluwer Academic.

[70] Hellio C.& Yebra D.. 2009 Advances in marine antifouling coatings and technologies. Boca Raton, FL: CRC.

[71] D.Gordon, S. Mawatari S. (1992) Atlas of marine-fouling Bryozoa of New Zealand ports and harbours.. New Zealand: Miscellaneous Publishers, New Zealand Oceanographic Institute.

[72] Dobretsov S.. (2009) Expected effect of climate change on fouling communities and its impact on antifouling research. Advances in marine antifouling coatings and technologies (eds , Hellio C.& Yebra D.), pp. 222–239Boca Raton,

[73] Martin Wahl (1989) Marine epibiosis. I. Fouling and antifouling: some basic aspects Vol.58: 175-189, Institute of Zoology, Kiel University.

[74] Alexander I. Railkin (2003), Marine Biofouling: Colonization Processes and Defenses ISBN 9780849314193 - CAT# 1419.

[75] Ruey-Jing Tang, Joseph J. Cooney (1998) Effects of marine paints on microbial biofilm development on three materials. Journal of Industrial Microbiology and Biotechnology ;20:275–280.

[76] Aslı KACAR, (2009) Effects Of Anti-Fouling Paints On Marine Bacterial Biofilm Development , Dokuz Eylul University Graduate School of Natural and Applied Sciences.

[77] Lily D. Chambers, Keith Stokes,Frank C. Walsh, Robert Wood (2006) Modern approaches to marine antifouling coatings

[78] Elisabete Almeida , Tereca C. Diamantino , Orlando de Souza (2007) Marine paints: The particular case of antifouling paints @ Progress in organic coatings Volume 59 Issue 1, pages 2-20

[79] Maureen E. Callow, Robert Fletcher (1994) The influence of low surface energy materials on bioadhension-A review a- review biodeterior & biodegr 34-333-348.

[80] Felicia Wong Yen Myan, Odetta ay Ling Paramor, James Walker (2013) The interaction of marine fouling organisms with topography of varied scale and geometry: A reviewDOI: 10.1186/1559-4106-8-30

[81] Gregory D. Bixler and Bharat Bhushan (2012) Biofouling: lessons from nature DOI:10.1098/rsta.2011.0502.

[82] M.Nosonovsky, B. Bhushan (2008) Multiscale dissipative mechanisms and hierarchical surfaces. New York, NY: Springer.

[83] Barthlott W.& Neinhuis C.. 1997Purity of the sacred lotus, or escape from contamination in biological surfaces. Planta 202, 1–8.doi:10.1007/s004250050096.

[84] Jung Y. C.& Bhushan B.. 2009Wetting behavior of water and oil droplets in three-phase interfaces for hydrophobicity/philicity and oleophobicity/philicity. Langmuir **25**, 14165–14173.doi:10.1021/la901906h

[85] Scardino A. J., Guenther J.& de Nys R.. 2008Attachment point theory revisited: the fouling response to a microtextured matrix. Biofouling **24**, 45–53.doi:10.1080/08927010701784391

[86] James F. Schumacher , Michelle L. Carman , Thomas G.Estes , Adam W. Feinberg, Leslie H. Wilson, Maureen E. Callow, James A. Callow, John A. Finlay & Anthony B. Brennan (2006) Engineered antifouling microtopographies – effect of feature size, geometry, and roughness on settlement of zoospores of the green alga *Ulva* Pages 55-62

[87] Carman ML, Estes TG, Feinberg AW, Schumacher JF, Wilkerson W, Wilson LH, Callow ME, Callow JA, Brennan AB (2006) Engineered antifouling microtopographies – correlating wettability with cell attachment. Biofouling 22:11–21

[88] Wan F, Pei X, Yu B, Ye Q, Zhou F, Xue Q: Grafting polymer brushes on biomimetic structural surfaces for anti-algae fouling and foul release. ACS Appl Mater Inter 2012, 4:4557–4565.

[89] Scardino AJ, Harvey E, De Nys R: Testing attachment point theory: diatom attachment on microtextured polyimide biomimics. *Biofouling* 2006, 22:55–60.

[90] J. Köhler, PD Hansen & M. Wahl (1999) Colonization Patterns at the Substratum‐water Interface: How does Surface Microtopography Influence Recruitment Patterns of Sessile Organisms? Pages: 237-248.

[91] Aldred N, Scardino A, Cavaco A, de Nys R, Clare AS: Attachment strength is a key factor in the selection of surfaces by barnacle cyprids (Balanus amphitrite) during settlement. Biofouling 2010, 26:287–299.

[92] Anthony F. Molland (2008) , The Maritime Engineering Reference Book, P.319 Hardcover ISBN: 9780750689878 , eBook ISBN: 9780080560090

[93] Felicia Wong Yen Myan (2017) The influence of physical attributes of surface topographies in relation to marine biofouling - Taylor's University – Malaysia

[94] Michael Schultz (2007) Effects of coating roughness and biofouling on ship resistance and powering Biofouling, 23:5, 331-341, DOI: 10.1080/08927010701461974

[95] Chelakara Subramanian, Trond M. Ostren, Sathya N. Gangadharan (2004) Noncontact Measurement of Marine Biofouling Roughness – Marine Technology, Volume 41,Number 2, pp. 67-73(7) @Society of Naval Architect and Marine Engineers

[96] Irma Yeginbayeva , Mehmet Atlar, (2018) An experimental investigation into the surface and hydrodynamic characteristics of marine coatings with mimicked hull roughness ranges P.1001-1018.

[97] Mohamed Ahmed Mosaad (1986) Marine Propeller Roughness Penalties, PhD thesis , New Castle University

[98] J.S.Carlton (2012) Marine Propellers and Propulsion, 3rd Edition, ISBN: 978-0-08-097123-0

[99] K. M. Berntson, H Andreasson, P.R. Jonnson, L. Larsson, K. Ring, S.Petronis & P. Gatenholm (2000) Reduction of barnacle recruitment on micro‐textured surfaces: Analysis of effective topographic characteristics and evaluation of skin friction Pages: 245-261

[100] Holtrop J., Mennen G.G.J. (1982) An Approximate Power Prediction Method. International Shipbuilding Progress, 29, 335, , 166–170.

[101] J.S.Carlton (2012) Marine Propellers and Propulsion, 3rd Edition, ISBN: 978-0-08-097123-0

[102] Holtrop J. (1988) A Statistical resistance prediction method, International Shipbuilding Progress 25(290) 253-256

[103] Volker Bertram, B.Herbeth Schneekluth, (1998). Ship Design for Efficiency and Economy.2nd edition.Butterworth Heinemann. ISBN 0-7506-4133-9 (978-0-7506-4133-3)

[104] Georg P. Weinblum (1951) , The Thrust Deduction @ The Journal Of The American Society for Naval Architects , Vol. 63, Issue 2 Pages 363-380

[105] Cora Bijsterveld as Resp. (2019) Systematic Propeller Series, Lecture notes OpenCourseWare of Delft University of Technology

[106] John.S Carlton (2007) Marine Propellers and Propulsion, 2nd. Edition ISBN:978-0-7506-8150-6

[107] G.Patience,(1983) Propeller surface roughness and fuel economy. Technical report, StoneManganese Marine Limited.

[108] C. W. B. Grigson (1982) Propeller roughness, its nature and its effect upon the drag coefficients of blades and ship power.Technical report, R.I.N.A.

[109] DirkStruik, (1961) Lectures on classical differential geometry. Dover Publications, Inc., New York. ISBN: 978-0486656090

[110] Christopher Wojciech Dekanski (1993), Design and Analysis of Propeller Blade Geometry using the PDE Method, PhD Thesis

[111] A.J.Musker, (1977), 'Turbulent shear-flows near irregularly rough surfaces with particular reference to ship hulls', Ph.D. Thesis, University of Liverpool.

[112] M. Atlar , E.J. Glover, M. Candries , R.J. Mutton, C.D. Anderson (2002) The effect of a foul release coating on propeller performance

[113] Stone Marine (2016) Propeller Surface Roughness , Open Source-Technical Papers

[114] Michigan Wheel and Federal Propellers (2000) Propeller Geometry: Terms and Definitions, PROPGEOM. 31AUG00Master Document from web open source.

[115] Chang-SupLee, Young-DalChoi, Byoung-KwonAhn, Myoung-SupShin, Hyun-GilJang (2013) Performance optimization of marine propellers @ International Journal of Naval Architecture and Ocean Engineering, Volume 2, Issue 4, December 2010, Pages 211-216

[116] Alexander H. Day (1997) Resistance Optimization of Displacement Vessels on the Basis of Principal Parameters, Journal of Ship Research volume 41,issue 4

[117] Jingwei Jiang,Haopeng cai, Cheng Ma, Zhengfanf Qian,Ke Chen, Peng Wu (2016) A ship propeller design methodology of multi-objective optimization considering fluid–structure interaction @Journal Engineering Applications of Computational Fluid Mechanics, Volume 12, 2018 - Issue 1.

[118] L.Morino, C.Kuo (1974) Subsonic potential aerodynamics for complex configurations - A general theory, AIAA Journal, vol. 12, Feb. 1974, p. 191-197.

[119] Yin Lu Young,Liu Zhanke (2007) Hydroelastic Tailoring of Composite Naval Propulsors, Proceedings of the 26th international conference on offshore mechanics and Arctic engineering, OMAE2007-29648, pp. 777-787; 11 pages

[120] Qun Zhang , Song Cen (2016) Multiphysics Modeling Numerical Methods and Engineering Applications Elsevier and Tsinghua University Press Computational Mechanics Series, Pages 125-156 ISBN: 978-0-12-407709-6

[121] Tanumay Sinha, (2019) Marine insight , 10 Factors Considered For Efficient Ship Propeller Design

[122] Antoine Brient (2002) Integrated Design Applied to Marine Propellers: Effects of Surface Roughness on Hydrodynamic Performance, IDMME 2002, At Clermont-Ferrand (France)

[123] Philip Mallozzi, (1936) Dynamic Balancing of Ship Propellers, Journal of the American Society for Naval Engineers, volume 48, issue 3, Pages 327-360

[124] Lother Birk (2019) Propeller Geometry, Fundamentals of Ship Hydrodynamics, Fluid Mechanics, Ship Resistance and Propulsion.ISBN: 9781118855485

[125] Mogens Blanke, Karl-Petter Lindegaard, Thor I.Fossen (2000) Dynamic Model for Thrust Generation Of Marine Propeller

[126] DNVGL Regulations, Part 4 Systems and components

[127] Zabi Bazari, 2015. Energy Efficient Ship Design and Technical Energy Efficiency Measures Presentation notes, Online, National Workshop On Marpol Annex VI and Technology Transfer, Batumi Georgia, International Maritime Organisation

[128] Sydney Arthur Walling, John Campbell Hill (1943) Nautical Mathematics New edition's ISBN: 9781107642522

[129] D.H Norrie (1962) Marine Propeller Vibration Research At The University Of Adelaide, The Royal Institution Of Naval Architects Boz.No:4762,GPO, Paper No: 62/N.

[130] Stefano Gaggero, Tomaso Gaggero, Enrico Rizzuto, Giorgio Tani, Diego Villa, MicheleViviani (2016) Ship Propeller Side Effects: Pressure Pulses And Radiated Noise , De Gruypter Open Source Paper, Noise Mapp. 2016; 3:295–315 DOI 10.1515/noise-2016-0021

[131] M. Felli, M. Falchi Propeller tip and hub vortex dynamics in the interaction with a rudder, Springer-VerlagExp Fluids, 2011,51:1385–1402.

[132] F. Ochi, T. Fujisawa, T. Ohmori, and T. Kawamura,(2009) "Simulation of propeller hub vortex flow", FirstInternational Symposium on Marine Propulsors, Norway.

[133] Insanu Abdilla Cendikia Abar, I Ketut Aria Pria Utama, Muhammad Iqbal (2018) An Investigation into the Effect of Slope Angle of Hub Cap Geometry against the Efficiency of Ship Propeller inthe Presence of PBCF, Proceeding of Marine Safety and Maritime Installation (MSMI 2018)

[134] Michael Brown,Seth Schroeder, Elias Balaras, (2015) Vortex Structure Characterization of Tip-Loaded Propellers, Fourth International Symposium on Marine Propulsorssmp'15, Austin, Texas, USA

[135] Jaroslaw Artyszuk (2003) Wake fraction and thrust deduction duringship astern manoeuvres ,Transactions on the Built Environment vol 68, 2003 WIT Press, Online ISSN: 1743-3509.

[136] C.Kawakita, T.Hoshino (1999) Design System of Marine Propellers with New Blade Sections @ 22.Symposium on Naval Hydrodynamics, chapter 4, propulsor hydrodynamics/hydroacoustics

[137] J.Basumatary (2017) Cavitation erosion-corrosion in marine propeller materials, PhD. Thesis, University of Southampton

[138] Daniel T. Valentine (1993) Reynolds-Averaged Navier-Stokes Codes and Marine Propulsor Analysis, Hydromechanics Directorate Research and Development Report, CRDKNSWC/HD-1262-06 , Carderock Division,Naval Surface Warfare Center,United States Navy

[139] Rudolph Diesel (1858-1913) A German mechanical engineer and inventor who borned in France.

[140] Bomboma Kalgora,Thsibuyi Mutinga Cristian (2016) The Financial and Economic Crisis, Its Impacts on the Shipping Industry, Lessons to Learn: The Container-Ships Market Analysis DOI: 10.4236/jss.2016.41005

[141] Martin Stopford (2009), Maritime Economics, ISBN: 9780415275576

[142] Sebastian Opitza,Henry Seidelb,Alexander Szimayerc (2015)The shipping crisis starting in 2008: Could it have been prevented? Hamburg Financial Reearch Center (HFRC) Working Paper Series No.14

[143] Cristofer H. Marques,Jean-D. Caprace, Carlos R. P. Belchior, Alberto Martini, (2019) An Approach for Predicting the Specific Fuel Consumption of Dual-Fuel Two-Stroke Marine Engines @Journal Of Marine Science and Engineering,

[144] IHS Group Market report, (2019) IMO 2020: What Every Shipper Needs To Know, whitepapers March 2019.

[145] World's Regional Oil Demand Growth Graph and Marine Bunker's Product Demand International Energy Agency (IEA) Fuel Report, March 2019

[146] United Nations Conference on Trade and Development, UNCTAD (2019) Review Of Maritime Transport 2019,

[147] Peter Sands (2019) Bunker Prices In Major Bunkering Hubs On The To Share Market Insights In Malaga,Spain and Amsterdam,Netherlands, World (BIMCO) 2019

[148] Snorri Gudmundsson, (2014) , General Aviation Aircraft Design, ISBN: 978-0-12-397308-5

[149] Tadeusz Borkowski, Lech Kasyk, Przemysáaw Kowalak , (2011) Assessment Of Ship's Engine Effective Power Fuel Consumption And Emission Using The Vessel Speed , Journal of KONES Powertrain and Transport, Vol. 18, No. 2

[150] MAN B&W,(2017) Technical Paper: Calculation of Specific Fuel Oil Consumption (*Sfoc) Description: 3700405-6.2*

[151] ACCESS (2014), D 2.42 - Calculation of fuel consumption per mile for variousship types and ice conditions in past, present and in future, Arctic Climate Change Economy and Society (ACCESS) ,Project no. 265863

[152] Koji Sekimizu (2014),Third IMO GreenHouse Gas (GHG) Study 2014Executive Summary andFinal Report.

[153] Thomson, H.; Corbett, J.J.; Winebrake, J.J. (2015) Natural gas as a marine fuel. Energy Policy, 87, 153–167. doi:10.1016/j.enpol.2015.08.027.

[154] ICCT (2011) Marginal CO_2 abatement costs of analyzed technologies, Reducing Greenhouse Gas Emissions from Ships Cost Effectiveness Of Available Options, White Papers

[155] IMO (2014) Third IMO GreenHouse Gas (GHG) Study 2014Executive Summary andFinal Report

[156] ENTEC, (2002) Market Survey of Marine Distillates with 0.2% Sulphur Content , European Commission, A European Green Deal final report 2002

[157] David Cooper,Tomas Gustafsson (2004) Methodology for calculating emissions from ships: 1. Update of emission factors, Swedish Methodology For Environmental Data, Report series SMED and SMED&SLU Nr 4

[158] ITU Ninova (2019) Additional Lecture Notes For "Hydrodynamic Characteristics Of Propellers" , Istanbul Technical University

[159] Aysegul AKDOGAN, 25 Feb 2009 @ "Design and Material Choice" lecture notes in Yıldız Technical University.

[160] Timo Teravista,Dag Tjostheim,Clive W.J.Granger,(1994) Chapter 48 Aspects Of Modelling Nonlinear Time Series, Handbook Of Econometrics, Volume 4, Pages 2917-2957

[161] Richard S. Westfall (1962) The Development of Newton's Theory of Color, book page 1 , ISIS A Journal Of the History of Science Society,Volume 53,Number 3 Sep.1962 in The University of Chicago Press Journals.

[162] Utku Büyüksahin, 2014 Vision Based Sensor Technologies - Webcam: A Multifunctional Sensor @ Comprehensive Materials Processing Volume 13,2014 Pages 375-392

[163] Adobe [®] Photpshopnews online version entery note by unknown author, Adobe [®] Photoshop CC Help , 2.2.2018 online PDF version

[164] Robert A. Hummel (1975) Histogram modification techniques, Computer Graphics, vol. 4, no. 3, pp. 209–224

[165] V. Magudeeswaran, C. G. Ravichandran (2013) Fuzzy Logic-Based Histogram Equalization for Image Contrast Enhancement, Mathematic Problems On Engineering, Volume 2013,Article ID 891864,10 pages, doi:10.1155/2013/891864

[166] Karin Smith (2018) History of 3D Scanners, Modena AEC Web marketing page.

[167] Mostafa Abdel-Bary EBRAHIM (2013) 3D Laser Scanners' Techniques Overview @ International Journal of Science and Research (IJSR) ISSN (Online): 2319-7064, Index Copernicus Value (2013): 6.14 | Impact Factor (2014): 5.611

[168] Ron K.C. Cheng (2008), Inside Rhinoceros® 5, Open source-marketing web-document

[169] Yeşim Ak Örek, Sinan Mavruk (2016) Ichthyoplankton of the Mediterranean Sea, The Turkish Part Of The Mediterranean Sea Marine Biodiversity, Fisheries, Conservation And Governance, pp.226-247

[170] Ismail B. Celik (1999) Lecture Notes for Introductory Turbulence Modeling, Open Webpage, West Virginia University

[171] Meteorological Depertmant of TRNC (2019), Temperature analysis form Code No: F.MTD.77.

[172] Nils Turnblom (2010) Underwater 3D Surface Scanning using Structured Light, ISSN: 1401-5757, UPTEC F10 063

[173] George Vosselman, Ben G.H. Gorte, Geroge Sithole,T Rabbani B.(2003) Recognising Structure In Laser Scanner Point Clouds , The International Archives Of The Photogrammetry, Remote Sensing And Spatial Information Sciences , Doi:10.1.1.118.6228

[174] Peter Schuchert zoologist (1998). How many hydrozoan species are there? Commemorative volume for the 80th birthday of Willem Vervoort in 1997 ISSN 0024-1652/ISBN 90-73239-68-0 and marine hydrozoa database of World Register of Marine Species organization (WoRMS)

[175] Boardman RS, Cheetam AH, Oliver WA Jr. (1973) Animal Colonies. Stroudburg, Pennsylvannia: Dowden, Hutchinson & Ross.

[176] Leo W. Buss , Evan D. Buss, Christopher P. Anderson, Michael Power, Joseph Zinter (2016) Control of Hydroid Colony Form by Surface Heterogeneity PLoS ONE 11(6): e0156249. https://doi.org/10.1371/journal.pone.0156249.

[177] Melissa R. McQuoid and Kjell Nordberg (2003) Environmental Influence on the Diatom and Silicoflagellate Assemblages in Koljö Fjord (Sweden) over the Last Two Centuries, Vol. 26, No. 4, Part A (Aug., 2003), pp. 927-937.

[178] Robert G. Wetzel, (1990) Land-water interfaces: metabolic and limnological regulators. Verhandlungen der Internationalen Vereinigung für Limnologie 24: 6-24

[179] Ulrike Müller. 1994: Seasonal development of epiphytic algae on Phragmites australis (CAV.) Trin. Ex Sten. in a eutrophic lake. Archiv für Hydrobiologie 129(3): 273-292.

[180] Guiry, Michael. "Worms – World Register Of Marine Species – Licmophora Abbreviata C.Agardh, 1831". Marinespecies.org. N.p., 2005. Web. 26 May 2016.

[181] Kudela Lab. Biological and Satellite Oceanography Laboratory, University of California Santa Cruz Phytoplankton Identification a look at the tiny drifters along the California coast.

[182] Olenina, I., Hajdu, S., Edler, L., Andersson, A., Wasmund, N., Busch, S., Göbel, J., Gromisz, S., Huseby, S., Huttunen, M., Jaanus, A., Kokkonen, P., Ledaine, I. and Niemkiewicz, E. (2006)

[183] John.R.Haynes (1981) Section: The Miliolida, Foraminifera PP 145-179 , ISBN: 978-1-349-05399-5

[184] Omaña, L.; Alencaster, G.; Buitrón, B.E. Lourdes Omaña, Gloria Alencaster, Blanca Estela Buitrón (2016). "Mid-early late Albian foraminiferal assemblage from the El Abra Formation in the El Madroño locality, eastern Valles–San Luis Potosí Platform, Mexico:

Paleoenvironmental and paleobiogeographical significance" (PDF). Boletín de la Sociedad Geológica Mexicana. 68 (3): 477–492. doi:10.18268/BSGM2016v68n3a6.

[185] Kumar Saraswati, (2001) Growth and habitat of some recent miliolid foraminifera: Palaeoecological implications Pratul.

[186] Jens Boenigk, Sabina Wodniok,Edvard Glücksman (2015) Biodiversity and earth History ISBN:9783662463932.

[187] Hans Hillewaert (2012) Benthic forams, taken with a Leica DFC 490 camera mounted on a Leica M205C binocular microscope

[188] Roger P. Harris, in Encyclopedia of Ocean Sciences (Second Edition), 2001

[189] Christopher J. Cutts, (2003) Culture of Harpacticoid Copepods: Ptential as Live Feed For Rearing Marine Fish, Advances in Marine Biology Volume 44, Pages 295-316.

[190] Havens KE, Pinto-Coelho RM, Beklioğlu M, Christoffersen KS, Jeppesen E, Lauridsen TL, Mazumder A, Méthot G, Alloul BP, Tavşanoğlu UN, Erdoğan Ş. (2015) Temperature effects on body size of freshwater crustacean zooplankton from Greenland to the tropics. Hydrobiologia.; 743(1):27-35.

[191] Kulkarni D, Gergs A, Hommen U, Ratte HT, Preuss TG. (2013) A plea for the use of copepods in freshwater ecotoxicology. Environmental Science and Pollution Research.; 20(1):75-85.

[192] Patrick Lavens , Patrick Sorgeloos As Editors (1996), FAO Fisheries Technical Paper 361, Manual on The Production and Use of Live Food for Agriculture, Open library of Food and Agriculture Organization of the United Nations, M-44 ISBN 92-5-103934-8.

[193] Ann M. Tarrant, Birgitte Nilsson, Benni Winding Hansen (2019) Molecular physiology of copepods - from biomarkers to transcriptomes and back again , Comparative Biochemistry and Physiology Part D: Genomics and Proteomics, Volume 30, Pages 230-247.

[194] David V Alford (2012), Pests of Ornamental Trees, Shrubs and Flowers (Second Edition), 2012

[195] Alexey Alexandrovich Zotin, (2009) The growth and energy metabolism of Lymnaea stagnalis (Lymnaeidae, Gastropoda): I. Early postlarval period

[196] Jonathan R. Hendricks, (2017) The digital encyclopedia of ancient life.

[197] Douglas S.Glazier,(2014) Amphipoda DOI:10.1016/B978-0-12-409548-9.09437-9

[198] Barnard, J. Laurens; Ingram, Camilla L. (1986). "The supergiant amphipod *Alicella gigantea* Chevreux from the North Pacific Gyre". Journal of Crustacean Biology. 6 (4): 825–839. doi:10.2307/1548395. JSTOR 1548395

[199] Frank M. Wilhelm and David C.(1998) Seasonal Trends in the Head Capsule Length and Body Length/Weight Relationships of Two Amphipod Species @ *Crustaceana* Vol. 71, No. 4 (Jun., 1998), pp. 399-410

[200] Weronika Podlesińskaa Henryka Dąbrowska (2019) Amphipods in estuarine and marine quality assessment – a review , Ocenalogia, Voluma 61,issue 2, Pages: 179-196

[201] B.Morton , G. Lotha (2019) Animal Diversity Web, Brittanica Encyclopedia

[202] M.Mcgurk, D.Warborton,V.Komori (1990) Outer Continental Shelf Environmental Assesment Program, final reports of principle investigators volume 71, Page: 276

[203] Yoshihisa Kurita, Hiroshi Wada (2011) Evidence that gastropod torsion is driven by asymmetric cell proliferation activated by TGF-β signalling, Biology Letters, 7(5) , Pages:759-762 PMCID: PMC3169068

[204] Takao Ubukata (2000) Geometric Pattern Growth Rate Of Prismatic Shell Structure İn Bivalvia

[205] Thomas R. Waller , 1981 Functional Morphology and Development of Veliger Larvae of the European Oyster, Ostrea edulis Linne

[206] Kyoko Kamiya, Keiji Yamashita, Toshiharu Yanagawa, Toyoki Kawabata, Kenji Watanabe (2012) Cypris Larvae (Cirripedia: Balanomorpha) Display Auto-Fluorescence in Nearly Species-Specific Patterns, Zoological Science, 29(4):247-253 (2012). https://doi.org/10.2108/zsj.29.247

[207] D.T. Anderson. (1994). Barnacles: structure, function, development and evolution. ISBN: 978041244420

[208] Tara Essock-Burns, Neeraj V. Gohad , Beatriz Orihuela , Andrew S. Mount , Christopher M. Spillmann , Kathryn J. Wahl , Daniel Rittschof (2017) Barnacle biology before, during and after settlement and metamorphosis: a study of the interface Journal of Experimental Biology 220, 194-207 doi:10.1242/jeb.145094

[209] H. Barnes (1953) Size Variations In The Cyprids Of Some Common Barnacles, Marine Biology Assosications, Volume 32, pages 297-304

[210] Y.Yan (2003) Dimensions of cultured larval stages of *Chinochthamalus scutelliformis* Larval Development Of The Barnacle Chinochthamalus Scutelliformis (Cirripedia: Chthamalidae) Reared In The Laboratory, Journal Of Crustacean Biology, 23(3): 513–521, 2003

[211] Nick AldredJens T. HøegDiego MaruzzoAnthony S. Clare , (2013) Analysis of the Behaviours Mediating Barnacle Cyprid Reversible Adhesion, https://doi.org/10.1371/journal.pone.0068085

[212] Robert Lee Wallace, Claudia Ricci and Giulio Melone (1996), A Cladistic analysis of pseudocoelomate (aschelhelminthes) morphology, Invertebrate Biology Vol. 115, No. 2 pp. 104-112.

[213] K.Soetart, Nikolas Lampadariou,Mario Franco,Agnes WN Muthumbi (2009) Factors affecting nematode biomass, length and width from the shelf to the deep sea , Marine Ecology Progress Series 392:123-132 , DOI: 10.3354/Meps08202

[214] A. M. A. Aguinaldo, J. M. Turbeville, L. S. Linford, M. C. Rivera, J. R. Garey, R. A. Raff, & J. A. Lake, (1997) Evidence for a clade of nematodes, arthropods and other moulting animals. Nature 387: 489-493.

[215] Melanie F.Kho, Balasubramani Venkatasamy, Audrey Bellier, Yan Hu, (2011) The Pore-Forming Protein Cry5B Elicits the Pathogenicity of Bacillus sp. against Caenorhabditis elegans DOI: 10.1371/journal.pone.0029122.

[216] Anthony J. Musker,(2012) Explicit Expression for the Smooth Wall Velocity Distribution in a Turbulent Boundary Layer, doi.org/10.2514/3.61193

[217] Anthony Kendall , Manoochehr Koochesfahani (2006) A Method for Estimating Wall Frictionin Turbulent Boundary Layers , 25'th AIAA Aerodynamic Measurement Technology and Ground testing Conference,5- 8 June 2006, San Francisco, California.

[218] ENTEC (2002) European Commission Quantification of emissions from ships associated with ship movements between ports in the European Community Final Report Part 2 July 2002 Entec UK Limited

[219] Da-Qing Li, Jan Hallander, Roger Karlsson (2015) Progress In Predicting Pressure Pulses And Underwater Radiated Noise Induced By Propeller With Pressure Side

[220] Kerwin, S.; Hadler, J. Principles of Naval Architecture 'Series'-Propulsion, 1st ed.; SNAME: New York, NY, USA, 2010 Cavitation, Nutts 18 2015, At Cortona Italy

- **TURNITIN REPORT**

CURRICULUM VITAE